공학박사 학위논문

A Cooperative Control Method of Active and Reactive Power for Droop Control-Based Standalone Microgrids

Droop 제어기반 독립형 마이크로그리드의

유·무효전력 연계제어에 관한 연구

2016년 2월

서울대학교 대학원

전기·컴퓨터공학부

김 윤 수

A Cooperative Control Method of Active and Reactive Power for Droop Control-Based Standalone Microgrids

지도교수 문 승 일

이 논문을 공학박사 학위논문으로 제출함
2015년 12월

서울대학교 대학원
전기·컴퓨터공학부
김 윤 수

김윤수의 공학박사 학위논문을 인준함
2015년 12월

위 원 장 _____ (인)

부위원장 _____ (인)

위 원 _____ (인)

위 원 _____ (인)

위 원 _____ (인)

Abstract

A Cooperative Control Method of Active and Reactive Power for Droop Control-Based Standalone Microgrids

Yun-Su Kim

School of Electrical Engineering and Computer Science

The Graduate School

Seoul National University

A microgrid that is operated autonomously due to its electrical isolation from the main grid (e.g., a remote island area) is called as a standalone microgrid. In grid-connected mode, the main grid forms and maintains the frequency and voltage stably whereas islanded or standalone mode cannot. So the standalone microgrid emulates the conventional power system to adopt frequency and voltage droop control. However, the standalone microgrid has characteristics of low system inertia and weak grid. Subsequently, the frequency and voltage stability of the microgrid is vulnerable to the change of load or output of intermittent renewable energy source (RES).

This dissertation presents control methods of distributed generations (DGs) in a standalone microgrid in order to maintain the frequency and voltage stably during disturbances such as load change and/or output change of intermittent RES. Since the conventional frequency droop control method uses frequency deviation from its nominal value to share active power, the frequency deviation is inevitable. To overcome frequency deviation, an active power sharing method of using the state of charge (SOC) of the battery energy storage system (BESS) is proposed. The BESS forms constant frequency and voltage magnitude without any droop method and other controllable DGs are controlled to output desired level of active and

reactive power. Thus, the output and the SOC of the BESS are changed if the active power load is changed. Other controllable DGs will share the active power load based on the SOC deviation. The DGs in the proximity of the BESS will measure the output of the BESS directly for primary SOC control. The DGs in the distance from the BESS will receive the SOC data via communication system with time delay for secondary SOC control. To enhance system reliability, the BESS controller is designed to be changed to the conventional frequency droop control mode if the communication system fails.

For improvement of the voltage stability, a new droop method is proposed. Voltage–reactive power (*V*–*Q*) droop control method has been adopted conventionally in standalone microgrids to alleviate voltage deviation and to share reactive power. This method uses the voltage deviation from its nominal value to control reactive power. Subsequently, it cannot fundamentally prevent voltage deviation. Especially, if the output of intermittent RES fluctuates heavily, the voltage variation will be severer. To eliminate this voltage fluctuation, active power–reactive power (*P*–*Q*) droop control method, which changes the reactive power proportional to the change of active power of RES, is proposed. The droop coefficient is determined based on the sensitivity matrix. Moreover, active power–active power (*P*–*P*) droop control is also developed for low voltage network based standalone microgrid where reactive power compensation barely affects system voltage.

The proposed method was modeled and simulated by MATLAB/SimPowerSystems. It is compared with the conventional droop control method to prove its effectiveness. The proposed method can be applied to the electrically isolated power system with high hosting capacity of RES. It can maintain the frequency and voltage steadily. Consequently, increment of the RES hosting capacity into the microgrid and prosperity of the energy self-supporting islands are looked for.

Keywords : Constant frequency, SOC-based active power control, Droop

control, Standalone microgrid, Battery energy storage system, Renewable energy source
Student Number : 2010-20776

Contents

List of Tables

List of Figures

Chapter 1. Introduction

1.1 Motivations and purposes

Change of energy paradigm

Due to growth in the global population and the increase of the use of various devices that consume electricity, the electrical energy demand has grown to unprecedented levels [1]. Since the electrical energy in the classical power system flows in one-direction, that is from the generation system to the distribution system via transmission system, the only way to resolve the energy demand growth problem is to establish more generation and transmission systems. For the past century since at the beginning of the power system industry, this method has been seemed to be effective to solve energy balancing problem.

However, recently, the supply increment strategy has been gradually reaching its limit on account of environmental, social, and geographical issues. For instance, most of the electrical energy for the peak load demand is acquired from the fossil-fueled power plant which emits greenhouse gas and thereby causes the air pollution. Most of the electrical energy for the base load demand comes from the nuclear power plant that inevitably discharges the nuclear waste which threatens the people as well as the environment. Moreover, the local residents have a complicated stake in the establishment of generation and transmission system. Usually, due to the health, safety, and aesthetic problems, they oppose to the construction of the generation and transmission system in the proximity of their habitats. For some countries especially with high population density, geographical problems can also be arisen.

To overcome the problems mentioned so far, many technologies such as demand response (DR), high voltage direct current (HVDC), flexible alternating current transmission system (FACTS), electric vehicle (EV), renewable energy

source (RES), distributed generation (DG), energy storage system (ESS), and microgrid have been developed. Thanks to these technologies, the strategy of the power system industry is changing from the supply increment to the demand management and from the centralized control to the decentralized control.

Motivations for studying standalone microgrids

Among the technologies that have been developed up to date, the microgrid and the RES are the most promising ones in the perspective of resolving energy balancing problem locally and environmental problems. The microgrid concept was first introduced in [2] and [3]. It is a low or medium voltage distribution network which is composed of DGs, ESSs, controllable loads, a static switch, RESs, and etc. The microgrid has an ability to be connected to or isolated from the main utility by closing or opening the static switch at the point of common coupling (PCC). In grid-connected mode, the microgrid can be seen as a controllable load in the perspective of the main utility. In islanded or standalone mode, it can be continuously operated even in abnormal situations of the main utility such as faults or maintenance, thereby enhancing the system reliability. This characteristic gives a great advantage to a standalone microgrid. However, since the system inertia is low and the grid is weak, the frequency and voltage problems are bound to be occurred due to instantaneous load change or intermittent output active power of RESs such as wind turbines (WTs) and photovoltaic (PV) systems. Moreover, with increasing environmental awareness, the hosting capacity of RES has increased gradually [4], [5]. This has led to many projects, such as [6]–[8], which attempt to interconnect RESs into isolated power systems such as remote islands, thereby constructing a standalone microgrid.

In South Korea, Ulleung Island is designated as ‘Green Island’ to make it energy self-supporting island [6]. The peak load of Ulleung Island is about 10 MW and around 18 MW of RES is planned to be interconnected with the applications of ESS, energy management system (EMS), DR, and etc. and thereby substitute the

conventional generators [6], [9]. Korean government is planning to promote the projects of standalone microgrids with high hosting capacity of RES to vitalize renewable energy certificate (REC) deal, expand information and communication technology (ICT)-based energy market, and develop business models of new energy industry.

The project of Samso Island is one of the most well-known renewable energy island programs. It is a small Danish island that would be expected to convert all its energy supply to 100 % RES within 10 years since 1997 [7]. The means to achieve this project included: Cuts in consumption and increased efficiency in terms of heat, electricity and transport; Expansion of the district heating supply systems combined with utilization of local biomass resources; Expansion of individual heating systems using heat pumps, solar heating, biomass-plants and other means; Construction of onshore and offshore wind power plants to cover electricity production [7].

Reference [8] analyzed about the feasibility of supplying the whole energy demand of the largest island in the Irish Republic from the RES. It concludes that the potential of renewable energy, especially wind and tidal power, is high enough to supply the whole energy demand of the island, however a modern electrical grid is necessary.

Some demonstration projects such as a standalone microgrid system with WTs, PV arrays, diesel engines, and ESSs on Kythnos Island in Greece [9] and a standalone microgrid consisting of multiple energy forms and seawater desalination installations on Dangan Island in Zhuhai, China [10] have also been established.

It can be noted that the study of the standalone microgrid is consistent with recent technical trends by seeing the projects about the standalone microgrid and the interconnection of the RES to the standalone microgrid.

Purposes of this dissertation

There are many technical issues about a microgrid. Typically, protection,

seamless mode transition, harmonics, power sharing, frequency stability, and voltage stability issues are of major concerns. Particularly in standalone microgrids, the frequency and voltage stability is severe problem due to low system inertia and weak grid network. Subsequently, this dissertation is mainly focused on the frequency and voltage stability issue of standalone microgrids.

The frequency deviation of a standalone microgrid is occurred mainly due to the load change or the output change of the RESs. In other words, the frequency deviation has direct bearing on the active power balance between demand and supply. Conventionally, the system frequency of the standalone microgrid is formed by the rotational speed of the rotor of synchronous generator or by the inverter-interfaced DG adopting frequency droop control. Using these mechanisms necessarily causes the frequency deviation. Hence, one of the purposes of this dissertation is to prevent frequency deviation and thereby to enhance frequency stability by proposing a novel mechanism for sharing active power.

The other purpose of this dissertation is to alleviate voltage fluctuation due to the output fluctuation of intermittent RES thereby to improve the voltage stability. Commonly, the system voltage is largely related to the reactive power. Hence, voltage–reactive power (V–Q) droop is usually adopted for voltage regulation and reactive power sharing. However, the active power is also related to the voltage, especially for the weak grid such as a standalone microgrid. Subsequently, this dissertation proposes the voltage control strategy related to the active power.

1.2 Highlights and contributions

Decoupling of frequency and active power

One of the main highlights and contributions of this dissertation is decoupling of the system frequency and the active power. This work is implemented by ditching the use of the frequency droop control. A standalone microgrid or any other isolated power systems require at least one source that is able to regulate voltage and frequency and respond quickly to changes in load [12]. These sources can be categorized as two types. One of these sources is the synchronous generator whose mechanical rotational speed is the system frequency. If the demand and supply of active power is balanced the frequency is at its nominal value. The frequency falls/rises if the load increases/decreases since the synchronous generator uses its kinetic energy stored in the rotational mass. Since the reaction of the rotor is relatively slow, the frequency deviation cannot be restored instantaneously. The other type of source is the inverter-interfaced DG. Unlike synchronous generators, inverter-interfaced DG units can change the output voltage angle instantaneously [13]. Hence they are able to regulate the frequency at the desired value. However, for active power sharing, the frequency droop control which inevitably causes frequency deviation should be adopted. Consequently, it can be concluded that neither type of source can prevent the frequency deviation.

In terms of preventing the frequency deviation, this dissertation proposes to decouple the frequency and the active power. To this end, the state of charge (SOC) of the battery energy storage system (BESS) instead of the frequency is coupled with the active power. A single inverter-interfaced BESS is controlled to form constant frequency and voltage without any droop control and the other DG units are controlled to output desired value of the active and reactive power.

Maintaining SOC of a BESS

By adopting a BESS as to be controlled as explained, a BESS cannot be

operated consistently since it has the capacity limit. Moreover, because it is controlled only to keep constant frequency and voltage, it cannot adjust its own SOC by itself. Thus, the controllable DG units receive the current SOC data and are adjusted to maintain the SOC at the desired level. Naturally, the active power sharing is implemented based on the deviation of the SOC. The SOC-maintaining units are categorized as two types – primary and secondary SOC control units. The primary SOC control unit is in the proximity of the BESS to directly measure the SOC of the BESS and the secondary SOC control unit is in the distance of the BESS. So, the secondary SOC control unit receives the SOC data via the communication system which might cause low reliability of the system.

Preventing reliability degradation

Since the use of the communication infrastructure might cause the degradation of the system reliability due to its failure, the proposed operation strategy is designed to cope with the communication system failure without any trouble. With a change of the BESS control mode during communication system failure, the standalone microgrid can be operated as same as the one that adopts conventional frequency droop control method. Though the advantages of the proposed method might be lost by the transition of the BESS control mode, it is essential to keep running the system. Note that if the communication system fails, the SOC cannot be maintained and then the BESS, which is the only source that forms the system frequency and voltage, will run out of its power.

New droop method for reactive power control

One of the major problems caused by the intermittent RES such as WTs and PV systems when they are interconnected to the standalone microgrid which has low inertia and weak grid network is the voltage stability problem. The voltage is highly related to the reactive power which is a major reason for why the generation system adopts *V*–*Q* droop conventionally for voltage regulation or reactive power

sharing. However, the voltage and the active power also have a relationship which is high for the weak grid such as standalone microgrids. Moreover, *V–Q* droop is triggered by the voltage deviation so it cannot fundamentally prevent the voltage fluctuation due to the variation of active power output of intermittent RES. To prevent voltage fluctuation occurred by the active power fluctuation, the *P–Q* droop concept is developed. The *P–Q* droop coefficient is calculated considering the grid impedance. By adopting this droop control method, the voltage stability enhancement can be achieved.

Increasing the hosting capacity of RESs

Many control methods that suppresses energy extraction below its available value have been developed for intermittent RESs, particularly WTs, to enhance frequency stability and controllability [14]–[16]. These control methods can enhance the stability whereas they are inefficient in the economical perspective. However, by adopting the proposed control strategy, the use of energy from the RESs can be maximized and the frequency and voltage stability can be enhanced. Consequently, the hosting capacity of RESs is allowed to be increased significantly in standalone microgrids.

1.3 Dissertation organization

Chapter 1 presents the motivations and purposes of this dissertation and then the highlights and contributions of this dissertation are followed. The last part of this chapter describes the organization of this dissertation.

Chapter 2 explains about technical issues about control of a standalone microgrid and its components. The concept and components of a standalone microgrid, control methods of energy sources, and types of energy sources are discussed in this chapter.

Chapter 3 describes about the SOC-based active power control method proposed in this dissertation. The proposed control strategy is applied to both a synchronous generator-based and an inverter-based standalone microgrids. A control scheme for each energy source is described also. A few simulation tests for the proposed strategy are implemented also.

Chapter 4 illustrates about the voltage control strategy proposed in this dissertation. Two newly proposed droop controls, which are *P–Q* and *P–P* droop controls, concepts are introduced in this chapter. Particularly in *P–Q* droop control method, the cooperative control characteristics between active and reactive power are also discussed. To determine which one of them to adopt depends on whether the network voltage is high or low. As same as Chapter 3, a couple of simulation tests are implemented to prove the effectiveness.

Chapter 5 shows the simulation results for case studies. Case studies include the output fluctuation of RESs, the communication system failure, trip out of the BESS from the system, and control of the BESS.

Chapter 6 concludes this dissertation.

Additionally, the system parameters including the proportional-integral (PI) gains of the controllers of the energy sources, the synchronous generators, and the network impedances are shown in Appendix A. The case of forecasting error and relationship between expected life and SOC of a battery are shown in Appendix B

and C, respectively.

Chapter 2. Standalone Microgrid and Its Components

2.1 Concept of standalone microgrid

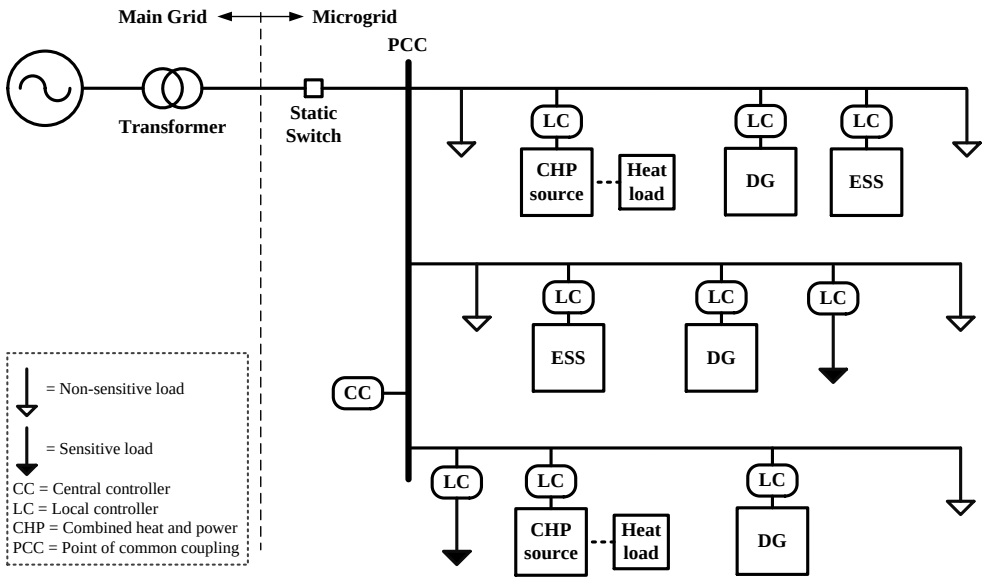

Fig. 2.1 Typical microgrid configuration.

Typical Microgrid

Microgrid concept was first introduced in [2] and [3]. It is a small-scale, low or medium voltage combined heat and power (CHP) supply network designed to supply electrical and heat loads for a small community, such as a housing estate or a suburban locality, or an academic or public community such as a university or school, a commercial area, an industrial site, a trading estate or a municipal region [17]. Microgrid is essentially an active distribution network because it is the conglomerate of DG systems and different loads at distribution voltage level. A typical microgrid configuration is shown in Fig. 2.1.

Fig. 2.1 shows that the microgrid contains a central controller (CC), local controllers (LCs) [18], a static switch, loads, and various types of energy sources.

Types of energy sources will be separately discussed in Section 2.2.

Static switch and mode transition

Typically, the static switch is placed at the PCC of the microgrid. The static switch plays a significant role to bring a representative characteristic of microgrid into relief, that is, it can change the operation mode of the microgrid. By opening/closing the static switch, the microgrid is isolated from/connected to the main grid. It is called islanded mode when the microgrid is isolated from the main grid and grid-connected mode when it is connected to the main grid. The grid-connected microgrid gives an advantage that the microgrid can be seen as a controllable load in the perspective of the main grid. On the other hand, the islanded microgrid gives an advantage that the electrical energy consumers of the microgrid-side can be supplied energy continuously and securely even if emergency events, such as faults and maintenances, happened.

Local controller

The main function of LC is to control the power and/or frequency and voltage of DGs (e.g., CHPs, ESSs, and etc.), or controllable loads in response to any disturbance and load changes. LC is able to control energy sources without any communications from the CC. It also participates in economic generation scheduling and load tracking. In islanded mode, LC should rapidly respond to the load change to share load demand and should be able to change its mode to grid-connected mode with the aid of CC. In both modes, LC is monitoring the local voltages to quickly react for voltage compensation with reactive power control during disturbances. Two other key features are that an LC will not interact independently with other LCs in the microgrid and that it will override the CC directives that may seem dangerous for its energy source [17].

Central controller

The CC executes the overall control of the microgrid including protection, power sharing, mode transition, economic generation scheduling, and etc. Its main objectives are to maintain the system frequency and voltage at the specified level and to operate microgrid economically beneficial. One of the major functions of the CC is to implement EMS function. EMS collects data about load forecasting, wind speed forecasting, solar irradiance forecasting, SOC of the ESS, and etc., to send optimized command to dispatchable DG units and controllable loads as shown in Fig. 2.2 [19]. If the environment of the microgrid is changed, microgrid model, settings, algorithms, and policies applied to the EMS can be changed to optimize the microgrid operation strategy suitable to the changed environment.

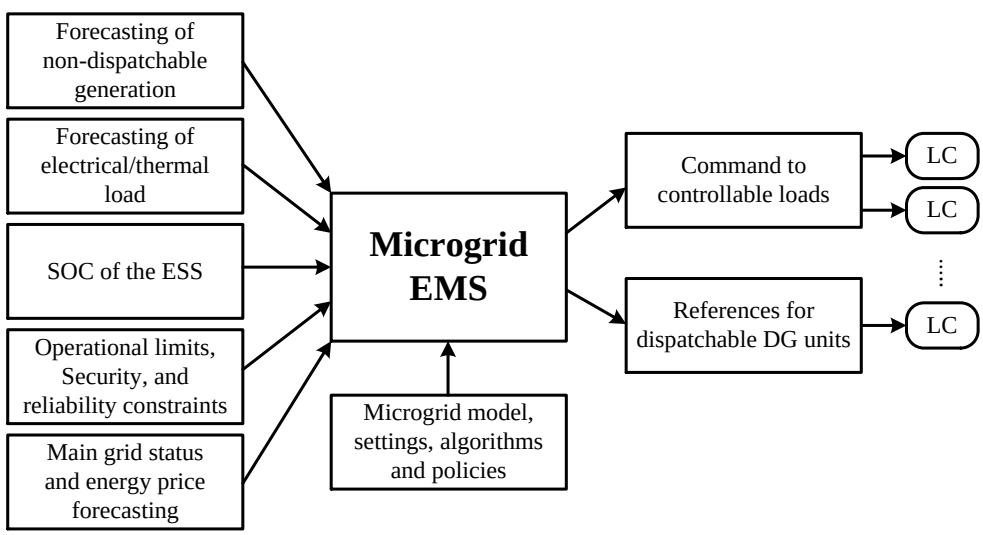

Fig. 2.2 Data flow of EMS for a microgrid [19].

Standalone microgrid

Typical microgrids can be operated either grid-connected mode or islanded mode. However, in remote island areas, the transmission line cannot be installed to interconnect their power system network to the main grid mainly due to economical and geographical factors (e.g., islands, mountains). By the way,

renewable sources such as wind and solar irradiance are abundant in remote island areas [20]–[22] thereby standalone microgrids have been established in such areas [6]–[8], [20], [22], [23]. The standalone microgrid is an autonomously operated microgrid that is not able to be connected to the main grid due to economical and geographical factors [22]–[24]. Usually, terminologies “standalone” and “islanded” are used interchangeably. However, in this dissertation, those words will be used distinctively – “standalone” for a microgrid that cannot be interconnected to the main grid and “islanded” for a one that can be interconnected to the main grid.

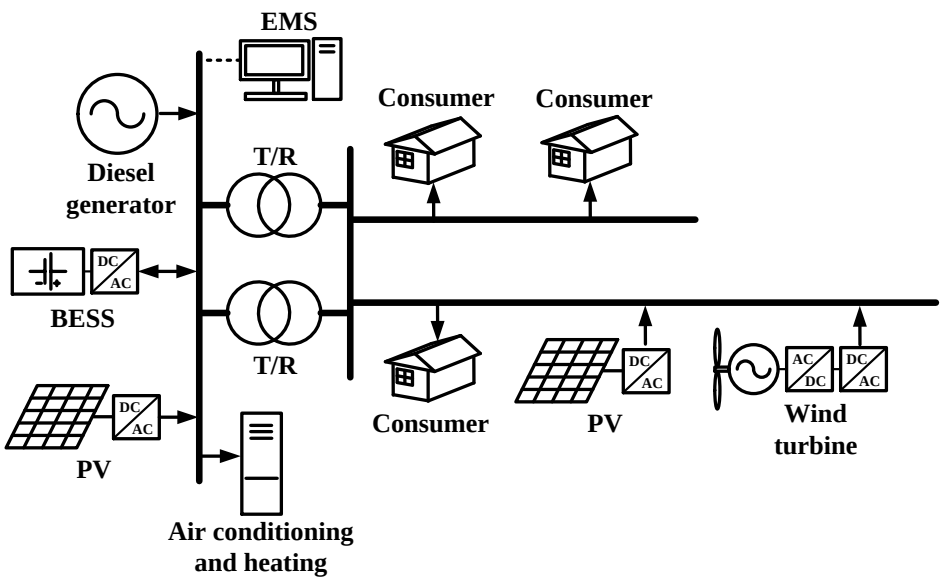

Fig. 2.3 Configuration of standalone microgrid of Gasa Island.

While connected to the main grid, the system requirements of a frequency and a voltage of the microgrid are met by the main grid. However, in remote island areas, such as standalone microgrids, the frequency and voltage are maintained by energy sources installed in a microgrid where diesel generators are most widely employed [25], [26]. The other energy sources can be categorized as controllable and uncontrollable types. Controllable energy sources, such as BESSs, microturbines, fuel cells, and etc., are usually adjusted for power sharing,

frequency support, and voltage control. Uncontrollable energy sources, such as WTs and PV systems, are usually adjusted by using maximum power point tracking (MPPT) method to maximize their use of clean energy. However, there are also some researches [14]–[16], which compulsively decrease their use of energy below the available power, to enhance grid code requirements. Fig. 2.3 illustrates the configuration of one of typical standalone microgrids in South Korea which is installed in Gasa Island. As can be seen from Fig. 2.3, the components of the standalone microgrid are as same as those of typical microgrids except that it does not have a static switch which connects the main grid.

2.2 Control of distributed generations (DGs)

2.2.1 Types of DG

Since there are so many terminologies referring to various types of energy sources in a microgrid, in this dissertation, a terminology, DG, is applied to all these types of energy sources including ESSs (e.g., BESSs, compressed air systems), RESs (e.g., WTs and PV systems), and etc. (e.g., gas turbines, microturbines, fuel cells) for convenience sake. The generation technologies suitable for a typical microgrid are as follows [53]:

- Internal combustion engines
- Mini- to small-size combustion turbines
- Microturbines
- Fuel cells
- Photovoltaic systems
- Wind turbines
- Energy storage systems

Among the above DGs, ESSs play an important role in a microgrid in order to shave peak load demand and to store surplus energy from RESs.

Internal combustion engines

The internal combustion engine (ICE) is the most commonly applied DG for commercial and industrial onsite generation applications [53]. In ICE, fuel is burnt in air in a combustion chamber with or without oxidizers. Combustion creates high-temperature and high-pressure gases that are allowed to expand and act on movable bodies like pistons or rotors. The commonly used fuels are diesel, gasoline, and petroleum gas [17]. Propane gas is also sometimes used as fuel. With some modifications to the fuel delivery components, most ICEs designed for gasoline can run on natural gas or liquefied petroleum gases. ICEs have been used

to produce electric power for nearly 100 years and are the most mature DG technology available [53]. ICEs are used for various applications such as standby power, peak shaving, CHP, and base load electricity production.

Microturbines

Microturbines are widely popular as generating units in DG systems and as energy producers in CHP systems [17]. Microturbines are extremely small turbines with less than a 1-MW rating and are available as single-shaft or split shaft units. A single-shaft unit and a split-shaft unit are shown in Figs. 2.4 and 2.5, respectively [17]. The single-shaft unit is a high-speed synchronous machine with compressor and turbine mounted on the same shaft. For these machines, the turbine speed ranges from 50,000 to 120,000 rpm [17]. On the contrary, the split-shaft unit uses a power turbine rotating at 3,000 rpm [17] and a conventional generator connected via a gearbox for speed multiplication. Unlike traditional backup generators, microturbines are designed to operate for extended periods of time and require little maintenance [17].

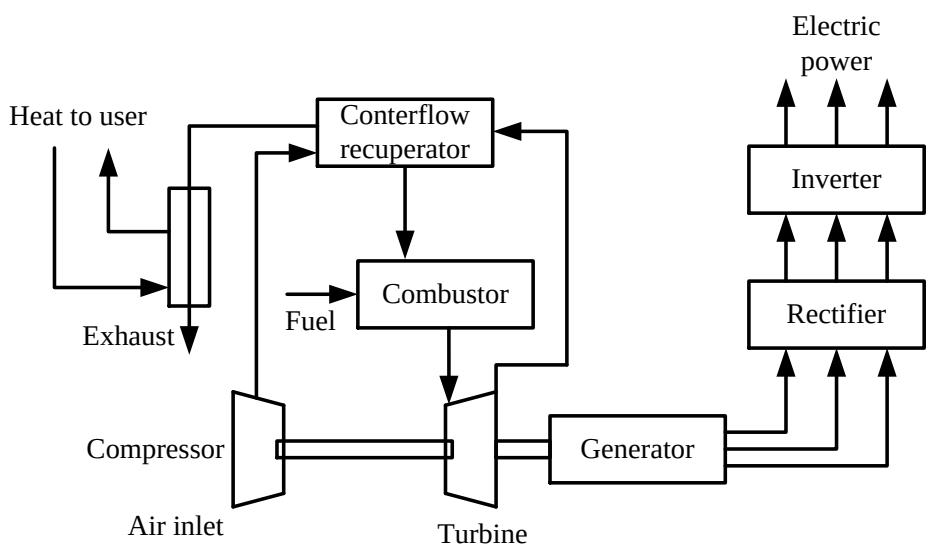

Fig. 2.4 Single-shaft microturbine [17].

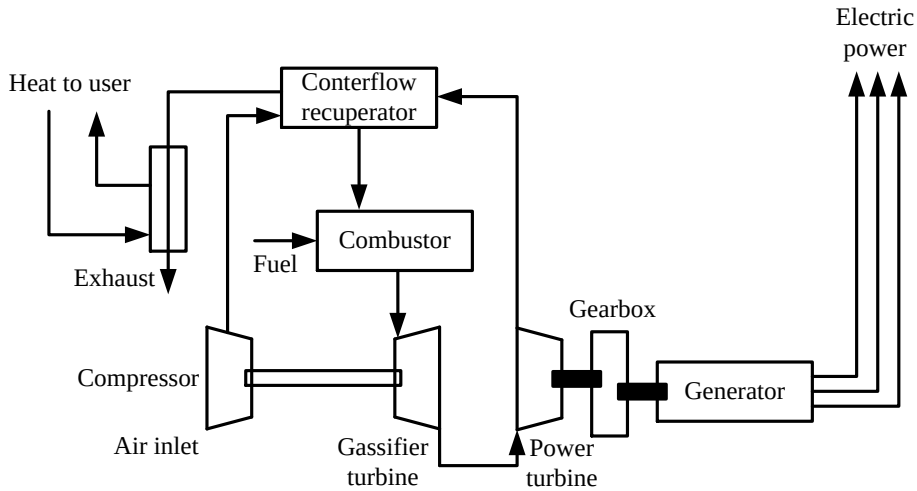

Fig. 2.5 Split-shaft microturbine [17].

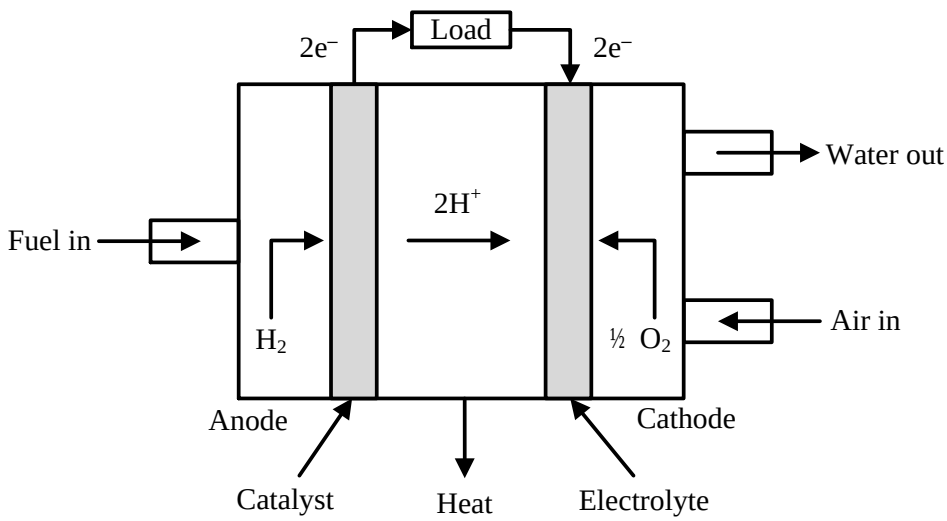

Fig. 2.6 Basic construction of a fuel cell [17].

Fuel Cells

Fuel cells convert chemical energy of fuels directly into electrical energy and consist of two electrodes (an anode and a cathode) and an electrolyte, retained in a matrix. The operation is similar to that of storage battery except that the reactants and products are not stored, but are continuously fed to the cell [17]. During operation, the hydrogen-rich fuel and oxidant are separately supplied to the

electrodes. Fuel is fed to the anode and oxidant to the cathode, and the two streams are separated by an electrode–electrolyte system. Electrochemical oxidation and reduction take place at the electrodes to produce electricity. Heat and water are produced as byproducts. Fig. 2.6 shows the basic construction of a fuel cell [17]. Fuel cells will likely play a major role in DG and microgrids in the near future [53].

Photovoltaic (PV) systems

PV systems are a rapidly emerging DG technology [1], [53]. They extract electricity power from free and inexhaustible solar energy. The major advantages of a PV system are as follows [17]:

- Sustainable nature of solar energy as fuel
- Minimum environmental impact
- Drastic reduction in customers' electricity bills due to free availability of sunlight
- Long functional lifetime of over 30 years with minimum maintenance
- Silent operation

Though PV systems can be effectively used as DG in a microgrid, yet they suffer from the disadvantages of high installation cost and low energy efficiency. The electrical conversion efficiency of PV is between about 5 and 20 %, depending on the type PV panel technology employed [53]. As the voltage and the current output of a single cell are very small, a large number of cells are arranged in series–parallel combination to produce PV arrays or modules of higher voltage and power rating. There are mainly four different types of PV cells as follows [17]:

- Monocrystalline silicon
- Multicrystalline silicon
- Thin-film silicon
- Hybrid

A comparison between each technology in UK is shown in Table 2.1 [17].

Table 2.1 Comparison of PV technologies [17].

PV technology	Monocrystalline	Multicrystalline	Thin-film	Hybrid
Cell efficiency at Standard Test Conditions (STC) (%)	16–17	14–15	8–12	18–19
Module efficiency (%)	13–15	12–14	5–7	16–17
Area needed per kW (for modules) (m^2)	7	8	16–17	6–6.5
Annual CO_2 savings per kW (kg/kW)	471	460	454	491
Annual CO_2 savings per m^2 (kg/m^2)	61	57	28	79–85

Wind turbines (WTs)

Depending on controllability of a generator rotor speed, WTs can be categorized as fixed-speed WTs and variable-speed WTs and depending on controllability of rotor blade angle, they can be categorized as stall control, pitch control, and active stall control WTs.

Typical configurations for WTs categorized in four types in the perspective of speed control are shown in Fig. 2.7 [54]. Type A, a fixed-speed type WT, employs a squirrel cage induction generator (SCIG) directly connected to the grid via a transformer. It only generates power at a specific rotational speed. To protect over current flowing into the grid, a soft-starter is interconnected between a generator and the grid. Since the SCIG always draws reactive power from the grid, a capacitor bank is used for reactive power compensation. Type B is a variable-speed WT and employs a wound rotor induction generator (WRIG). A variable resistance is interconnected to a rotor of the generator in order to adjust the rotor resistance thereby to control the slip. Type C and D are also variable-speed WTs. Type C, also known as a doubly-fed induction generator (DFIG), uses a partial-scale frequency converter rated at approximately 30 % of nominal generator power [54]. Type D uses a full-scale frequency converter. A wound rotor synchronous generator

(WRSG) also can be applied to this type and a gearbox is not always necessary.

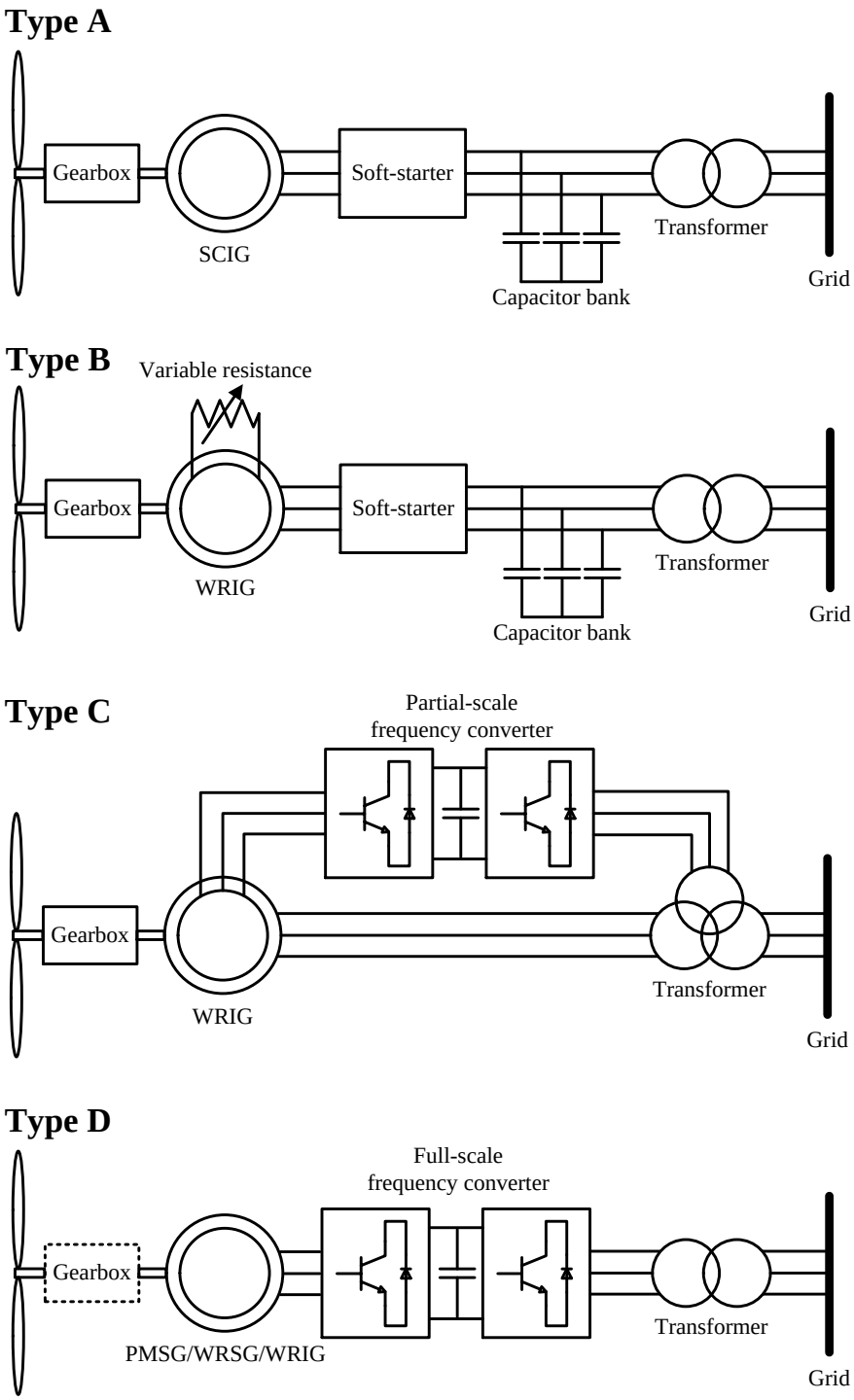

Fig. 2.7 Typical WT configurations [54].

Table 2.2 WT categorization depending on control methods [54].

Speed control	Power control		
	Stall	Pitch	Active stall
Fixed-speed		Type A	
Variable-speed	Not in use	Type B	Not in use
	Not in use	Type C	Not in use
	Not in use	Type D	Not in use

Types of WTs can be summarized as listed in Table 2.2. Pitch, stall and active stall control method uses aerodynamics to control or limit output power of WTs. The details of these control methods can be found in [55]. Nowadays, stall and active stall control are only applied to fixed-speed type with power ratings of under hundreds of kW.

Energy storage systems (ESSs)

Since there are various forms of energies (e.g., chemical, electrical, mechanical, thermal) that can be stored, numerous types of ESSs have been developed. The major technologies for these types are ultra-capacitors, flywheels, compressed air systems (CASs), super magnetic energy storages (SMESs), and batteries. Among them, only a few can be met requirements for use in the distributed power system [53]. These energy storage technologies are lithium-ion batteries and lead-acid batteries [53]. These BESSs have been used for various purposes of microgrid operational improvement [19], [22], [23].

In this dissertation, details of each DG characteristics are not modeled since only management of active and reactive power within the grid of standalone microgrid is handled to improve system frequency and voltage stability. For instance, all types of RESs are modeled as non-dispatchable (uncontrollable) DG and the others are modeled as dispatchable (controllable) DG.

2.2.2 Types of inverter controller

Most of DG units are interfaced with an inverter. Hence up to date, extensive technical literatures have been discussed about control of electronically coupled DG units in microgrids. A general overview of grid-side converter controllers is given in [38], in which controllers are categorized based on their reference frame: synchronous (*dq*), stationary (*αβ*), and natural (*abc*). The synchronous reference frame is associated with DC variables and proportional-integral (PI)-based controllers. The stationary reference frame is associated with sinusoidal variables and proportional-resonant (PR) controllers. The natural reference frame utilizes controllers realized in the form of PI, PR, hysteresis, or dead-beat [38]. All the controllers considered in this dissertation are PI controller since it is the most common controller used in industrial application today [56].

Based on the control purpose of inverters, they can be categorized as grid-forming and grid-feeding control [12].

Grid-forming control

A grid-forming control type inverter adjusts output voltage and frequency of the inverter regardless of those of the grid. Hence it can be considered as a voltage source as shown in Fig. 2.8 [12], in the perspective of the grid where V_{ref} is a reference value of a voltage magnitude, f_{ref} is a reference value of a frequency, v_{ref} is a reference 3-phase voltage, and Z is impedance.

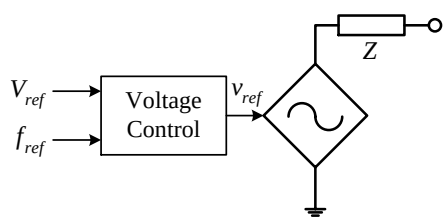

Fig. 2.8 Grid-forming control type source [12].

For stable operation of isolated power systems, such as standalone microgrids, at least one source is required that is able to regulate voltage and frequency and respond quickly to changes in load [12]. Thus, at least one grid-forming control inverter should be operated online in standalone microgrids. For grid support, frequency and voltage droop control can also be applied to the inverter controller. This form of the controller is categorized as a grid-supporting-grid-forming controller as shown in Fig. 2.9 [12] where P and Q represents output active and reactive power of the inverter, respectively.

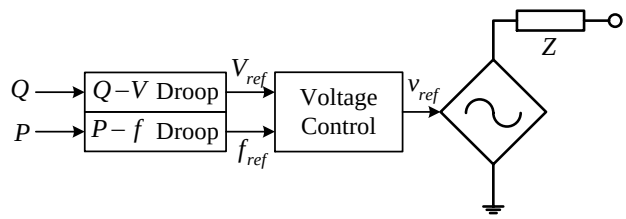

Fig. 2.9 Grid-supporting-grid-forming control type source [12].

As shown in Fig. 2.9, active power–frequency (P–f) and reactive power–voltage (Q–V) droop controls are usually employed to emulate power sharing method of conventional power systems. The principle of P–f and Q–V droop controls are depicted in Figs. 2.10 and 2.11 respectively.

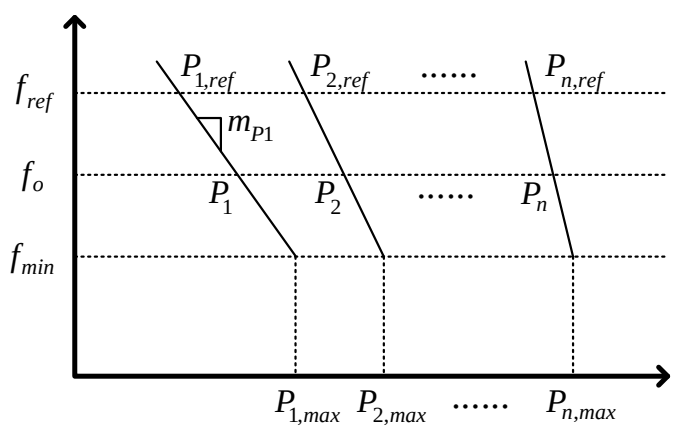

Fig. 2.10 P–f droop characteristics.

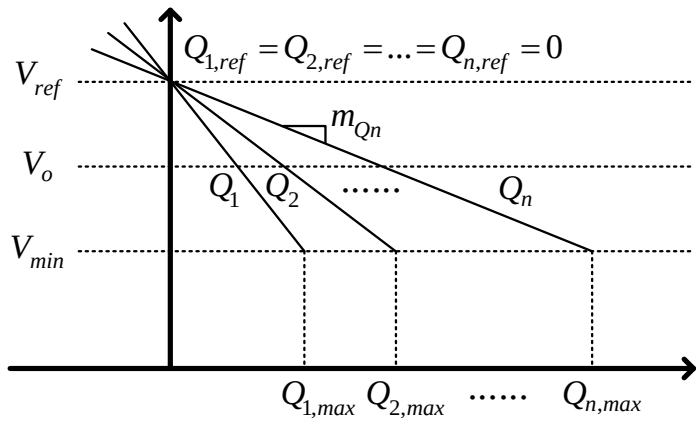

Fig. 2.11 *Q–V* droop characteristics.

By adopting *P–f* droop control to output control inverters, they share the active power and adjust output frequency as per pre-specified slope, m_P (frequency droop coefficient), of each DG unit as shown in Fig. 2.10 where f_{ref} is the reference (nominal) value of output frequency, f_o is the output frequency of each DG unit, f_{min} is the minimum output frequency of each DG unit, $P_{n,ref}$ is the reference output active power of DG unit *n*, $P_{n,max}$ is the maximum output active power limit of DG unit *n*, and P_n is the output active power. When the load demand is changed, DG units adopting this droop control change their output frequency. By sensing this frequency deviation from the nominal value, which is usually f_{ref}, secondary controllers are adjusted to restore the frequency. The relationship between active power and frequency is presented as:

$$f_o = f_{ref} - m_P(P_{ref} - P) \tag{2.1}$$

$$m_P = \frac{(f_{ref} - f_{min})}{(P_{ref} - P_{max})}. \tag{2.2}$$

Similarly, reactive power is shared and adjusted as per pre-specified slope, m_Q (voltage droop coefficient), of each DG unit as shown in Fig 2.11 where V_{ref} is the reference (nominal) value of output voltage magnitude, V_o is the output voltage magnitude of each DG unit, V_{min} is the minimum output voltage of each DG unit,

$Q_{n,ref}$ is the reference output reactive power of DG unit n, $Q_{n,max}$ is the maximum output reactive power limit of DG unit n, and Q_n is the output reactive power. As similar as frequency droop control, the voltage magnitude also can be restored by secondary control.

$$V_o = V_{ref} - m_Q(Q_{ref} - Q) \tag{2.3}$$

$$m_Q = \frac{(V_{ref} - V_{min})}{(Q_{ref} - Q_{max})}. \tag{2.4}$$

However, unlike frequency droop control, the reactive power cannot be shared equally since the voltage drop depends on the network impedance. This issue has been dealt in many technical literatures such as [57].

Grid-feeding control

A grid-feeding control type inverter controls its active and reactive power output and refers grid frequency. It acts as a current source as shown in Fig. 2.12 [12] where P_{ref} and Q_{ref} are reference values of active and reactive power output of ab inverter, respectively, and i_{ref} is reference value of 3-phase output current of an inverter.

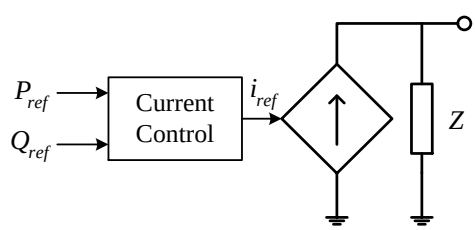

Fig. 2.12 Grid-feeding control type source [12].

This type of inverter is also referred as a current-controlled inverter and about 81 % [58] of inverters applied in industry are current-controlled inverter. The others are voltage-controlled inverters, which are grid-forming inverters. Regardless of load change in the system, a grid-feeding control type inverter

outputs their reference value. Hence, to support grid during disturbances, additional controllers are necessary as shown in Fig. 2.13 [12].

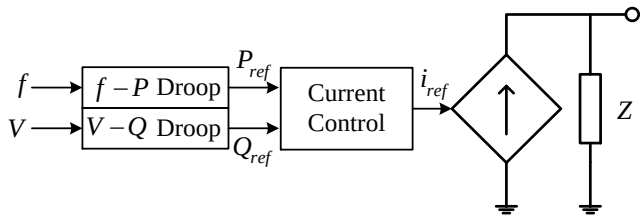

Fig. 2.13 Grid-supporting-grid-feeding control type source [12].

Though both grid-supporting controllers shown in Figs. 2.11 and 2.15 seem to act similar in a way of supporting frequency and voltage of the grid, they differ in the perspective of response to grid disturbances. Unlike *P–f* and *Q–V* droop control used in Fig. 2.9, *f–P* and *V–Q* droop are used in Fig. 2.13. The former reacts and readjusts frequency and voltage after active and reactive power demand (or generations) is changed while the latter reacts and readjusts active and reactive power output after the grid frequency and voltage are changed. Either way, its major disadvantage is its load-dependent frequency and amplitude deviations [70].

2.3 Technical issues on a standalone microgrid

Typically, power systems cover geographically extensive area so a fully centralized control is unable to be implemented due to the necessity of vast amount of computation and extensive communication infrastructure. Likewise, a fully decentralized control is also infeasible to be implemented since a variety of factors that cannot be acquired by using LCs only are strongly coupled with each other units. Therefore, a compromise between fully centralized and fully decentralized control schemes can be achieved by means of a hierarchical control scheme consisting of three control levels: primary, secondary, and tertiary [19]. These control levels differ in the followings [19]:

- Speed of response and the time frame in which they operate
- Infrastructure requirements (e.g., communication requirements)

In the secondary and tertiary control level of microgrids, predictions for the load demand and the output power of RESs are implemented and are used for scheduling. However, no matter how accurate the predictions are, forecasting errors are inevitable. Moreover, the errors become larger for smaller time-scale where the primary control level is responsible for. Hence, to alleviate disadvantages due to sudden power mismatches such as output power fluctuation of RESs and load changes, this dissertation focuses on the primary control level of DGs. Islanding detection, energy source's output control, and power sharing/balance control are categorized in this control [32]–[34]. Among these, output control and power sharing/balance control are the most major objectives of the primary control. These are closely related to frequency and voltage control which should be kept stable under different load conditions and during load variations [19], [69]. If not, the system may be collapsed just as Ulleungdo case that the 600-kW wind turbine makes the diesel generator trip out of the system [66].

Commonly, two types of generation units are directly adjusted by primary control. One of them is a synchronous generator, which is the most widely used

unit to supply power demand. A synchronous generator implements output control and power sharing by using a voltage regulator, a governor, an excitation system, and inertia of a generator rotor. Control method of a synchronous generator has been developed for a long period and can be found in a numerous literatures so it is substituted by referring [35] in this dissertation.

The other is an inverter which can be categorized as two types with regard to its sources – whether it is voltage or current. Voltage-sourced inverter (VSI) is more widely used in industry than current-sourced inverter (CSI) since it is more efficient for low or medium power applications [36]. CSI is more efficient for high power application above 20 MW (e.g., HVDC). Hence, only VSI will be discussed in this dissertation. VSI controllers are composed of output controller and power sharing controller. Power sharing controllers are responsible for the adequate share of active and reactive power mismatches in the microgrid, whereas inverter output controllers should control and regulate the output voltages and currents [32], [33], [37]–[39]. Output controllers typically consist of inner current control loop and outer voltage control loop and power sharing controller typically consist of *P–f* and *Q–V* droop controllers that emulate the droop characteristics of synchronous generators [40].

Conventional frequency control strategies of standalone microgrids can be categorized as a synchronous generator-based operation and an inverter-based operation in a viewpoint of a generation system that forms the grid frequency. The former acts as same as typical power systems and the latter emulate the former by using *P–f* droop control. The details of each control strategy are depicted in the next sections.

2.3.1 Synchronous generator-based standalone microgrid

In conventional isolated power systems, as same as typical power systems, the system frequency is formed by synchronous generators as shown in Fig. 2.14.

Hence, the system frequency is directly related to the rotational speed of the generator rotor. With this mechanism, relationship between the electromagnetic torque and the angular velocity of the rotor is as follows [35]:

$$J\frac{d\omega_m}{dt} = T_m - T_e \tag{2.5}$$

where J is combined moment of inertia of generator and turbine, ω_m is the angular velocity of the rotor, T_m is the mechanical torque, and T_e is the electromagnetic torque. From (2.5), it can be noticed that, if the load (T_e) is changed, the system frequency (ω_m) will be changed inversely proportional to the system inertia (J). Thus, the system frequency of isolated power systems such as standalone microgrids which have small system inertia is vulnerable to the load change.

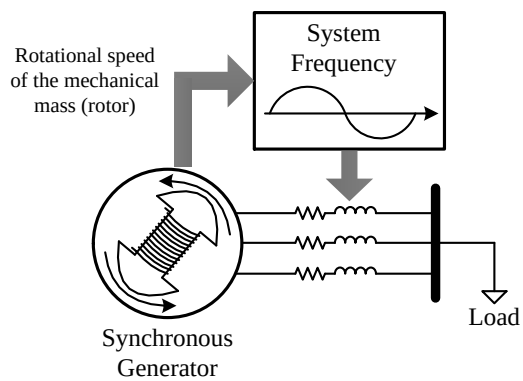

Fig. 2.14 System frequency formed by a synchronous generator [23].

After frequency deviations due to change of load and/or output of non-dispatchable generation systems, the system frequency has to be restored to the nominal value as per the grid code requirements. The frequency restoration is conducted via secondary control, which is referred to as automatic generation control (AGC) or load–frequency control (LFC) [35]. LFC units increase or decrease their output power based on degrees of deviations of frequency from its nominal value (typically 50 or 60 Hz). This is accomplished by adding PI control to an active power controller of LFC unit as shown in Fig. 2.15 where P_{ref} and Q_{ref} are

the reference values of active and reactive power, respectively, P and Q are the active and reactive power output, respectively, f_{nom} is the nominal value of the system frequency, f is the current system frequency, and PI represents the PI controller. The integral control action ensures zero frequency error in the steady state.

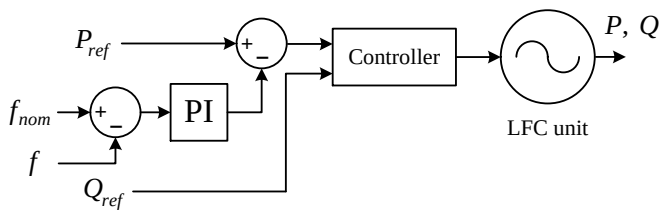

Fig. 2.15 LFC unit control scheme.

If there is a single LFC unit is the system, it has full responsibility to restore the frequency deviations whereas if there are two or more LFC units, they share the active power to be increased or decreased proportional to their controllers' gain.

2.3.2 Inverter-based standalone microgrid

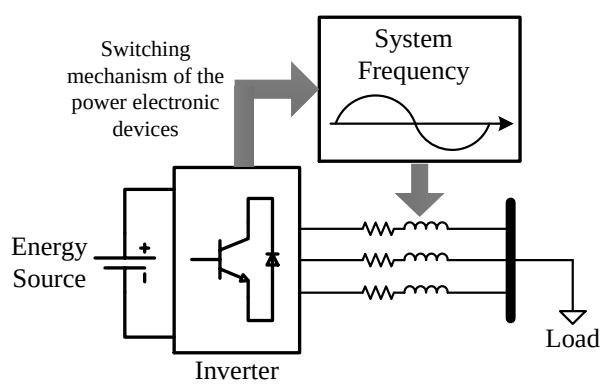

Fig. 2.16 System frequency formed by an inverter [23].

As power electronics technologies have been gradually developed, inverter-interfaced DGs have been increasingly interconnected to microgrids. Subsequently,

many technical literatures [39], [45], [51], [57], [59] have been discussed about microgrids without any synchronous generator. Unlike synchronous generators, since inverters can change its output voltage angle instantaneously [13], the system frequency can be tightly held on at the desired value. Whereas output frequency of a synchronous generator depends on mechanical inertia of its rotor, output frequency of an inverter can be quickly adjusted electrically as shown in Fig. 2.16 where the energy source can be assumed as wind speed, solar irradiance, fuel cell, microturbines, and etc.

Since inverters have no mechanical inertia and able to maintain output frequency at desired level, frequency deviations would not be happened after load change if output frequency is constantly controlled. If there are no frequency deviations, conventional power systems cannot perceive generation mismatches. Hence, to mimic conventional power systems, *P–f* droop control is employed and thereby inverters compulsorily make frequency deviations if generation mismatches occurred in microgrids. By doing so, the system can perceive generation mismatches based on frequency deviations and the frequency restoration is implemented by secondary control.

2.3.3 Relationships between line parameters and voltage control

There have been numerous devices and control methods for voltage control. Whether devices are used or specific control methods are applied, each manner has pros and cons for its use.

The voltage magnitude at every bus in the system has significant relations with the network impedances. This relationship can be explained with network equations of simple power system shown in Fig. 2.17 where P and Q are active and reactive power, respectively, flow through network impedance, R and X are the resistance and reactance of the network impedance, respectively, V_s and V_r are the voltage magnitudes of sending and receiving end, respectively, and δ is the sending

end voltage angle.

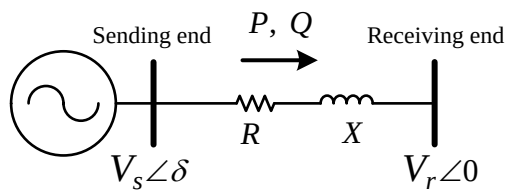

Fig. 2.17 Simplified power system network.

From Fig. 2.17, the current which flows through the network impedance is expressed as:

$$I = \frac{RV_s\cos\delta + XV_s\sin\delta - RV_r}{R^2 + X^2} + j\frac{RV_s\sin\delta - XV_s\cos\delta + XV_r}{R^2 + X^2}. \quad (2.6)$$

The active and reactive power is real and imaginary part of complex power, respectively. The complex power *S* sent to the receiving end can be calculated as:

$$S = V_r I^*. \quad (2.7)$$

Then, the active and reactive power can be presented as (2.8) and (2.9), respectively, as shown below:

$$P = \mathrm{Re}\{S\} = \frac{RV_rV_s\cos\delta + XV_rV_s\sin\delta - RV_r^2}{R^2 + X^2} \quad (2.8)$$

$$Q = \mathrm{Im}\{S\} = \frac{-RV_rV_s\sin\delta + XV_rV_s\cos\delta - XV_r^2}{R^2 + X^2}. \quad (2.9)$$

In medium or high voltage networks, the resistance is assumed to be much smaller than the reactance ($R \ll X$) and the voltage angle difference is assumed to be very small ($\delta \approx 0$, then $\sin\delta \approx \delta$ and $\cos\delta \approx 1$). Thereby, the active and reactive power can be simplified as:

$$P \approx \frac{V_rV_s\delta}{X} \quad (2.10)$$

$$Q \approx \frac{V_rV_s - V_r^2}{X}. \quad (2.11)$$

From (2.10) and (2.11), it can be noticed that the active and reactive power are

correlated with voltage angle and voltage magnitude, respectively. This relationship is not valid to low voltage networks which will be discussed in the later section. From (2.11), the voltage magnitude of the receiving end can be rearranged as:

$$V_r^2 - V_s V_r + XQ = 0. \tag{2.12}$$

By using the quadratic formula, the voltage magnitude of the receiving end can be solved as:

$$V_r = \frac{V_s \pm \sqrt{V_s^2 - 4XQ}}{2}. \tag{2.13}$$

Hence, it can be concluded that the receiving end voltage magnitude can be controlled by reactive power flow and/or voltage magnitude of the sending end and/or by reactance impedance of the network. Most of the conventional voltage control methods have been conducted based on this rule. However, this rule cannot be applied to every power systems especially with low voltage networks which will be discussed in the later section.

In the next sections, conventional voltage control devices and strategies are briefly discussed before the proposed control methods are presented.

2.3.4 Voltage control devices and methods

Excitation systems

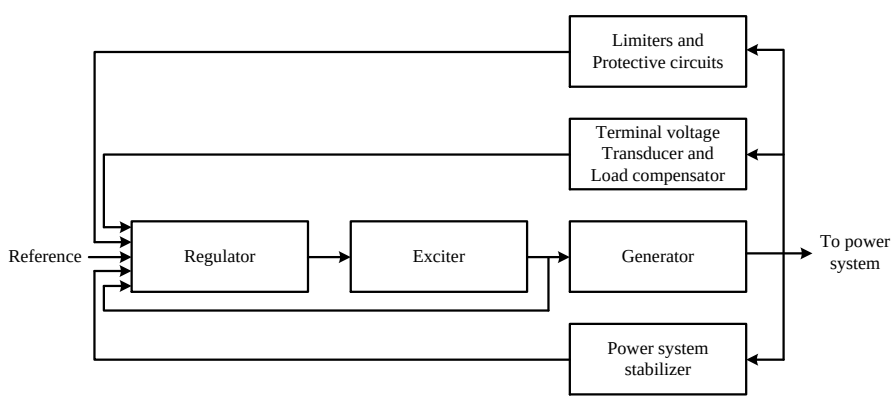

Fig. 2.18 Functional block diagram of a synchronous generator excitation system [35].

Excitation systems are fundamental functions to adjust terminal voltage of synchronous generators. The basic function of the excitation system is to provide DC current to field winding of the synchronous generator. With this action, the excitation system is able to control reactive power by controlling the field current and thereby the field voltage. A typical excitation control system for a large synchronous generator is shown in Fig. 2.18 [35].

The followings are the brief explanations about the subsystems shown in Fig. 2.18 [35].

- Exciter: Provides DC power to the synchronous machine field winding.
- Regulator: Processes and amplifies input control signals to an appropriate level for control of the exciter.
- Terminal voltage transducer and load compensator: Senses generator terminal voltage, rectifies and filters it to DC quantity, and compares it with a reference value.
- Power system stabilizer: Provides an additional input signal to the regulator to damp power system oscillations.
- Limiters and protective circuits: Include a wide array of control and protective functions which ensure that the capability limits of the exciter and synchronous generator are not exceeded.

Together with the governor system, the excitation system plays a significant role in controlling the synchronous generator. Both governor and excitation system adjust frequency and voltage, respectively, and thereby make the synchronous generator able to act as a grid-forming source shown in Fig. 2.8.

Further discussions about the excitation systems are beyond the topics of this dissertation. Hence, more details of the excitation systems are substituted by introducing [35].

Shunt reactors and shunt capacitors

Shunt reactors are used to compensate for the effects of line capacitance,

particularly to limit voltage rise on open circuit or light load. Since the shunt reactor makes the reactance inductive, it can be noticed in (2.13) that the receiving end voltage magnitude will be decreased if the magnitude of the reactance increases. Shunt reactors are usually required for extra high voltage overhead lines longer than 200 km [35] or for a weak system. For strong system, they may not be needed to be connected to the line permanently. In such cases, the reactors may be switchable for flexible uses.

On the contrary to shunt reactors, shunt capacitors supply reactive power and boost local voltages. The principle of these actions can be explained with (2.13) as like those of shunt reactors did. Shunt capacitors are used throughout the system and are applied in a wide range of sizes but there is the principal disadvantage that their reactive power output is proportional to the square of the voltage. Consequently, the reactive power output is reduced at low voltages when it is likely to be needed most [35].

Synchronous condensers

A synchronous condenser is a synchronous machine running without a prime mover or a mechanical load. Let us assume that Fig. 2.17 is an equivalent circuit of a synchronous machine. Then, the sending end voltage is the internal voltage of the machine, the receiving end is the terminal voltage of the machine, R and X are the armature resistance and leakage reactance, respectively, and δ is the power angle. From (2.10) and (2.11), it can be noticed that the active power can be controlled to zero with zero power angle and the reactive power can be controlled as desired by controlling field excitation.

Other devices for voltage control (or reactive compensation)

There are many other control devices for voltage control or reactive compensation. Static VAR compensators are one of them which are shunt-connected static generators and/or absorbers whose outputs are varied so as to

control specific parameters of the electric power system [35]. Under-load tap changers (ULTCs) are one of other types for voltage control devices which can change tap position during online. They are transformers controlling voltage of secondary winding side by changing the tap position and thereby changing turn ratio of winding. Many others for voltage control can be found in numerous literatures.

Voltage control methods

The most well-known and widely used voltage control (or supporting) method is voltage droop control (Q–V droop for grid-forming source and V–Q droop control for grid-feeding source), which was already explained in Chapter 2.2.2 with Fig. 2.11. This control method is categorized as primary control and implemented by excitation systems of synchronous generators, inverter controllers, and etc. Devices such as shunt reactors and capacitors are controlled mostly for secondary control such as scheduling. The goal of voltage droop control is to maintain the local voltage within the allowable range by controlling reactive power output of device based on the voltage deviation from the nominal value or sometimes to share reactive power. Unfortunately, voltage droop control methods have also been applied to standalone microgrids which have weak system characteristics. However, voltage droop control methods are only effective to medium or high voltage networks where the assumption that the network resistance is much smaller than the reactance is valid. Moreover, the droop control based on voltage deviation cannot fundamentally prevent voltage fluctuation, which may threaten voltage stability, since it is triggered only if the voltage deviation is occurred. To develop suitable voltage control methods for standalone microgrids, in the next section, novel voltage control methods that effectively prevent voltage fluctuation in medium voltage networks as well as in low voltage networks are discussed.

So far, fundamental control theories about microgrids and components have been discussed. On the basis of these technical issues, the details of the proposed

methods will be illustrated in Chapters 3 and 4.

Chapter 3. SOC-Based Active Power Control Methods of DGs

Frequency stability is one of the major issues of power system stability and understood as the ability to regain an equilibrium state after being subjected to a disturbance. In a power system network, considerable drop in frequency could result in high magnetizing currents in induction motors and transformers [35]. Additionally, the extensive use of electric clocks and the use of frequency for other timing purposes require accurate maintenance of synchronous time which is proportional to integral of frequency [35]. Consequently, the system frequency is strictly regulated by grid code requirements and thereby the frequency should remain nearly constant for satisfactory operation of a power system. Particularly, standalone microgrids have low inertia, which may cause severe frequency deviation. To enhance frequency stability, a novel control strategy of DG units in a standalone microgrid is discussed in this chapter.

3.1 Control methods for synchronous generator-based standalone microgrid

Since standalone microgrids have small system inertia, their frequency stability is vulnerable to change of load and/or output power of non-dispatchable DGs, such as intermittent RESs (e.g., WTs, PV systems). Thus, to cope with increasing hosting capacity of intermittent RESs in standalone microgrids, enhancing frequency stability is necessary. To this end, a BESS is employed to form grid frequency in this dissertation. The BESS is an inverter-interfaced ESS and hence it can instantaneously adjust its output voltage angle as mentioned previously. To prevent frequency deviations due to generation mismatches, frequency droop control is not used in the proposed method of the BESS control.

Instead, the BESS operates in order to output constant voltage and frequency as shown in Fig. 3.1 where V_{nom} is the nominal value of voltage magnitude, f_{nom} is the nominal value of frequency, and $v_{iabc,ref}$ is the reference value of 3-phase output voltage. Since the BESS is expected to be act as grid-forming DG, the output voltage is controlled. The reference of 3-phase output voltage is sent to sine-pulse width modulation (S-PWM) controller to generate gate pulses, which controls the inverter.

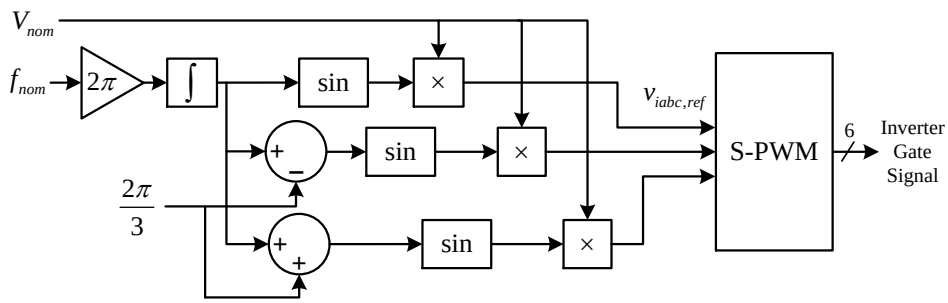

Fig. 3.1 Basic control scheme of BESS for constant frequency and voltage [23].

The BESS, instead of other inverter-interfaced DGs, is chosen to fulfill the proposed strategy since it has a chargeable characteristic unlike any other inverter-interfaced generation systems. This enables the BESS to take over twice amount of load change than the others with same power rating. For instance, a 1-kW BESS is capable of taking over a 2-kW load change (from –1 to 1 kW) while the others of same power rating are capable of taking over 1-kW load change only.

Typically, BESSs employ grid-feeding type control in order to control output active and reactive power since they are expected to manage their SOC value at desired level. However, by using the BESS controller shown in Fig. 3.1, which is grid-forming type controller, the SOC cannot be adjusted by controlling the BESS itself. The BESS only outputs constant frequency and voltage and thereby its output active and reactive power varies as per generation mismatches in the system. Thus, the SOC should be regulated by other controllable DGs in order to maintain

the SOC at the desired level and thereby to operate the BESS online. Note that the BESS is the only grid-forming type generation system in the proposed method and that at least one grid-forming type generation system should be online for stable operation of standalone microgrids.

The method of maintaining the SOC at the certain level and enhancing frequency stability is illustrated in the next consecutive two sections. Each section represents different environmental situation of standalone microgrids.

3.1.1 Control method for constant frequency and SOC

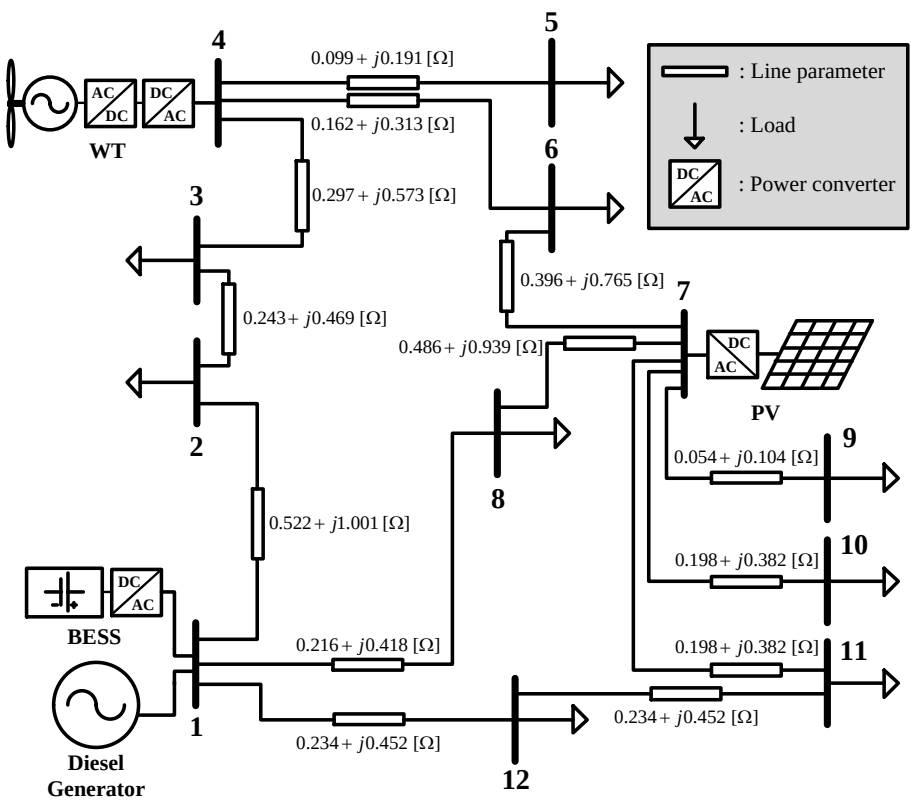

Fig. 3.2 Synchronous generator-based standalone microgrid configuration [23].

As mentioned previously, the frequency of standalone microgrids is formed either by synchronous generators or inverter-interfaced DG units. In this section, a standalone microgrid with the grid frequency forming by a synchronous generator

is investigated. Among various types of energy sources supplying synchronous generators, diesel engines are most widely used for isolated power systems [6], [9]. Hence, a synchronous generator used in this study is modeled as a diesel generator. WTs and PV arrays are also used to represent characteristics or RES units.

Table 3.1 System load demand [23].

Bus Number	Day [MW]	Night [MW]
2	3	1.5
3	2	1
5	1	0.5
6	1	0.5
8	2	1
9	0.2	0.1
10	0.2	0.1
11	0.1	0.05
12	0.5	0.25
Total	10	5

Fig. 3.2 and Table 3.1 show the configuration of studied synchronous generator-based standalone microgrid, which is the power system of Ulleung Island, and the system load demand, respectively [23]. Bus numbers, line parameters, loads, and power generation systems that will replace the conventional versions are shown in Fig. 3.2. The line parameters were calculated by considering the distance between loads and the locations of loads were obtained from Korean Electric Power Corporation (KEPCO). The line impedance is considered as a type of ACSR 160-mm^2, 6.6-kW cable. The power rating of the diesel generator (employing synchronous generator), BESS, WT, and PV power are 14, 15, 9.7, and 1 MW, respectively. The nominal system frequency and voltage are 60 Hz and 6.6 kV, respectively, and the load demands during the day and night are shown in Table 3.1 which is based on the real data of the power system of Ulleung Island referred to in [11].

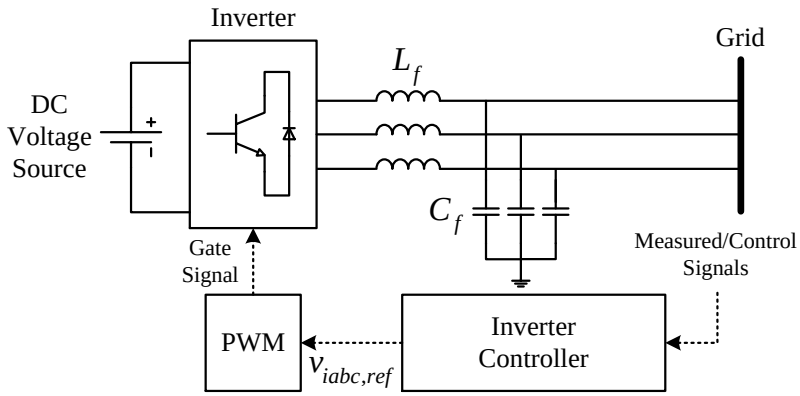

Fig. 3.3 Inverter-interfaced generation system [23].

The generation systems were modeled in MATLAB. Since the proposed control strategies focus mainly on the grid-side inverters, the DC-link and prime mover parts of the BESS, the PV array, and WT are simplified as ideal DC voltage sources as shown in Fig. 3.3 where $v_{iabc,ref}$ is the reference value of 3-phase output voltage of the inverter and L_f and C_f are the output filter inductance and capacitance, respectively. The inverters were modeled as two-level type and S-PWM with switching frequency of 1.8 kHz was adopted to generate the gate signals of the inverter. The inverter controller provides the reference of 3-phase voltage at the inverter terminal by using the control input and measured data signals. For the BESS, the controller shown in Fig. 3.1 is adopted.

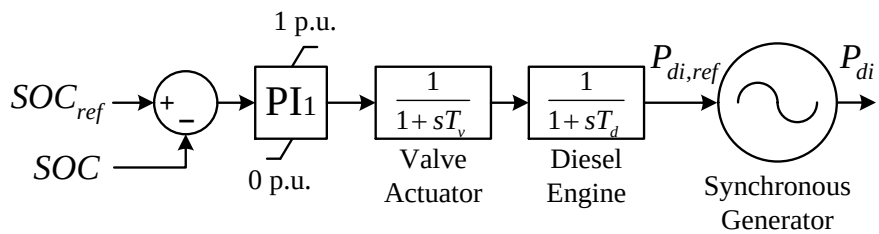

Fig. 3.4 Control scheme of diesel generator for adjusting SOC.

As mentioned previously, the SOC cannot be adjusted by the BESS itself to maintain at the desired level by using the controller shown in Fig. 3.1. To overcome

this problem, the only controllable (or dispatchable) generation system in the standalone microgrid, which is the diesel generator, is controlled by the control scheme shown in Fig. 3.4 where SOC_{ref} is the reference or desired value of the SOC, PI_1 represents the PI controller (where subscript 1 is the index number of the PI controller), T_v and T_d are the time constants of the valve actuator and diesel engine, respectively, $P_{di,ref}$ is the reference value of output active power of the diesel generator, and P_{di} is the output active power of the diesel generator. The time constants T_v and T_d are set to 0.05 and 0.5, respectively, as in [26]. The parameters of the PI controller and the synchronous generator are shown in Appendix A. Since the diesel generator is connected to the same bus with the BESS, the SOC level is assumed to be measured directly by the diesel generator controller without any communication. An error signal between SOC_{ref} and SOC goes into the PI controller (PI_1), which enables to make zero SOC error. The output comes from the PI controller (PI_1) goes through the valve actuator and the diesel engine, which are substituted by the time constants, and provides the reference output active power to the synchronous generator. With this control, the diesel generator acts as load–SOC control, which is a similar concept as load–frequency control of the conventional power systems. Load–SOC control makes zero SOC error while load–frequency control makes zero frequency error. The control of the reactive power is not largely related to the frequency control hence it will be discussed in Chapter 4. The excitation system applied to the diesel generator is described in Appendix A.

The energy source of the WT is a wind speed. The power that can be extracted from the wind is given as [54]:

$$P_{wind} = \frac{1}{2}\rho\pi r^2 C_p v_w^3 \tag{3.1}$$

where ρ is the air density, r is the radius of the rotor blade, C_p is the power coefficient, and v_w is the wind speed. If we assume that the WT is operated with MPPT method, C_p can be regarded as a constant value. Then the reference value of WT active output power can be simply represented as a function of v_w as follow:

$$P_{WT,ref} = K_{WT} v_w^3 \tag{3.2}$$

where K_{WT} is a constant value.

The energy source of PV power system is a solar irradiance. By neglecting the diode saturation current of PV module, the output current I_A of a PV array with N_P modules in parallel may be represented as [60]:

$$I_A = N_P I_{SC} \tag{3.3}$$

where I_{SC} is the short circuit current of a solar module. It can be represented as [60]:

$$I_{SC} = I_{SC,ref}\left[\left(\frac{S}{1000}\right) + \frac{J}{100}\left(T - T_{ref}\right)\right] \tag{3.4}$$

where $I_{SC,ref}$ is a short circuit current at reference irradiance and cell temperature, S is the irradiance, J is a temperature coefficient at short circuit current, T is a cell temperature, and T_{ref} is a reference cell temperature. If we assume the cell temperature to be a reference value and neglecting its change, (3.3) can be expressed as:

$$I_A = N_P I_{SC,ref} \frac{S}{1000}. \tag{3.5}$$

With (3.5), the power that can be extracted from solar irradiance can be given as

$$P_{pv} = V_A I_A = V_A N_P I_{SC,ref} \frac{S}{1000} \tag{3.6}$$

where V_A is the PV array terminal voltage. Since all of the right-hand side terms of (3.6) except S are constant values, the reference value of output active power of PV system can be simplified as a function of S as follow:

$$P_{PV,ref} = K_{PV} S \tag{3.7}$$

where K_{PV} is a constant value.

By using (3.2) and (3.7), the active power of WT and PV system can be adjusted with the wind speed and the solar irradiance, respectively. The controller for both the WT and the PV system is shown in Fig. 3.5 where i_{id} and i_{iq} are the *d*- and *q*-component of inverter output current, respectively, v_{id} and v_{iq} are the *d*- and

q-component of inverter output voltage, v_{sd} and v_{sq} are the d- and q-component of the filter (see Fig. 3.3) terminal voltage, respectively, ω_s is the angular frequency of the filter terminal voltage, θ_s is the angle of the filter terminal voltage or the reference angle of dq-axis, and the subscript *ref* denotes the reference value. The parameters of the PI controllers are shown in Appendix A and they are determined by the method used in [72].

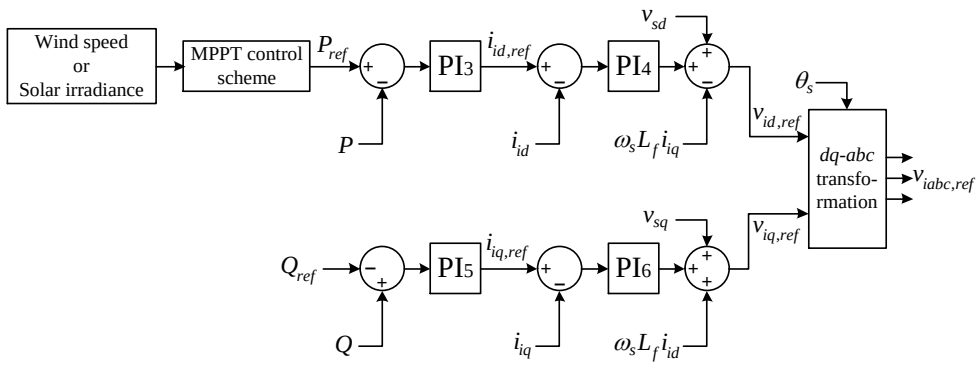

Fig. 3.5 Control scheme for both WT and PV system using simplified MPPT method.

3.1.2 Simulation test of the proposed method for synchronous generator-based standalone microgrid

To verify the effectiveness of the proposed method, the system shown in Fig. 3.2 was modeled and implemented by using MATLAB/SimPowerSystems. The conventional and the proposed methods are compared to each other for the case of sudden load change. The test settings are shown in Table 3.2.

As shown in Table 3.2, two control methods were tested and compared with each other. In the conventional method, the diesel generator with isochronous governor and the BESS with controlling constant power without droop control are applied whereas in the proposed method, the control scheme shown in Figs. 3.1 and 3.4 are applied to the BESS and the diesel generator, respectively. To investigate

frequency deviation with respect to the load change only, WT and PV system are considered to output constant power. Day time load data shown in Table 3.1 is used and the load demand of bus 8 is steeply changed about –0.5 MW at 30 s of simulation time. Since the simulation time scale is roughly tens of seconds, the capacity of the BESS is scaled down to 1/20 of its practical value, 30 MWh, in the simulation to illustrate the change of the SOC clearly.

Table 3.2 Simulation settings for the case of load change.

Settings		
	Conventional method	Proposed method
BESS	Constant power without droop	Constant frequency and constant voltage (Fig. 3.1)
Diesel generator	Isochronous governor	Load–SOC control (Fig. 3.4)
WT and PV system	Assumed to output constant power	
Total load demand	Day time load data shown in Table 3.1 is used	
Load change	Load demand of bus 8 is changed about –0.5 MW at 30 s of simulation time	

Figs. 3.6–3.8 show the simulation results of the active power, the SOC, and the frequency, respectively, for the case of employing the conventional method. As shown in Fig. 3.6, the diesel generator take cover the entire power mismatch occurred by load change at bus 8 and the BESS keeps its output power constantly. Though the BESS outputs zero active power, there are some power losses such as inverter switching loss, filter loss, and etc. Hence, the SOC is slightly decreased as time goes on as shown in Fig. 3.7. By employing the conventional method, the frequency is increased, as can be expected from (2.5), as shown in Fig. 3.8.

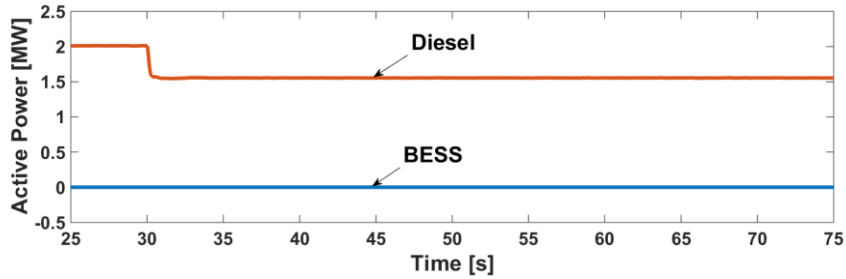

Fig. 3.6 Active power of the BESS and the diesel generator for the conventional method.

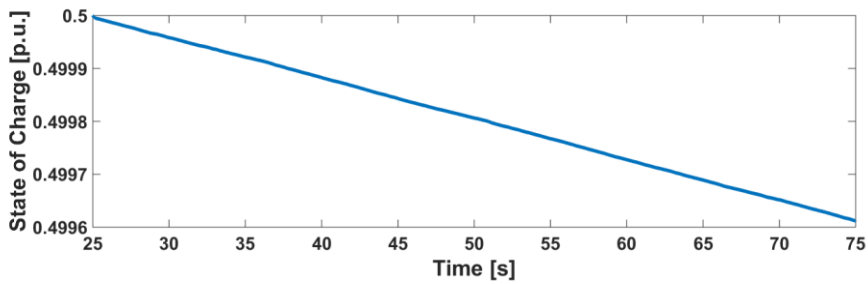

Fig. 3.7 SOC of the BESS for the conventional method.

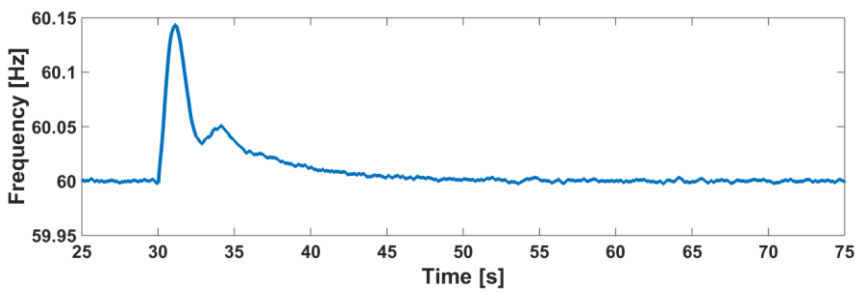

Fig. 3.8 Frequency for the conventional method.

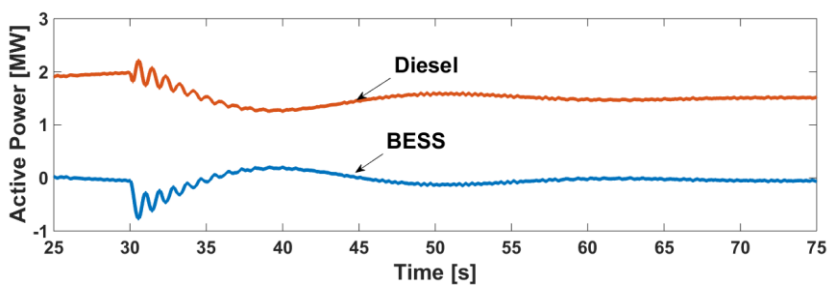

Fig. 3.9 Active power of the BESS and the diesel generator for the proposed method.

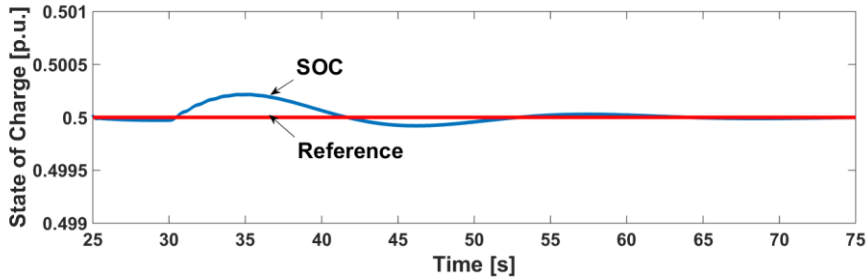

Fig. 3.10 SOC of the BESS and its reference value for the proposed method.

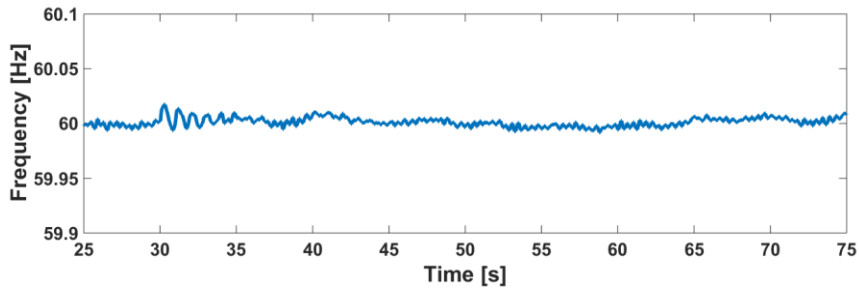

Fig. 3.11 Frequency for the proposed method.

Figs. 3.9, 10, and 11 show the simulation results of the active power, the SOC, and the frequency, respectively, for the case of employing the proposed method. As shown in Fig. 3.9, both the BESS and the diesel generator react after the load change. The BESS reacts to the load change since it has full responsibility of maintaining the frequency at the nominal value whereas the diesel generator reacts to the SOC change for implementing the load–SOC control scheme shown in Fig. 3.4. As a result, the SOC is able to be restored to the reference (desired) value after load change (at 30 s) as shown in Fig. 3.10. Moreover, the frequency is also able to be held to the nominal value rigorously as shown in Fig. 3.11 because the angle of the output voltage of the BESS can be adjusted instantaneously even though the load changed suddenly.

By comparing both control methods, it can be noticed that the proposed method is able to maintain the frequency as well as the SOC at the desired level. Consequently, it can be concluded that the proposed method is able to enhance the

frequency stability effectively. However, the diesel generator has its own efficiency characteristics versus the output power as shown in the next section. By the efficiency curve, it is effective for the diesel to output as much as rating power in the perspective of efficiency of fuel consumption. The details about the efficiency of the diesel generator are discussed in the next section. It is recommended to use other DGs such as fuel cells instead of diesel generators (since the diesel generator has efficiency problems) though the diesel generator is employed in this case in order to consider practical case of power system (the power system of Ulleung Island). More case studies for proving effectiveness of the proposed method will be discussed in Chapter 5.

Note that in this standalone microgrid configuration, there is only one controllable generation system, which is the diesel generator. Hence, specific method for active power control to maintain the SOC at the desired level is necessary for standalone microgrids with multiple controllable DG units, which is discussed in the next section.

3.1.3 Control strategy considering fuel efficiency

In the previous section, the frequency control strategy for synchronous generator-based standalone microgrid is proposed without considering the fuel consumption efficiency of the diesel generator since this dissertation focuses on maintaining the frequency and the SOC at the certain level. Since the control strategy may become more complicated by considering the fuel consumption, employing other controllable DGs (such as fuel cells) rather than diesel generators is recommended. However, a simple operational method considering fuel consumption of the diesel generator by using the proposed frequency control strategy is discussed in this section.

Efficiency of generic diesel generators

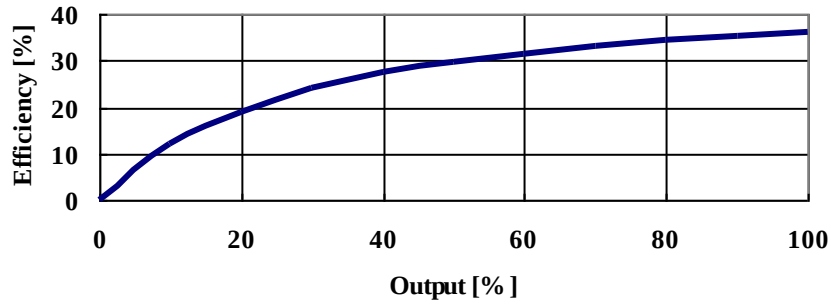

Fig. 3.12 Efficiency curve of diesel generator [61].

Fig. 3.12 shows the efficiency curve relating the fuel consumption to the power output for generic diesel generators [61]. It can be inferred from Fig. 3.12 that the efficiency of diesel generators is very poor at low output. However, as shown in Fig. 3.9, the diesel generator outputs around 1–2 MW (7.1–14.3 % of rating power, 14 MW) by adopting the proposed method and the efficiency corresponding to this output power is approximately 5–15 %. The efficiency can be doubled or more only by outputting the power of diesel generator over 50 %. Fuels such as diesel are precious sources especially for a remote island environment so increasing the fuel efficiency is of paramount importance. Hence, a strategy considering the fuel efficiency has to be developed and applied to the control method proposed in Chapter 3.2.2.

Proposed control strategy

In the proposed method, the SOC substitutes the frequency for controlling and sharing of active power. Unlike the frequency, the SOC is not a factor for grid code requirement and hence does not necessarily be maintained at the reference value unless it hits its minimum or maximum value. Hence, in order to control the diesel generator more flexible, the allowable SOC operating range is suggested to be determined in this study. By determining the allowable SOC range, the control

strategy of the diesel generator is as follow:

- Set the minimum and maximum value of the SOC (SOC_{min} and SOC_{max}, respectively).
- Only two operation modes for the diesel generator are allowed: 1) off-line and 2) on-line with 0.5–1.0 pu output.
- If the SOC tends to fall below SOC_{min}, the diesel generator is on-lined.
- If the SOC tends to exceed SOC_{max}, the diesel generator is off-lined.

The control scheme of the BESS is same as proposed in Chapter 3 (see Fig. 3.1) and a new control scheme of the diesel generator during on-line is shown in Fig. 3.13.

The ramp rate controller shown in Fig. 3.13 is used not to control the active power of the BESS but to limit an excessive difference between SOC_{max} and SOC. The lower limit is set to 0.5 pu in order to perform fuel efficiency of 50 % at least. The upper limit can be set to value between 0.5 and 1.0 pu. In this case, it is set to 1 pu in order to leave an output margin for the BESS to catch up a large load change. The reference value of the SOC is set to SOC_{max} and as mentioned previously, the diesel generator is off-lined when the SOC reaches SOC_{max}. This control strategy can reflect the fuel efficiency to some extent but scheduling (e.g., economic dispatch, unit commitment) should be implemented within the secondary control level for the optimum operation. However, investigating the secondary control level is out of the scope of this dissertation.

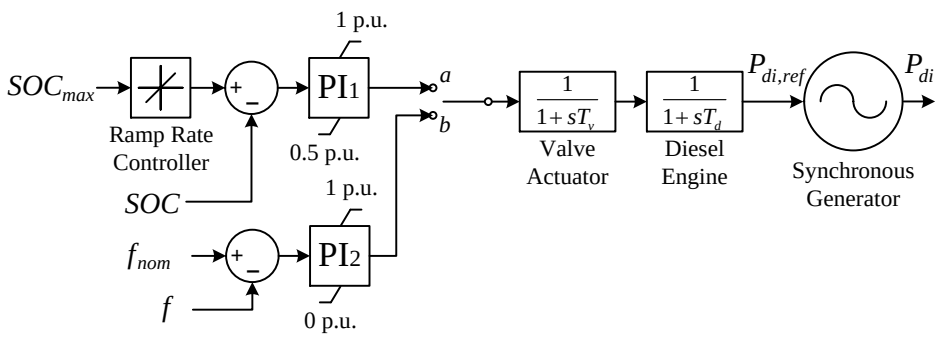

Fig. 3.13 Control scheme of diesel generator considering fuel efficiency.

Simulation test – When diesel generator is on-lined

A simulation test is implemented in order to perform the control strategy considering fuel efficiency. The simulation environment is same with Chapter 3.2.2 except the controller of the diesel generator. The day time data of Ulleung Island is applied and the RESs output constant power with average wind speed and solar irradiance values. A decrement of 0.5 MW load is occurred at 40 s of simulation time. In this case, the initial value of the SOC is at SOC_{min} in order to make a situation for the diesel generator to be on-lined. SOC_{min} is arbitrarily set to 0.5 pu in this study.

Fig. 3.14 shows the active powers of the diesel generator and the BESS, the SOC, and the frequency. It can be noticed that the diesel generator output power is maintained between 0.5 pu (7 MW) and 0.6 pu (8.4 MW) as shown in Fig. 3.14(a). As the load is changed at 40 s, the BESS decreases its output power as shown in Fig. 3.14(b). Note that the BESS takes full responsibility of the load change whereas the diesel generator maintains its output power within the allowable range (0.5–0.6 pu). The SOC is gradually increased since it reaches 0.5 pu (see Fig. 3.15(c)) and hence the diesel generator is on-lined. Since the fuel efficiency is the main focus of this study, the SOC does not need to be maintained at certain value any more. As can be expected, the frequency is maintained at the nominal value without any deviation (see Fig. 3.14(d)) though the load is changed at 40 s.

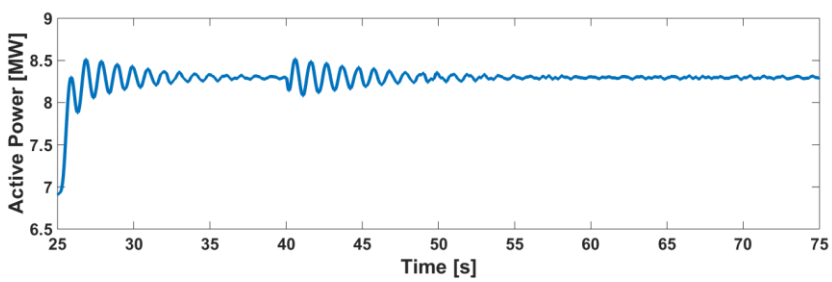

(a)

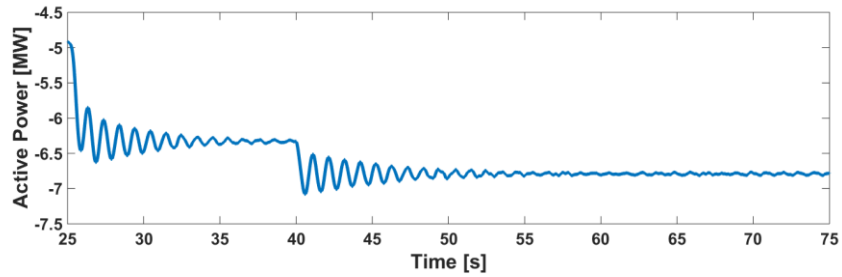

(b)

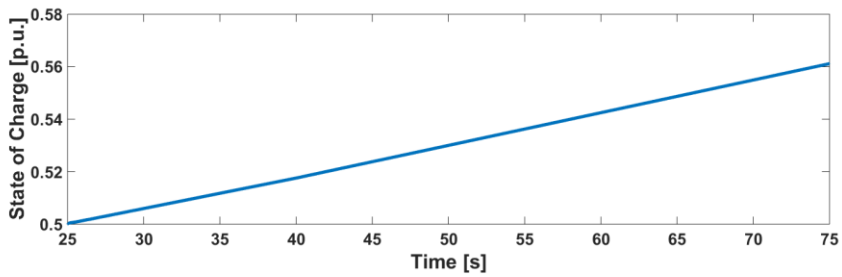

(c)

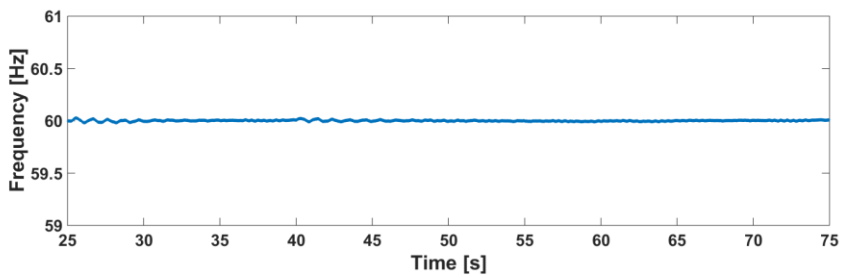

(d)

Fig. 3.14 Simulation results for control strategy considering fuel efficiency (when diesel generator is on-lined). (a) Active power of diesel generator. (b) Active power of BESS. (c) SOC. (d) Frequency.

Simulation test – When diesel generator is off-lined

In this case, the simulation environment is same as the previous case except that the initial value of the SOC is at SOC_{max} in order to make a situation for the diesel generator to be off-lined. SOC_{max} is arbitrarily set to 0.9 pu in this study.

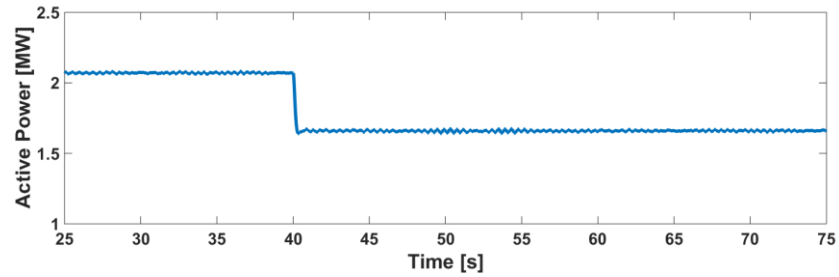

(a)

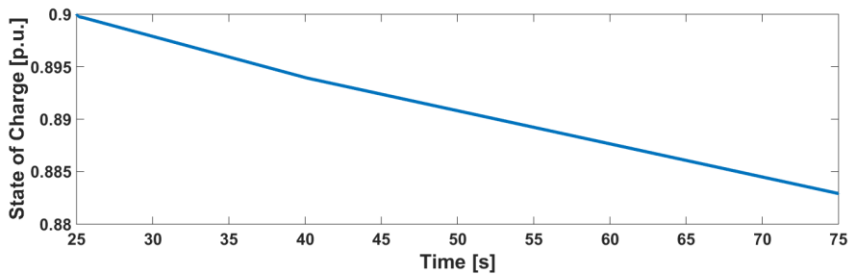

(b)

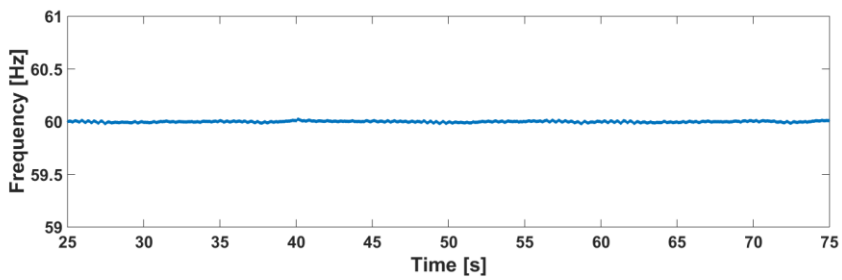

(c)

Fig. 3.15 Simulation results for control strategy considering fuel efficiency (when diesel generator is off-lined). (a) Active power of BESS. (b) SOC. (c) Frequency.

Fig. 3.15 shows the active powers of the BESS, the SOC, and the frequency. The active power of the diesel generator is not shown since the diesel generator is off-lined. The diesel generator is off-lined because the SOC reaches SOC_{max} (0.9 pu). The BESS responses to the load change at 40 s as shown in Fig. 3.15(a) and the SOC decreases as shown in Fig. 3.15(b) since the diesel generator is off-lined. The frequency is well maintained at the nominal value as intended.

The comparison between the control method proposed in Chapter 3.1.1 and in this chapter is shown in Table 3.3.

Table 3.3 Comparison between two proposed control methods.

Control method	Efficiency	SOC	Frequency
Chapter 3.1.1	5–15 %	Strictly maintained at the certain value	Well maintained at the nominal value
Chapter 3.1.3	At least 30 %	Maintained within allowable range	Well maintained at the nominal value

As can be seen Table 3.3, the control method proposed in this chapter seems to be better than that of Chapter 3.1.1. The frequency is well maintained with both control methods whereas the fuel efficiency is much more effective when using the control method for fuel efficiency. However, many other costs such as start-up cost should also be considered in the control method for fuel efficiency. This problem leads to secondary control issues which are beyond the scope of this dissertation. This dissertation mainly focuses on the primary control of DG units and the control of frequency and voltage. Hence, more details about economic issues (such as fuel efficiency, start-up cost) are neglected. The details of the relationship between life of battery and SOC are shown in Appendix C.

3.1.4 Active power sharing among multiple diesel generators

In the previous sections, the case of the synchronous generator-based standalone microgrid is discussed and the diesel generator is assumed as one 14-MW generator. Practically, however, two or more generators are installed at the plant for the case of maintenance, reserve power, mechanical failure, and etc. Hence, in this section, the active power sharing topology among multiple diesel generators is developed.

In conventional power systems, the active power sharing among synchronous generators are based on the frequency deviation [35]. Based on the frequency deviation, the frequency droop control is used to share active power among synchronous generators and the power sharing ratio is determined by the ratio among the droop coefficients. This dissertation proposes to mimic the power sharing method used in the conventional power systems however the frequency remains constant by using the proposed control method. Hence, the SOC is used instead of the frequency. The proposed active power sharing topology is shown in Fig. 3.16 where ΔSOC is the deviation of the SOC from its reference value, k_{pn} and k_{in} are nth generator's proportional and integral gains, respectively, and $P_{di,n}$ is output active power of nth generator, and $P_{di,tot}$ is the total generation power from the synchronous generators.

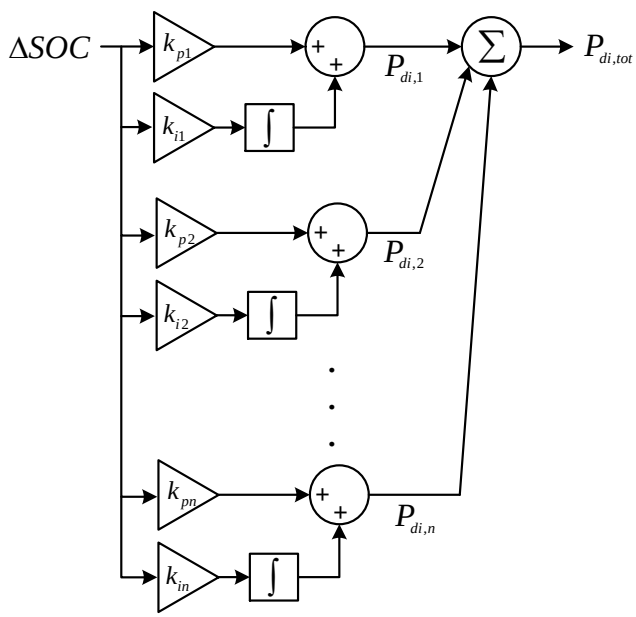

Fig. 3.16 SOC-based active power sharing topology.

The active power sharing ratio can be determined by the ratio between proportional and integral gains. It is noticeable that the ratio of k_{pn} and k_{in} should be same for all generators who participate in the active power sharing. For instance, if

the ratio of *i*th generator's gains is 1:1 (k_{pi}:k_{ii}), the ratio of k_p and k_i of the others must be 1:1 for accurate power sharing. If one is intended to share active power with the ratio of 2:1 among *i*th and *j*th generators, the ratio between gains should be k_{pi}:k_{ii}:k_{pj}:k_{ij} = 2:2:1:1. By using the proposed topology, the system frequency and the SOC can be kept constant and the active power sharing can be implemented accurately as intended.

3.2 Control methods for inverter-based standalone microgrid

3.2.1 Primary and secondary SOC control

This section represents two distinguishable characteristics of a standalone microgrid compared to the standalone microgrid system investigated in the previous section. In this section, inverter-based standalone microgrid with multiple controllable (dispatchable) DG units and a single uncontrollable (non-dispatchable) DG unit is investigated. The studied standalone microgrid, which is referred from [33] with slight modification, is shown in Fig. 3.17 [71]. It consists of a static switch, loads, transformers, a BESS, DG units, a central controller (CC), and local controllers (LCs). The power rating of each DG unit and transformer, the amount of each load, and network impedances are also indicated in Fig. 3.17.

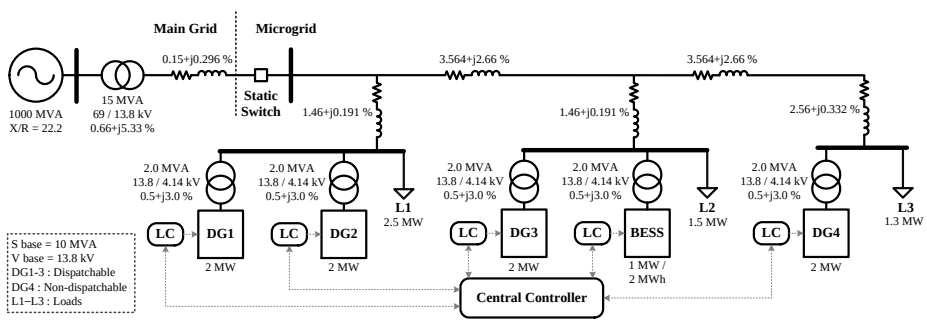

Fig. 3.17 Inverter-based standalone microgrid configuration [71].

Since there are 5 inverter-interfaced DG units, the practical simulation time would be tremendously long if all the inverters are considered as switching model types. Hence, all the inverters are designed as ideal sources for sake of convenience. This design is reasonable since this dissertation focuses not on the details of the inverter mechanisms but on the interactions of active and reactive power between DG units across the standalone microgrid system.

All the DG units in the standalone microgrid shown in Fig. 3.17 is categorized

as 3 types – the BESS, the controllable DG units, the uncontrollable DG unit. As mentioned previously, the BESS acts as per the controller shown in Fig. 3.1 except that $v_{abc,ref}$ goes into the ideal voltage source in this case. However, the BESS has a limited capacity which leads the BESS unable to operate consistently while it becomes fully discharged. To overcome this problem, other controllable DG units are subjected to be controlled to maintain the SOC at the certain level and to share the responsibility of the generation mismatch. These types of DG units are categorized as primary and secondary SOC control units as similar as the conventional primary and secondary frequency control units.

To adopt primary and secondary SOC control scheme, a relationship between active power and SOC is depicted by the following equations which present the relationship between the SOC and the active power [62]:

$$SOC = SOC_i - \int \frac{I_{DC}}{Q} dt \tag{3.8}$$

$$I_{DC} = \frac{P_{BESS}}{V_{DC}} \tag{3.9}$$

$$Q = \frac{I_{DC,rate} C_{BESS,rate}}{P_{BESS,rate}} \tag{3.10}$$

where SOC_i is the initial value of the SOC, I_{DC} is the output DC current from the DC-link of the BESS, V_{DC} is the DC voltage of the DC-link of the BESS, P_{BESS} is the output active power of the BESS, $I_{DC,rate}$ is the rate value of I_{DC}, $C_{BESS,rate}$ is the rate capacity of the BESS, and $P_{BESS,rate}$ is the rate active power of the BESS. Substituting (3.9) and (3.10) into (3.8) gives

$$SOC = SOC_i - \int \frac{P_{BESS,rate} P_{BESS}}{V_{DC} I_{DC,rate} C_{BESS,rate}} dt. \tag{3.11}$$

Taking the derivatives of (3.11) gives

$$\frac{dSOC}{dt} = -K_r P_{BESS} \tag{3.12}$$

where K_r is a constant value assuming that V_{DC} is constant.

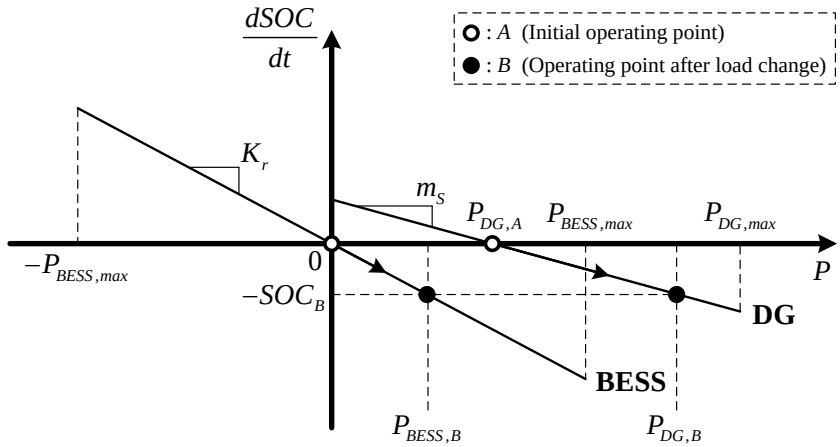

Fig. 3.18 Relationship between active power and SOC.

Since the relationship between the SOC and the active power includes integral term as expressed in (3.11), derivative term expressed in (3.12) is used to establish relationship shown in Fig. 3.18 where $P_{BESS,max}$ and $P_{DG,max}$ indicates the maximum output power of the BESS and the primary SOC control DG unit, respectively. Since the output active power of the BESS affects the derivative of the SOC proportional to K_r, the slope m_S can be determined for the primary SOC control unit in order to affect the SOC level. To keep the SOC level constant, P_{BESS} at steady state should be 0 (see point *A* of the BESS in Fig. 3.18). At this point, the output of the primary SOC control unit is $P_{DG,A}$. Since the BESS is the only grid-forming DG unit, the output active power of the BESS (and thereby the SOC) is the only output power that reacts to generation mismatches. If the mismatch occurs, the output of the BESS and the derivative of the SOC will move to the point *B* ($P_{BESS,B}$ and $-SOC_B$, respectively) in Fig. 3.18. Simultaneously, the primary SOC control unit will support the BESS with the amount of output power inversely proportional to m_S. Consequently, from (3.12) and Fig. 3.18, the following equations can be established:

$$(-SOC_B - 0) = K_r (P_{BESS,B} - 0) \tag{3.13}$$

$$(-SOC_B - 0) = m_S (P_{DG,B} - P_{DG,A}). \tag{3.14}$$

Substituting (3.14) into (3.13) gives

$$(P_{DG,B} - P_{DG,A}) = \frac{K_r}{m_S}(P_{BESS,B} - 0). \tag{3.15}$$

By using (3.15), the controller of primary SOC control unit is shown in Fig. 3.19 [71]. It is noticeable that reducing of the BESS power rating is allowable by decreasing m_S.

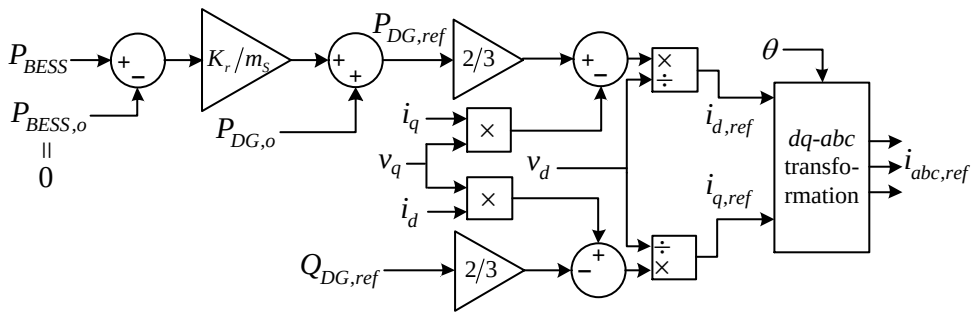

Fig. 3.19 Control scheme of the primary SOC control unit [71].

In Fig. 3.19, θ is the reference angle of *d*- and *q*-axis and $i_{abc,ref}$ is the reference value of 3-phase current goes into the ideal current source. The other DG units except the BESS are modeled as ideal current source since they are considered to be grid-feeding units. $P_{DG,o}$ is the operating point before the disturbance, hence it is same as $P_{DG,A}$ in (3.15). Since the active and reactive power can be expressed as

$$P = 1.5(v_d i_d + v_q i_q) \tag{3.16}$$

$$Q = 1.5(v_q i_d - v_d i_q), \tag{3.17}$$

$i_{d,ref}$ and $i_{q,ref}$ can be rearranged as

$$i_{d,ref} = (\frac{2}{3}P_{DG,ref} - v_q i_q) \Big/ v_d \tag{3.18}$$

$$i_{q,ref} = (v_q i_d - \frac{2}{3}Q_{DG,ref}) \Big/ v_d \,. \tag{3.19}$$

Therefore, the reference *d*- and *q*-component currents can be controlled as shown in Fig. 3.19. Note that the primary SOC control unit should be installed at the same

bus with the BESS as shown in Fig. 3.17 since it should rapidly sense the output power of the BESS (see Fig. 3.19) without any communication delay in order to support the SOC instantaneously (Remind that this unit is for "Primary" SOC control). The characteristics of the primary SOC control unit that it reacts to the output active power of the BESS, which is proportional to the derivative of the SOC, instead of the SOC further boosts up its reaction speed to the SOC change.

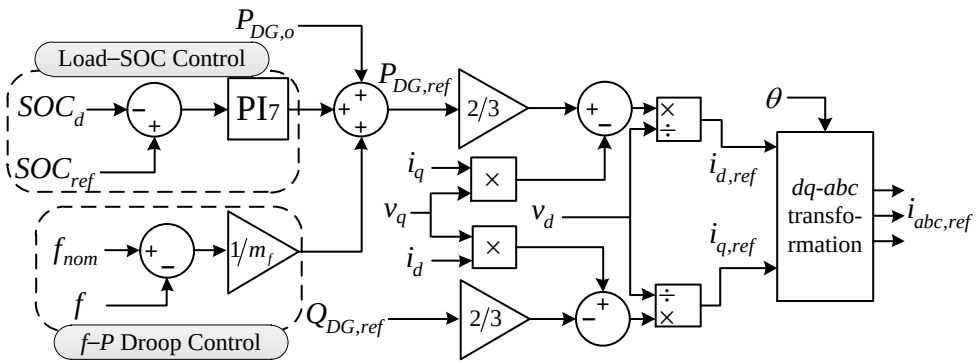

Fig. 3.20 Control scheme of the secondary SOC control unit [71].

However, by using the primary SOC control solely, the SOC cannot be restored to the desired value. To restore the SOC to the desired (reference) value, the secondary SOC control is adopted to some controllable DG units. This control acts as load–SOC control which restores the SOC at the desired level. The load–SOC control is as similar as load–frequency control in conventional power system which restores the frequency to the nominal value. However, the SOC is a local variable since it is only able to be measured in the proximity of the BESS whereas the frequency is a global variable since it is able to be measured anywhere in the system network. Hence, the SOC data should be sent to the secondary SOC control units through communication infrastructure. By using the communication system, the communication delay is inevitable for employing the secondary SOC control. The communication delay may threaten the stability of the standalone microgrid system, however the stability can be enhanced [45], [46]. The control scheme of

the secondary SOC control unit is shown in Fig. 3.20 [71] where SOC_d is the SOC level with communication time delay, SOC_{ref} is the nominal value of the SOC, m_f is the *f–P* droop coefficient, and the PI gain parameters is shown in Appendix A.

The main objective of the secondary SOC control unit is to restore the SOC at the certain value, which is SOC_{ref} in this case, after disturbances such as generation mismatches. The current SOC level is informed to the secondary SOC control unit via communication system (microgrid CC) so the time delay is occurred. The error between SOC_{ref} and SOC_d goes into the PI controller to maintain the SOC level. Though this control method helps to maintain the SOC at the desired level, use of the communication system may degrade the system reliability. The additional control scheme to enhance the system reliability and the role of the frequency droop control shown in Fig. 3.20 will be discussed in Chapter 5.

The rest DG unit (DG4) is assumed as uncontrollable (non-dispatchable) unit. The control scheme for this unit is same as shown in Fig. 3.20 except that the SOC control part including the PI controller does not exist.

3.2.2 Simulation test of the proposed method for inverter-based standalone microgrid

Table 3.4 Applied control method for each DG unit.

DG unit	Conventional method	Proposed method
BESS	*P–f* droop	Constant frequency and voltage
DG1 & DG2	*f–P* droop	The secondary SOC control (Load–SOC control)
DG3	*f–P* droop	The primary SOC control
DG4	Non-dispatchable	Non-dispatchable

To verify the proposed control strategy for inverter-based standalone microgrid with multiple controllable DG units, the system shown in Fig. 3.17 was modeled and implemented by using MATLAB/SimPowerSystems. The

conventional and the proposed methods are compared to each other for the case of sudden load change. The applied control methods for each DG unit are shown in Table 3.4.

As shown in Table 3.4, in the proposed method, the BESS is controlled as same as that used in the case of synchronous generator-based standalone microgrid. DG3, which is located in the proximity of the BESS for instantaneous sensing of the BESS without communication delay, is adjusted for the primary SOC control. It shares transient load with the BESS as per the relationship between active power and SOC depicted in Fig. 3.18, which is similar to the frequency droop concept of conventional power systems. DG1 and DG2 act as the secondary SOC control unit. They use integral control (included in the PI controller) in order to achieve zero SOC error after disturbances. This is the reason why the secondary SOC control is called as load–SOC control in this dissertation. The secondary SOC control units (DG1 and DG2) share the active power necessary for restoring the SOC proportional to the PI gain parameters. In this study, the parameters of both DG1 and DG2 are same.

In the simulation study, the load L3 in Fig. 3.17 will be changed from 1.3 MW to 0.8 MW at 1 s of the simulation time. Typically, communication time delay is in the order of 100–300 ms [63]. In this dissertation, 300 ms of communication delay is considered to account for the worst time delay – the system stability becomes worse if the communication delay becomes larger [45], [46]. Since the total simulation time is about 10 s, the capacity of the BESS is scaled down to 1/400 of its original value (2 MWh) to see change of the SOC clearly. The simulation results for the conventional method are shown in Figs. 3.21–23.

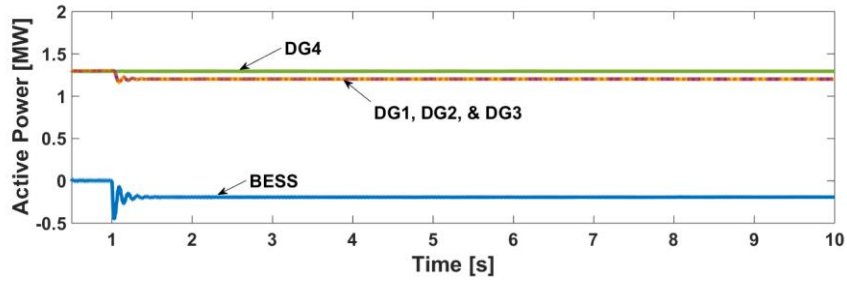

Fig. 3.21 Active power of the BESS and DG1–4 for the conventional method.

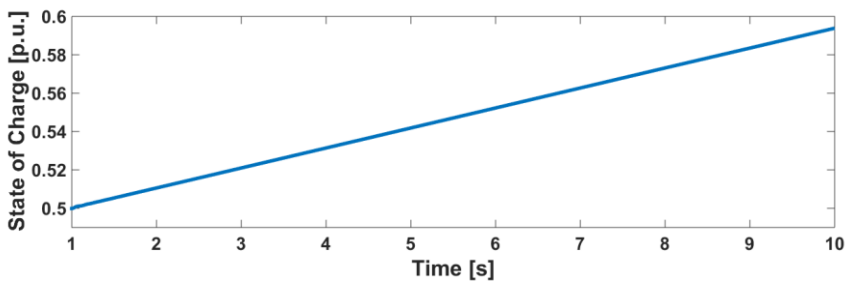

Fig. 3.22 SOC of the BESS for the conventional method.

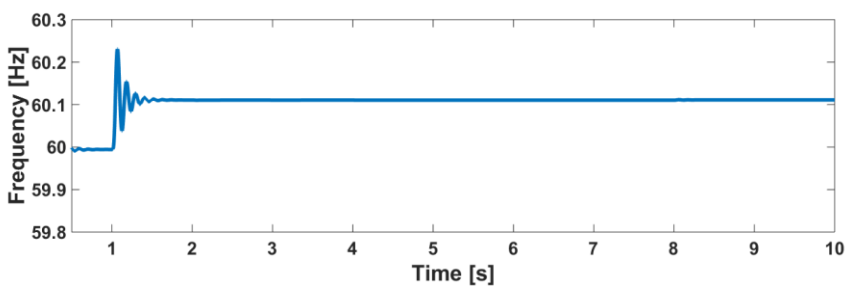

Fig. 3.23 Frequency for the conventional method.

The output active power of the BESS and DG1–4 is shown in Fig. 3.21. Since the load decreases about 0.5 MW at 1 s, the output of the BESS with *P–f* droop control is decreased. Subsequently, the SOC cannot be maintained steadily as shown in Fig. 3.22 and the frequency is increased as shown in Fig. 3.23. The DG units with *f–P* droop control (DG1–3) readjust their power as per the amount of frequency deviation from its nominal value whereas the other DG unit (DG4) does nothing. Note that DG4 is a non-dispatchable unit and its output is assumed to be

constant in this case. For comparing to the conventional control method, the simulation results for the proposed method are shown in Figs. 3.24–26.

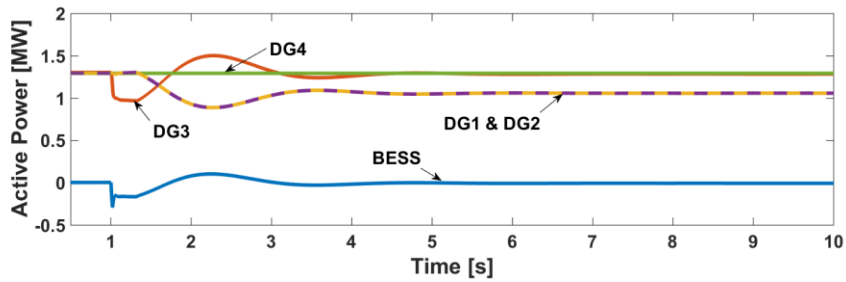

Fig. 3.24 Active power of the BESS and DG1–4 for the proposed method.

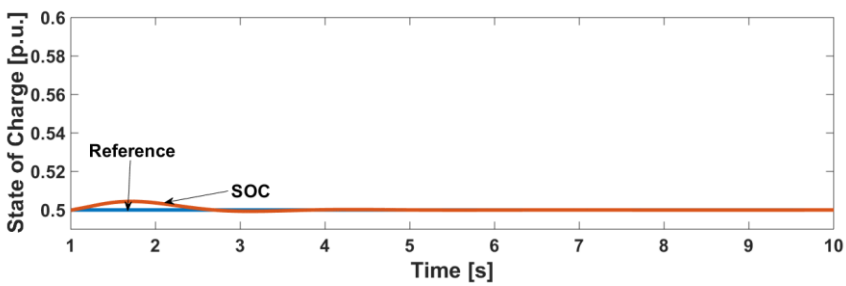

Fig. 3.25 SOC of the BESS for the proposed method.

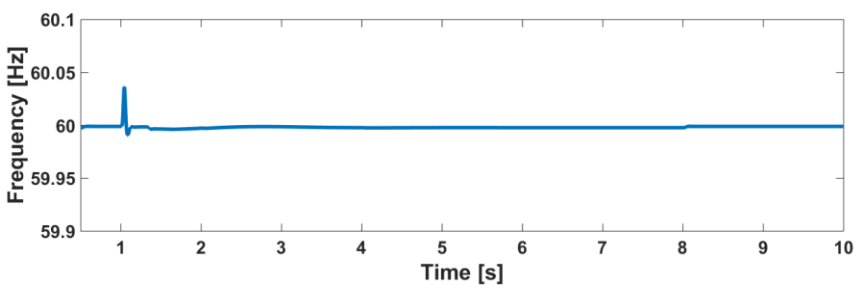

Fig. 3.26 Frequency for the proposed method.

As shown in Fig. 3.24, the BESS and the primary SOC control unit (DG3) shares transient active power mismatch immediately after the load change occurs. The non-dispatchable DG unit (DG4) does nothing with this disturbance since it is

not dispatchable. After a while, the secondary SOC control units (DG1 and 2) decrease their output power since the SOC becomes larger than the reference value as shown in Fig. 3.25. Due to the support of the secondary SOC control units, the SOC level can be restored to the reference value. Moreover, the frequency also can be maintained at the nominal value due to the constant frequency control of the BESS though there is a momentary frequency deviation immediately after the sudden load change as shown in Fig. 3.26.

The characteristics of the proposed method for enhancing frequency stability can be concluded by comparing with the conventional method as shown in Table 3.5.

Table 3.5 Comparison between both methods in the frequency stability viewpoint.

Content	Conventional method	Proposed method
Sensing active power mismatch	From frequency deviation	From SOC deviation
Frequency deviation	Usually happens for a long term, and sometimes, largely deviated	Barely and momentarily deviated
Integration of RES	Frequency instability might be caused	Stable frequency operation can be implemented
Suitable to	Large power systems	Small isolated power systems

In the proposed method, active power mismatch within the system is sensed from the frequency deviation whereas in the conventional method, it is sensed from the SOC deviation. Since the power mismatch raises frequency deviation, large integration of RESs might cause the frequency instability by using the conventional method. However, the frequency is able to be stably operated by using the proposed method even if large RESs are integrated to the system. In conclusion, since the conventional control method uses the system frequency, which is a global parameter that can be measured anywhere in the system, it is suitable to large power systems whereas the proposed control method is suitable to small isolated power systems since it uses the SOC, which is a local parameter that should be

transmitted via communication system.

The control strategy proposed in this chapter enhances the frequency stability dramatically. However, using only this control method is not enough to enhance the whole system stability for standalone microgrids, which have weak grid characteristic. Moreover, reactive power control method of the BESS and the dispatchable DGs are not even discussed in this chapter. Integration of DG units and power mismatches might also cause voltage instability. In the next chapter, the control method of reactive power of RESs and coordinated control method of reactive power of the BESS and the dispatchable DGs are discussed.

Chapter 4. New Droop Methods for Voltage Control

Voltage stability is the ability of a power system to maintain steady acceptable voltages at all buses in the system under normal operation conditions and after being subjected to a disturbance [35]. The major problem is usually the voltage drop that occurs when active and reactive power flow through resistive (for low voltage network) and inductive (for medium or high voltage network)) reactances of network grid, respectively. Recently, however, the voltage rise has also occurred usually due to reverse power flow mainly caused by integration of DG units. As similar as the frequency, the voltage is also regulated by the grid code requirements. Moreover, standalone microgrids have weak network grid which make the voltage drop and rise severer and this is critical to standalone microgrids which are targeted to integrate large RESs. To enhance the voltage stability of standalone microgrids, this chapter illustrates about the proposed control methods of DG units in standalone microgrids.

4.1 Droop method for medium voltage network standalone microgrid

Since a standalone microgrid has weak system characteristic, the voltage instability is more likely to happen than a large power system. Intermittent output change of RESs, sudden load change and trip out of generators may cause severe voltage fluctuation and/or deviation. Though standalone microgrids have weak network, most of the conventional voltage control methods are focused on a relationship between reactive power, voltage, and reactance. Those control methods are mostly suitable to high or extra high voltage networks. In this section, more suitable solutions for voltage control strategy of standalone microgrids are developed for both medium and low voltage networks.

4.1.1 Active power–reactive power (*P*–*Q*) droop control

Practically, unlike the assumptions that derive (2.10) and (2.11), network voltage is affected by both active and reactive power as noticed from (2.8) and (2.9). It is reasonable to apply (2.10) and (2.11) to large power systems with strong network grid but both active and reactive power should be considered for voltage control in a weak grid such as a standalone microgrid. Also, a novel method should be developed to prevent voltage fluctuation since the conventional voltage droop control methods are triggered by voltage deviation. To solve both problems, a novel droop control method for RES units is proposed. Since RES units are uncontrollable sources and thereby one of major problems that causes voltage fluctuation, the proposed control method is applied to RES units. Since the voltage problem is a local issue, this attempt to solve the voltage problem (by applying a solution control method directly to the target which causes problem) is reasonable.

A novel droop control method proposed in this dissertation is called *P*–*Q* droop control in this dissertation. Additional control schemes are added to the reactive power controller of RES shown in Fig. 3.5. As a result, the proposed controller of RESs is shown in Fig. 4.1.

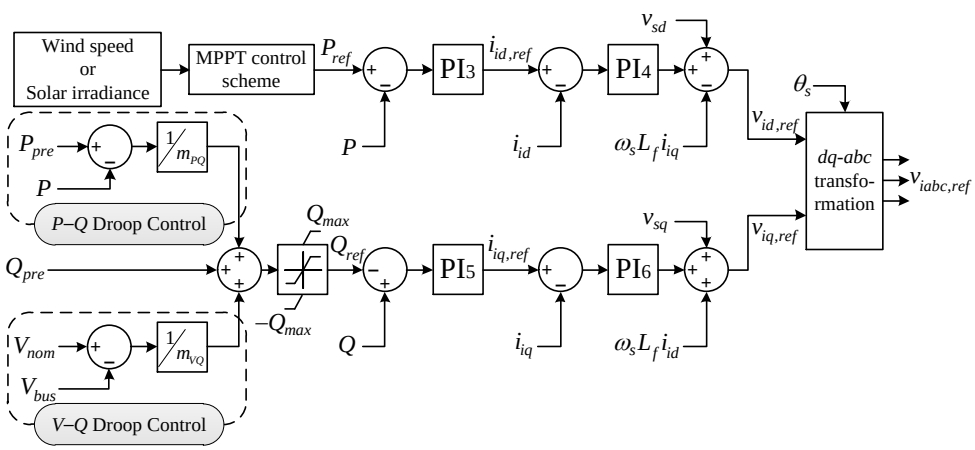

Fig. 4.1 Proposed control scheme of RESs to mitigate voltage fluctuation [23].

As can be seen in Fig. 4.1, both the proposed *P*–*Q* droop as well as the conventional *V*–*Q* droop are added to the reactive power controller. m_{PQ} and m_{VQ} are *P*–*Q* and *V*–*Q* droop coefficient, respectively, P_{pre} and Q_{pre} are the predicted (or scheduled) value of active and reactive power, respectively, V_{bus} is the RES bus voltage, and the rest of the notations are same as explained previously. The value of $1/m_{VQ}$ is based on the following equation [64]:

$$\frac{1}{m_{VQ}} = \frac{\Delta Q / P_{rate}}{\Delta V_{bus} / V_{base}} \tag{4.1}$$

where V_{base} and P_{rate} are the base voltage of the bus and the rate active power of the generation system, respectively. Typically, $1/m_{VQ}$ has a value between 0 and 25 [64]. Since m_{VQ} is determined based on the power rating, adding *P*–*Q* droop control might cause excessive reactive power output. To prevent this problem, Q_{ref} is limited at the maximum reactive power, Q_{max}, which is presented below:

$$Q_{max} = \sqrt{S_{rate}^2 - P^2} \tag{4.2}$$

where S_{rate} is the rating of apparent power of the inverter which is considered to be same as the power rating of the RES. From (4.2), it can be noticed that the maximum reactive power is determined by the output active power which means that maximizing the active power is prioritized over compensating the reactive power for mitigating voltage fluctuation. The parameters of PI controllers are given in Appendix A.

The role of the *V*–*Q* droop is same as that of conventional, that is to maintain the bus voltage within the allowable range or to share reactive power. However, this does not fully prevent the voltage fluctuation due to the active power fluctuation which is likely to happen for uncontrollable (non-dispatchable) RESs. Additionally, the voltage fluctuation due to active power fluctuation is severer for weak power systems such as standalone microgrids. For these reasons, combining the *P*–*Q* droop to the reactive power controller will be helpful for mitigation voltage fluctuation. However, determining proper *P*–*Q* droop coefficient still

remains as a problem. The voltage fluctuation will be barely alleviated when *P*–*Q* droop coefficient is too small and the system may be unstable when *P*–*Q* droop coefficient is too large [45]. To determine *P*–*Q* droop coefficient (m_{PQ}) properly, the sensitivity matrix is used in this dissertation.

The sensitivity matrix can be calculated from the Jacobian matrix equation given in [35]

$$\begin{bmatrix} \Delta\mathbf{P} \\ \Delta\mathbf{Q} \end{bmatrix} = \begin{bmatrix} \mathbf{J}_{\mathbf{P\theta}} & \mathbf{J}_{\mathbf{P|V|}} \\ \mathbf{J}_{\mathbf{Q\theta}} & \mathbf{J}_{\mathbf{Q|V|}} \end{bmatrix} \begin{bmatrix} \Delta\boldsymbol{\theta} \\ \Delta|\mathbf{V}| \end{bmatrix} \tag{4.3}$$

where $\Delta\mathbf{P}$ is the active power deviation at each bus, $\Delta\mathbf{Q}$ is the reactive power deviation at each bus, $\Delta\boldsymbol{\theta}$ is the voltage angle deviation at each bus, $\Delta|\mathbf{V}|$ is the voltage magnitude deviation at each bus, and $\mathbf{J}_{\mathbf{P\theta}}$, $\mathbf{J}_{\mathbf{Q\theta}}$, $\mathbf{J}_{\mathbf{P|V|}}$, and $\mathbf{J}_{\mathbf{Q|V|}}$ are the Jacobian matrices. Taking the inverse transform of the Jacobian matrix given in (4.3), the sensitivity matrix equation can be expressed as:

$$\begin{bmatrix} \Delta\boldsymbol{\theta} \\ \Delta|\mathbf{V}| \end{bmatrix} = \begin{bmatrix} \mathbf{S}_{\boldsymbol{\theta}\mathbf{P}} & \mathbf{S}_{\boldsymbol{\theta}\mathbf{Q}} \\ \mathbf{S}_{|\mathbf{V}|\mathbf{P}} & \mathbf{S}_{|\mathbf{V}|\mathbf{Q}} \end{bmatrix} \begin{bmatrix} \Delta\mathbf{P} \\ \Delta\mathbf{Q} \end{bmatrix}. \tag{4.4}$$

The voltage deviation occurring with the change in the active and reactive power is calculated as:

$$\Delta|\mathbf{V}| = \mathbf{S}_{|\mathbf{V}|\mathbf{P}}\Delta\mathbf{P} + \mathbf{S}_{|\mathbf{V}|\mathbf{Q}}\Delta\mathbf{Q}. \tag{4.5}$$

As can be noticed from (4.5), the voltage can be influenced by reactive power as well as active power. The objective of the *P*–*Q* droop control is to mitigate the bus voltage fluctuation caused by the output active power fluctuation of the RES which is interconnected to that bus. Hence, to make the voltage deviation of *i*th bus 0, the following equation must be satisfied:

$$\begin{aligned} \Delta|V|_i &= S_{|V|P,i,i}\Delta P_i + S_{|V|Q,i,i}\Delta Q_i \\ &= 0 \\ &= S_{|V|P,i,i}(P_{pre,i} - P_i) + S_{|V|Q,i,i}(Q_{pre,i} - Q_i). \end{aligned} \tag{4.6}$$

where the subscript i denotes the index of bus number or the index of rows and columns of vectors (or matrices). Assume that the day-ahead forecasting of RES

output is provided, $P_{pre,i}$ and $Q_{pre,i}$ are the predicted or scheduled value (based on the day-ahead forecasting) of active and reactive power, respectively, for the RES interconnected to *i*th bus of the system. Since the reactive power of DG is usually set to 0, (4.6) can be rearranged as:

$$Q_i = \left(S_{|V|P,i,i} \Big/ S_{|V|Q,i,i} \right) \left(P_{pre,i} - P_i \right) = \left(1 \Big/ m_{PQ} \right) \left(P_{pre,i} - P_i \right). \qquad (4.7)$$

As a result, *P*–*Q* droop coefficient m_{PQ} can be determined by using the sensitivity matrix. In this way, the proper droop coefficient that is neither too small to barely mitigate voltage fluctuation nor too large to cause the system instability can be determined.

4.1.2 Coordinated control of RESs and dispatchable DGs

As can be seen from (4.2), the reactive power of RES is limited by its power rating and output active power. Hence the RES's reactive power deficiency problem may be raised. Since reactive power control methods of the BESS, the diesel generator, and the other dispatchable DGs are not discussed in Chapter 3, they are discussed in this section with the objective of supporting the reactive power of RESs.

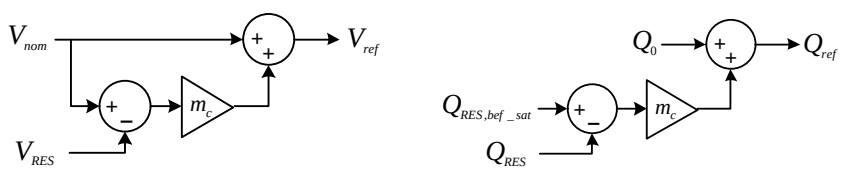

(a) (b)

Fig. 4.2 Control scheme to support reactive power of RES. (a) Reference voltage of BESS and diesel generator. (b) Reference reactive power of dispatchable DGs.

The purpose of the *P*–*Q* droop control is to mitigate the voltage fluctuation. During the active power fluctuation of the RES, the reactive power may be limited

by (4.2) at some point where the output active power is high. The more the amount of reactive power is limited, the more the degree of voltage fluctuation will be. In order to mitigate the RES's voltage fluctuation, the reference voltage of the diesel generator and the BESS and the reference reactive power of the dispatchable DGs are proposed as shown in Fig. 4.2 where m_c is the coefficient that can be adjusted. By adjusting this coefficient, the operator can determine the amount of reactive power supported for the RESs by the BESS and the DGs. Since the BESS and the diesel generator control the magnitude of the voltage, they sense the voltage deviation at the RES bus and then support it. On the other hand, since the dispatchable DGs (grid-feeding type) control the output reactive power, they sense the amount of reactive power limited by the output active power and then support it. The simulation test will be implemented and discussed in Chapter 5 to prove the effectiveness of the proposed control methods.

4.1.3 Simulation test of the proposed method for medium voltage network standalone microgrid

To prove the effectiveness of the *P*–*Q* droop control, a simulation test was implemented. The tested standalone microgrid is Ulleung Island power system shown in Fig. 3.2. The nominal voltage of this standalone microgrid is 6.6 kV which seems enough voltage level for medium voltage network. The day time load demand shown in Table 3.1 was adopted in this test. In the day time of Ulleung Island, the wind speed ranges from 10.5 to 11.5 m/s and averages 11 m/s [65], [66]. The solar irradiance ranges from 600 to 720 W/m^2 and averages 660 W/m^2 [65], [66]. By using the average values of wind speed and solar irradiance as the forecasted value, P_{pre} of both WT and PV system are determined. Based on the data given, $1/m_{PQ}$ of the WT and PV system are calculated to be 0.413 and 0.495, respectively and $1/m_{VQ}$ of the WT and PV system are determined as 5 and 25, respectively. Three different control methods – without any droop controls, only

with *V*–*Q* droop control, *P*–*Q* plus *V*–*Q* droop control – were tested to compare the voltage stability of each method during the fluctuation of output active power of RESs. The output active power of WT and PV system are shown in Figs. 4.3 and 4.4, respectively. The output fluctuation of both RESs begins at 30 s.

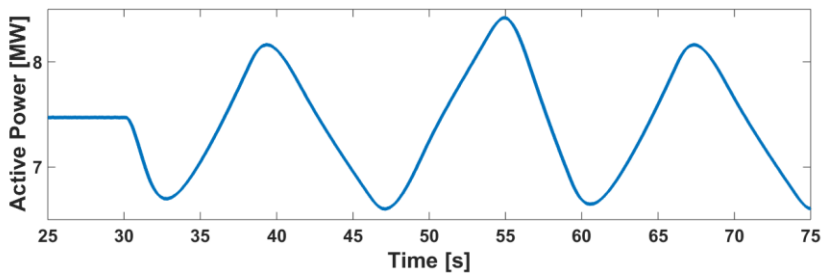

Fig. 4.3 Active power of WT during the day time.

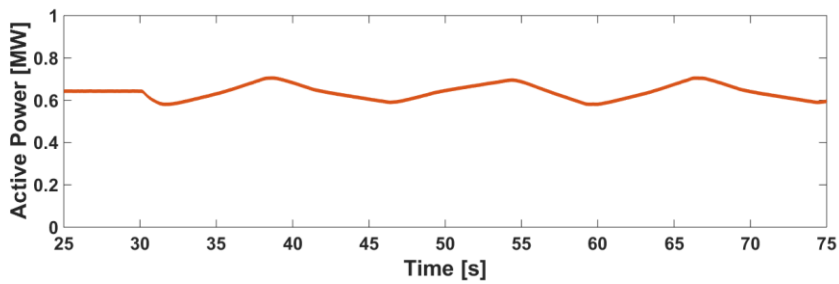

Fig. 4.4 Active power of PV system during the day time.

The reactive power of WT and PV system are shown in Figs. 4.5 and 4.6, respectively. Each figure shows the results of three different control methods – without droop (w/o droop), using *V*–*Q* droop only (*V*–*Q* droop), using both *V*–*Q* and *P*–*Q* droop (proposed).

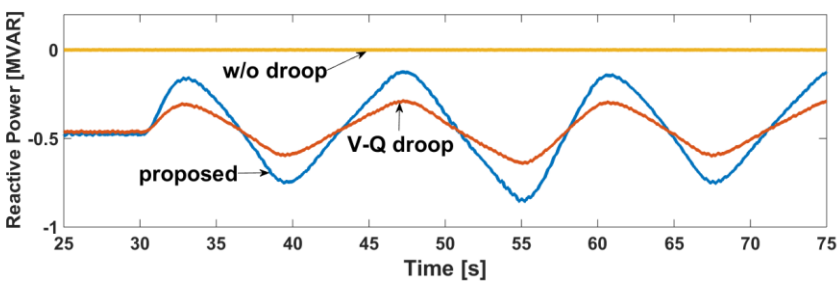

Fig. 4.5 Reactive power of WT during the day time.

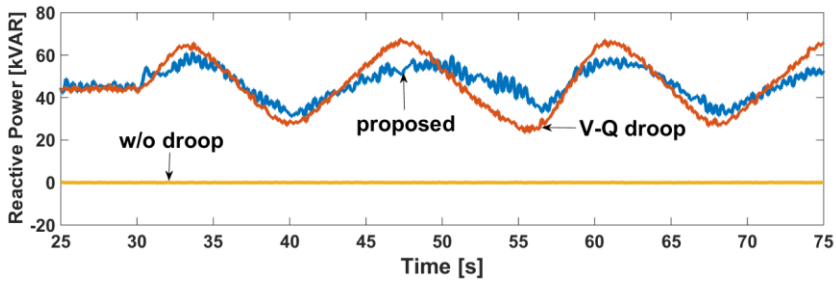

Fig. 4.6 Reactive power of PV system during the day time.

As can be seen from Figs 4.5 and 4.6, both RESs have the same power factor (unity power factor) without droop control, whereas they control the reactive power to compensate for the voltage deviation by applying the *V*–*Q* droop control. By applying the proposed control method (using both *V*–*Q* and *P*–*Q* droop), the reactive powers of both RESs are controlled not only for compensating for voltage deviation but also for mitigating the voltage fluctuation induced by their own active power fluctuations. In the case of PV system, there is little difference between the conventional droop control method (using *V*–*Q* droop only) and the proposed control method, since the output active power fluctuation is not very large. By contrast, in the case of WT, the proposed control method outputs more reactive power than the conventional control method due to its large active power fluctuations. With these reactive power compensations, the simulation results for bus voltage magnitude at WT and PV system are shown in Figs. 4.7 and 4.8, respectively.

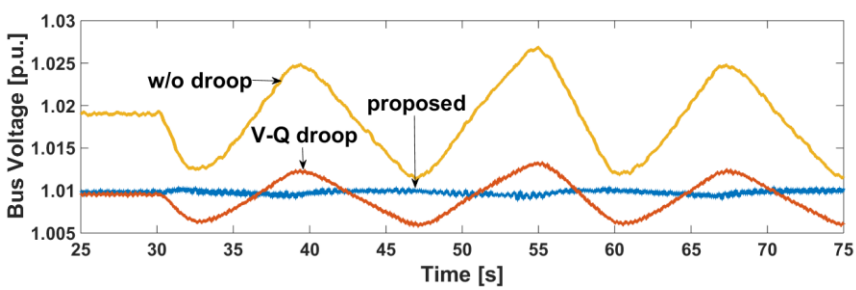

Fig. 4.7 Voltage at WT bus during the day time.

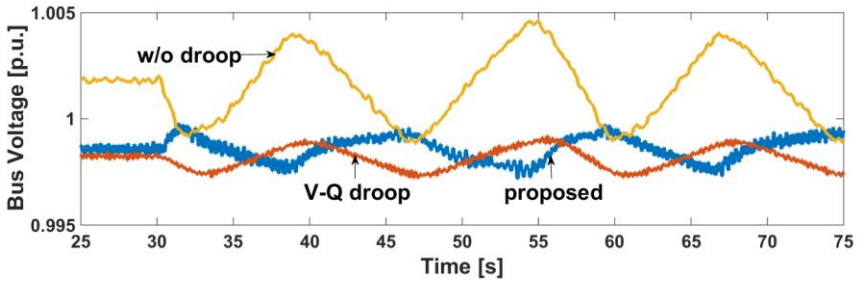

Fig. 4.8 Voltage at PV system bus during the day time.

Figs. 4.7 and 4.8 show that by using *V*–*Q* droop only, the bus voltage can be kept closer to the nominal value than without the droop control. However, it cannot effectively prevent the voltage fluctuations incurred by the output power fluctuations. By adding *P*–*Q* droop control, the voltage fluctuation can be eliminated. While the mitigation of the PV system bus voltage fluctuation is negligible, since its active power fluctuation is not very large, the WT bus voltage fluctuation is reduced dramatically. Therefore, it can be concluded that the proposed *P*–*Q* droop control of a RES has a damping effect on the voltage fluctuation incurred by its own active power fluctuation. However, it is worth note that the value of *P*–*Q* droop coefficient hinges on the network impedance and the forecasting data of load and RESs' generation. This means that the forecasting error affects the *P*–*Q* droop coefficient and hence the voltage control performance. This issue is discussed in Appendix B.

In this case, the reactive powers of both RESs did not be reached to their limitations. Hence, the reactive power was able to fully alleviate the voltage fluctuation. The case where the reactive power output is limited by its maximum value will be investigated in Chapter 5.

4.2 Droop method for low voltage network standalone microgrid

4.2.1 Voltage compensation methods with active power

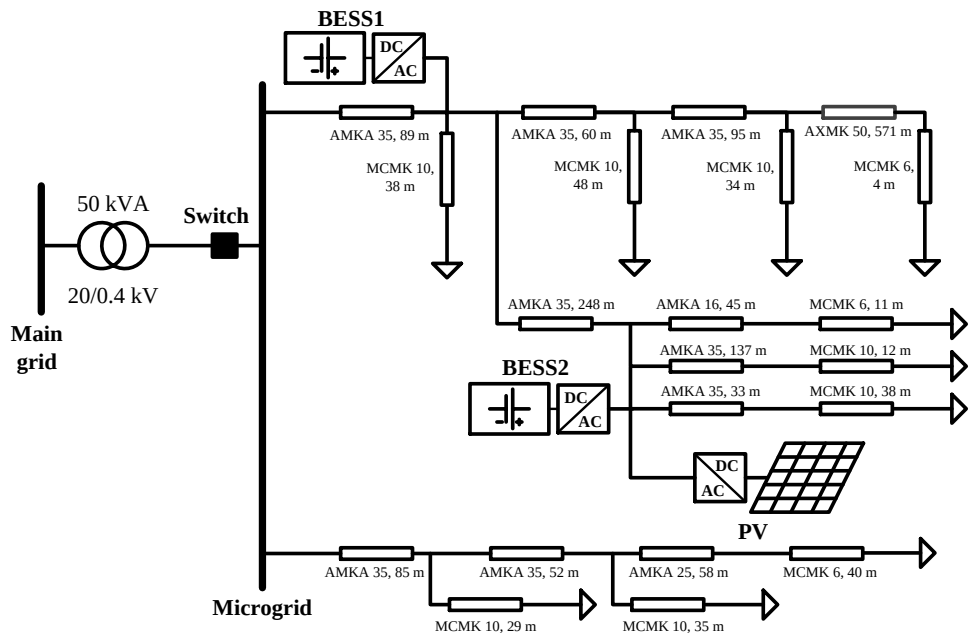

Fig. 4.9 Low voltage network microgrid [67].

In this section, a control strategy to enhance voltage stability in low voltage network standalone microgrids is developed. The studied low voltage network based microgrid, which is referred from [67] with slight modification, is shown in Fig. 4.9. The studied low voltage network is a typical Finnish rural overhead AMKA network. Loading ratio of the transformers through the loads can be adjusted between 0 and 150 % of nominal power of the transformer. In this study, the total load is set to 30 kW with each load of 3 kW. In order to realize standalone microgrid network, the switch is assumed to be opened. The resistances, reactances, and reactance/resistance (X/R) ratio of the lines used in the studied network (Fig. 4.9) are shown in Table 4.1 [67].

Table 4.1 Line parameters of low voltage network microgrid in Fig. 4.9 [67].

	X (Ω/km)	R (Ω/km)	X/R
AMKA 3×50+70	0.101	0.641	0.158
AMKA 3×35+50	0.104	0.868	0.120
AMKA 3×25+35	0.106	1.20	0.088
AMKA 3×16+25	0.108	1.91	0.057
AXMK 4×50S	0.088	0.641	0.137
MCMK 3×10+10	0.088	1.83	0.048
MCMK 3×6+6	0.090	3.08	0.029

Table 4.2 Typical line parameters [68].

Line voltage	X (Ω/km)	R (Ω/km)	X/R
Low voltage line	0.083	0.642	0.129
Medium voltage line	0.190	0.161	1.180
High voltage line	0.191	0.060	3.183

Typical line parameters for low, medium, and high voltage networks are shown in Table 4.2 [68]. Unlike high voltage networks that reactance is much larger than resistance, low voltage networks has much larger resistance than reactance. Hence, from (2.8) and (2.9) with some assumptions ($X \ll R$, $\delta \approx 0$, then $\sin\delta \approx \delta$ and $\cos\delta \approx 1$), the following equations can be derived:

$$P = \frac{V_r V_s - V_r^2}{R} \tag{4.8}$$

$$Q = \frac{-V_r V_s \delta}{R}. \tag{4.9}$$

By contrary to high voltage networks, in low voltage networks, a bus voltage magnitude is much more correlated with active power than reactive power.

On the basis of these assumptions, two new voltage control strategies for low voltage network standalone microgrid using active power compensation of a BESS is proposed in this dissertation. One of newly proposed voltage control methods is active power–active power (*P*–*P*) droop control. This droop control is named after the way how it activates – it measures active power deviation of a specific RES unit and then compensates with a BESS's active power. As same as *P*–*Q* droop

control developed in the previous section, the purpose of *P–P* droop control is to mitigate voltage fluctuation occurred by the active power fluctuation of intermittent RESs. To this end, *P–P* droop control scheme is added to the active power controller of the BESS (grid-feeding type) under the following assumptions:

- Standalone microgrid is low voltage network (with X/R ratio of under 0.2 at least).
- The BESS is located in the proximity of the RES unit so that the BESS can directly measure the output of the RES without communication delay.
- The outputs of the BESS and the RES at the steady state are optimally determined in scheduling stage.

With these assumptions, the BESS control scheme adopting *P–P* droop is developed as shown in Fig. 4.9.

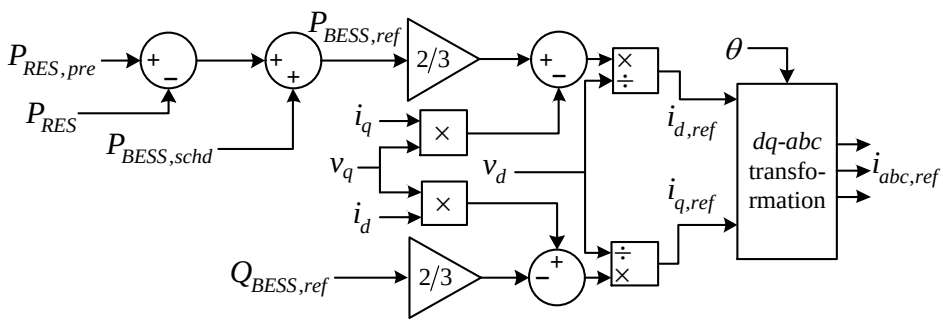

Fig. 4.10 BESS control scheme adopting *P–P* droop.

The simple proposed controller shown in Fig. 4.10 is applied to BESS2 in Fig. 4.9. At steady state, the PV system (RES)'s output active power (P_{RES}) is same as the forecasted or predicted value ($P_{RES,pre}$). Hence, the BESS outputs the optimally scheduled value ($P_{BESS,schd}$) at steady state. If the output active power of PV system (RES) is deviated from the predicted value, the BESS compensates active power as much as amount of the deviation of the PV system output. Since both the BESS and the PV system are located at the same bus, the net active power flow within the bus is same as that of before the deviation occurred. Consequently, not only the

voltage deviation but also the frequency deviation that might be incurred by the active power deviation of the PV system (RES) can be prevented. Nonetheless, the condition that the BESS should be interconnected to the same bus with the target RES remains as a problem because interconnecting two different units (BESS and RES) at the same bus might be restricted by economical, geographical, and/or some other reasons.

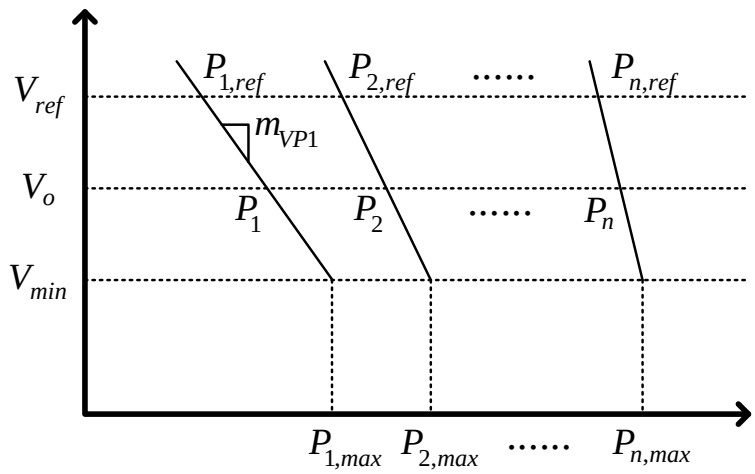

Fig. 4.11 *V–P* droop characteristics.

To resolve this problem, *V–P* droop control, which is occasionally used in low voltage networks, is investigated. This control is for the voltage control at a bus where it is located electrically far from a source of voltage deviation (output change of RES). *V–P* control plays a same role as conventional *V–Q* control of medium or high voltage network power systems. The characteristics of *V–P* droop is shown in Fig. 4.11 and is somewhat similar to *f–P* and *V–Q* droop characteristics shown in Figs. 2.10 and 2.11, respectively. The relationship between active power and voltage is presented as:

$$V_o = V_{ref} - m_{VP}(P_{ref} - P) \tag{4.10}$$

$$m_{VP} = \frac{(V_{ref} - V_{min})}{(P_{ref} - P_{max})}. \tag{4.11}$$

In this study, the proposed controller is applied to BESS2 in Fig. 4.9. Though this controller is for a DG units located electrically far from the RES, it is applied to BESS2 in this study in order to compare with *P*–*P* droop control (Fig. 4.10). The controller is shown in Fig. 4.12 where V_{bus} (equal to V_o in (4.10)) is the bus voltage, V_{nom} (equal to V_{ref} in (4.10)) is the nominal value of the voltage magnitude, m_{VP} is the droop coefficient, $P_{BESS,schd}$ (equal to P in (4.10)) is the scheduled value of active power of the BESS, and $P_{BESS,ref}$ (equal to P_{ref} in (4.10)) is the reference active power of the BESS. Though *V*–*P* droop control is applied to the BESS in this study, it may be applied to any other types of controllable DG units. Still, it might be the best option to apply *P*–*P* droop to the BESS since there are many advantages in interconnecting the BESS and the RES at the same bus (e.g., storing surplus energy from the RES to the BESS).

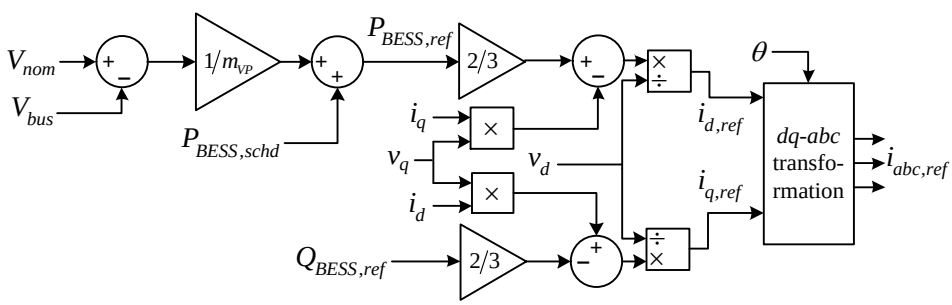

Fig. 4.12 BESS control scheme adopting *V*–*P* droop.

4.2.2. Simulation test of the proposed method for low voltage network standalone microgrid

To prove the effectiveness of the voltage control strategies for low voltage network standalone microgrids, the low voltage network microgrid shown in Fig. 4.9 is studied and four different control types – without droop, with *V*–*Q* droop, with *P*–*P* droop, with *V*–*P* droop – are applied to BESS2 shown in Fig. 4.9. BESS1 is controlled as grid-forming type with the controller shown in Fig. 3.1 and the

output of the PV system is deviated from the predicted value ($P_{RES,pre}$) for 0.5 s (between 0.5 and 1.0 s of simulation time).

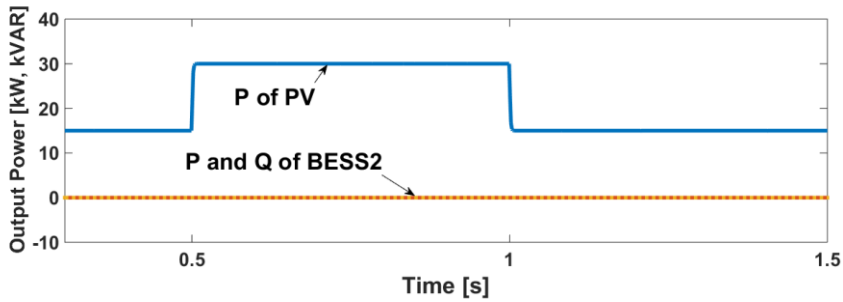

Fig. 4.13 Active power of PV system and BESS without droop control.

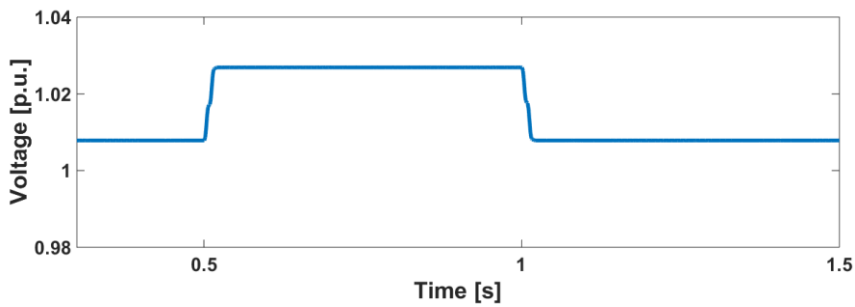

Fig. 4.14 Voltage at BESS and PV bus without droop control.

Fig 4.13 shows the output power of the PV system and the BESS without any droop control. The scheduled active and reactive power of BESS2 is 0 and the predicted value of the PV system is 15 kW. The active power deviation of the PV system is occurred during between 0.5 and 1.0 s. As a result, the voltage at BESS and PV bus is increased approximately about 0.02 pu as shown in Fig. 4.14. This voltage rising effect ensures that the active power and voltage are closely correlated in low voltage networks.

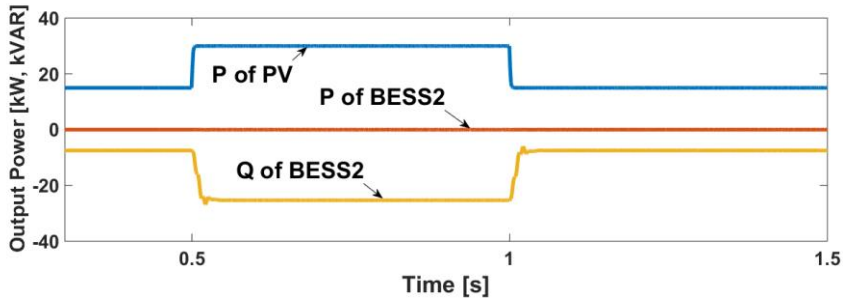

Fig. 4.15 Active power of PV system and BESS with *V*–*Q* droop control.

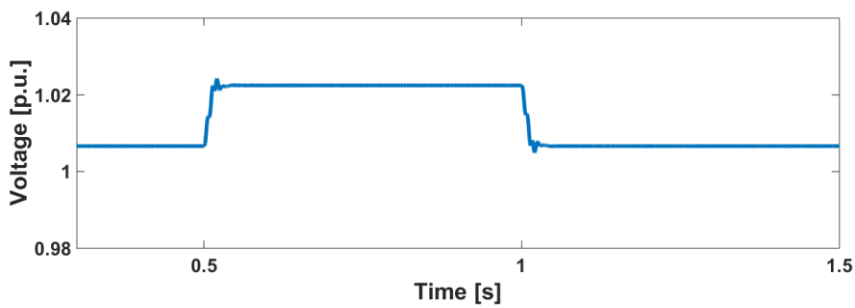

Fig. 4.16 Voltage at BESS and PV bus with *V*–*Q* droop control.

Fig. 4.15 shows the output power of the PV system and BESS with conventional *V*–*Q* droop control to mitigate voltage deviation. Based on [64] that recommends to determine $1/m_{VQ}$ as a value between 0 and 25, $1/m_{VQ}$ is determined as 25. As a result, the voltage deviation is barely prevented as shown in Fig. 4.16. The amount of voltage deviation is similar to the control method without any droop control (see Fig. 4.14) nevertheless *V*–*Q* droop is applied. This result ensures that reactive power and voltage are barely correlated in low voltage networks.

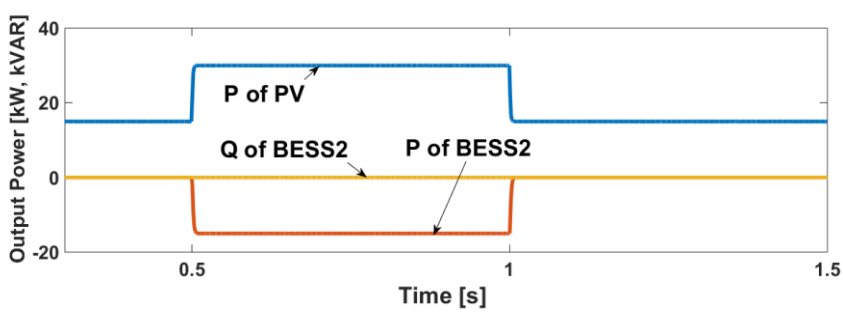

Fig. 4.17 Active power of PV system and BESS with *P*–*P* droop control.

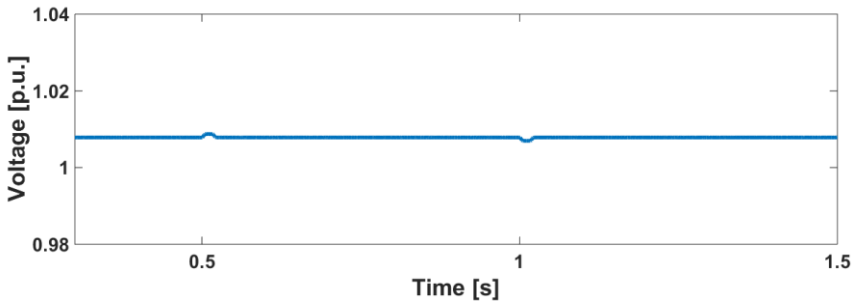

Fig. 4.18 Voltage at BESS and PV bus with *P*–*P* droop control.

Fig. 4.17 shows the output power of the PV system and BESS with *P*–*P* droop control to prevent voltage deviation due to the active power deviation of the RES (PV system). Since the assumption that the active power and the voltage are strongly correlated in low voltage networks is proved by simulations and (4.8), the BESS (BESS2) is attempted to compensate the active power exactly as much as amount of the PV system's active power deviation from the predicted value. As a result the voltage is well maintained at the level before the active power deviation occurred as shown in Fig. 4.18 though there are little bounces at 0.5 and 1.0 s. These bounces are due to time delays. Though the active power deviation of the PV system can be instantaneously sensed by the BESS, there are some time delays due to controllers and switching mechanisms of the inverter of the BESS. These time delays are simply modeled as a transfer function $(1/(sT_s+1))$ where T_s represents time delay and is 0.001 s in this study.

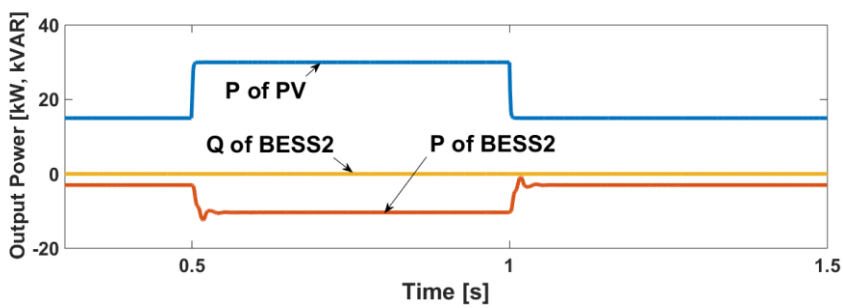

Fig. 4.19 Active power of PV system and BESS with *V*–*P* droop control.

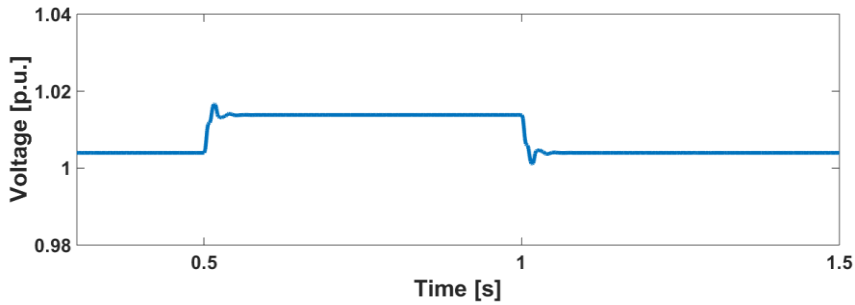

Fig. 4.20 Voltage at BESS and PV bus with *V–P* droop control.

Fig. 4.19 shows the output power of the PV system and BESS with *V–P* droop control for the case where the BESS is located far from the RES, though the BESS is connected at the same bus with the RES (PV system) to fairly compare its effectiveness with *P–P* droop control. The *V–P* droop coefficient is determined as same as that of *V–Q* droop. As a result, the voltage deviation is prevented, as shown in Fig. 4.20, more than those of by applying no droop (Fig. 4.14) or *V–Q* droop control (Fig. 4.16). But still, *P–P* droop control is the most effective for mitigating voltage deviation. Though the effectiveness is much weaker than that of applying *P–P* droop control, *V–P* droop control has an advantage over *P–P* droop control in the perspective of that it can be applied to BESSs and/or other controllable DG units located far from the RES.

The main disadvantage of *P–P* droop and *V–P* droop is that they may distort the SOC level from the pre-scheduled SOC value during the droop compensation. However, the SOC can be rescheduled after droop compensation and following the voltage regulation has ascendancy over the scheduling.

Chapter 5. Case Study

In this chapter, some case studies that prove the effectiveness of the control strategies developed in the chapters 3 and 4 will be discussed. Though some simple simulations were already tested in the previous chapters, in this chapter, case studies deal with more details and cases which were not tested in the previous chapters. The standalone microgrid networks and the controllers of DG units introduced in the previous chapters are used in this chapter.

5.1 Case 1 – Practical situation

Simulation settings for day time – Case 1-1

To see if the proposed control strategies work effectively and stably on a practical power system, Case 1-1 considers practical situation with real data (include line impedances, total load demand, power ratings of generation systems, wind speed, and solar irradiance) of the standalone microgrid. The standalone microgrid of 6.6 kV shown in Fig. 3.2 and the day time load demand shown in Table 3.1 are used. The controllers of the diesel generator, the BESS, and the RESs (PV and WT) are shown in Figs. 3.1, 3.4, and 4.1, respectively. In the day time of Ulleung Island, the wind speed ranges (varies) from 10.5 to 11.5 m/s and averages 11 m/s [65], [66]. The solar irradiance ranges from 600 to 720 W/m^2 and averages 660 W/m^2 [65], [66]. By using the average values of wind speed and solar irradiance as the forecasted value, P_{pre} (in Fig 4.3) of both WT and PV system are determined. Based on the data given, $1/m_{PQ}$ of the WT and PV system are calculated to be 0.413 and 0.495, respectively and $1/m_{VQ}$ of the WT and PV system are determined as 5 and 25, respectively. Three different control methods – without any droop controls (w/o droop), only with *f*–*P* and *V*–*Q* droop control for the BESS (conv.), constant frequency control for the BESS and *P*–*Q* plus *V*–*Q* droop control

for the RESs (prop.) – are tested to compare the frequency and voltage stability of each method during the fluctuation of output active power of RESs.

Simulation results and discussions – Case 1-1

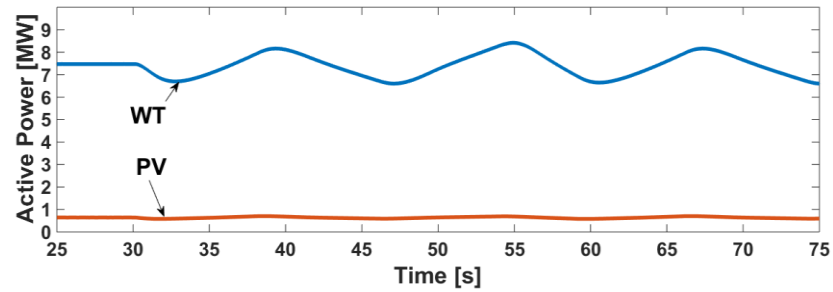

(a)

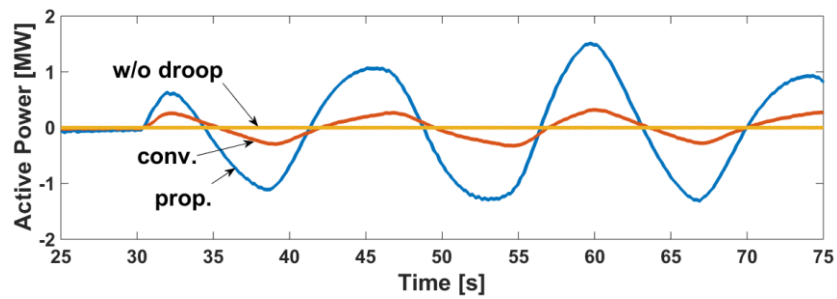

(b)

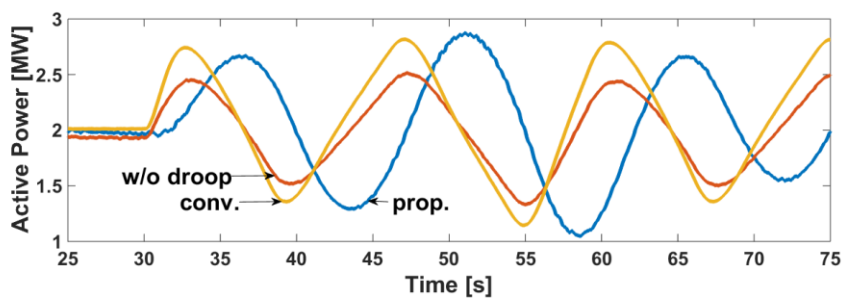

(c)

Fig. 5.1 Active power for Case 1-1. (a) PV system and WT. (b) BESS. (c) Diesel generator.

Fig. 5.1 shows the output active power of the PV system, the WT, the BESS, and the diesel generator for three different control methods. Without droop control,

the diesel generator takes full responsibility for the output fluctuations of the RESs, while the BESS supports the diesel generator with *f*–*P* droop control, although the diesel generator still strives to match the power demand. Conversely, the roles of the two power generations systems are exchanged if the proposed control method is applied. The BESS responds immediately to any output power fluctuations, whereas the diesel generator is used to maintain the SOC, thereby supporting the BESS.

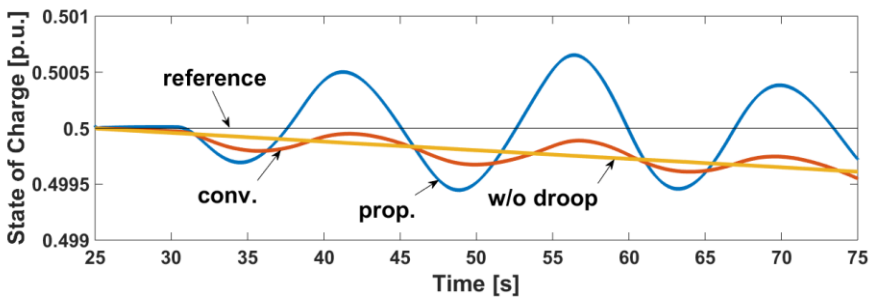

(a)

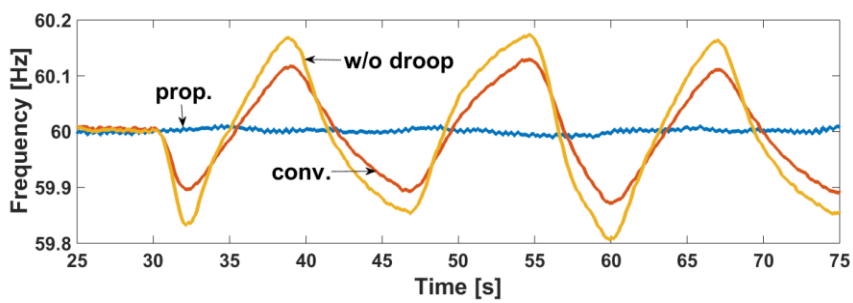

(b)

Fig. 5.2 SOC and frequency for Case 1-1. (a) SOC and its reference of the BESS. (b) Frequency.

Fig. 5.2(a) shows the SOC of the three control methods and the reference SOC for the proposed control method. There are the oscillations of the SOC around at the desired level in the proposed method. This is due to the slow dynamics of the diesel generator and the fluctuations of active powers of RESs. However, the SOC

can be stabilized to the desired (reference) level if there are no fluctuations of the active powers as it was already shown in Chapter 3. Without droop control, although the output active power of the BESS is close to 0 MW, the SOC decreases slightly due to small losses, such as the filter and inverter switching losses. By using the conventional control method, the SOC fluctuates as the BESS supports the diesel generator and its trend line is similar to that without the droop control. Nevertheless, although it fluctuates, the SOC is maintained at the reference value by using the proposed control method where the synchronous generator acts as the load–SOC control unit. As shown in Fig. 5.2(b), the frequency deviates from its nominal value without droop control. With conventional droop control, the deviation is mitigated, but is still not prevented completely. With these two control methods, the deviation and restoration of the frequency are dependent on the rotational speed and inertia of the synchronous generator. In comparison, with the proposed control method, the system frequency is generated by the BESS, which has rapid response characteristic and no mechanically rotating mass. Consequently, the frequency rarely deviates from its nominal value.

Figs. 5.3(a) and (b) show the reactive powers of the WT and the PV system, respectively. Without droop control, both WT and PV system have the same power factor, whereas by applying *V*–*Q* droop control, they control the reactive power to compensate the voltage deviation. By applying the proposed control method, the reactive powers of RESs are controlled not only for compensating the voltage deviation but also for mitigating the voltage fluctuation induced by their own active power fluctuations. In the case of PV system, there is little difference between the conventional droop control method and the proposed control method since the output active power fluctuation is not very large. By contrast, in the case of WT, the proposed control method outputs more reactive power than the conventional droop control method due to its large active power fluctuation.

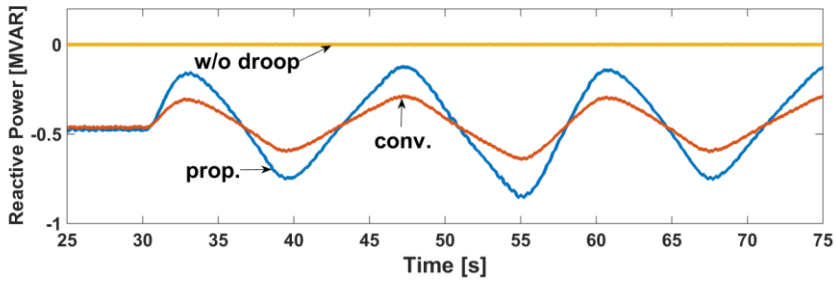

(a)

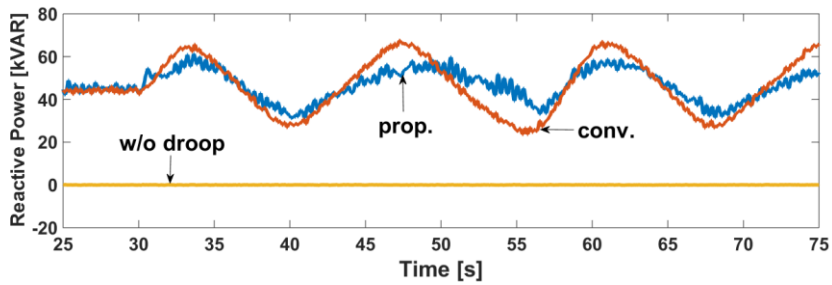

(b)

Fig. 5.3 Reactive power for Case 1-1. (a) WT. (b) PV system.

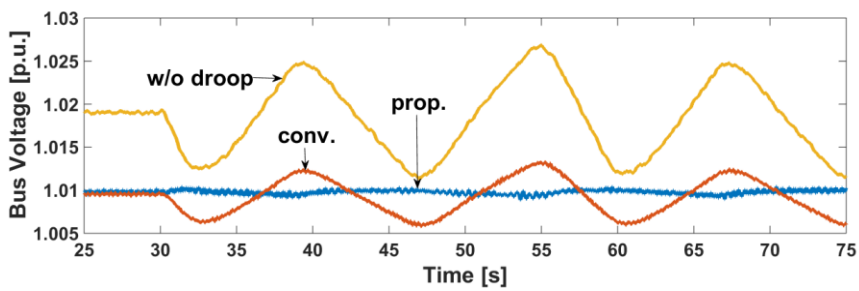

(a)

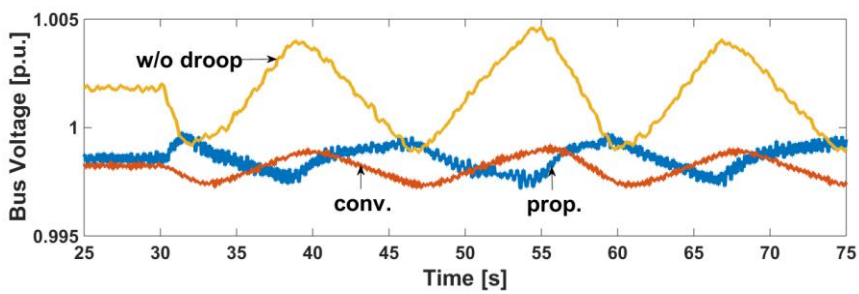

(b)

Fig. 5.4 Bus voltage for Case 1-1. (a) WT. (b) PV system.

Figs. 5.4(a) and (b) show the bus voltages of the WT and the PV system, respectively. This shows that by using the *V*–*Q* droop control, the bus voltage can be kept closer to the nominal value than without using the droop control. However, it cannot effectively prevent the voltage fluctuation incurred by the output power fluctuations. By adding *P*–*Q* droop control, the voltage fluctuation can be eliminated. While the mitigation of the PV system bus voltage fluctuation is negligible since its active power fluctuation is not very large, the WT bus voltage fluctuation is reduced dramatically. Therefore, it can be concluded that the proposed *P*–*Q* droop control of the RESs has a damping effect on the voltage fluctuation incurred by its own active power fluctuation.

Simulation settings for night time – Case 1-2

In this case (Case 1-2), the practical data of the night time are used. All the simulation settings are same as those of Case 1-1 except that the load data, wind speed, and solar irradiance of the night time are applied. In the night time of Ulleung Island, the wind speed ranges (varies) from 7.1 to 10.2 m/s and averages 8.5 m/s [65], [66]. The solar irradiance is 0 W/m^2 [65], [66]. Based on the data given, $1/m_{PQ}$ of the WT and PV system are calculated to be 0.473 and 0.514, respectively and $1/m_{VQ}$ of the WT and PV system are determined as 5 and 25, respectively.

Simulation results and discussions – Case 1-2

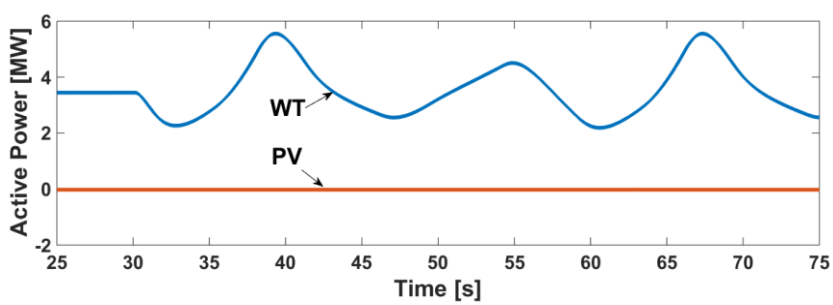

(a)

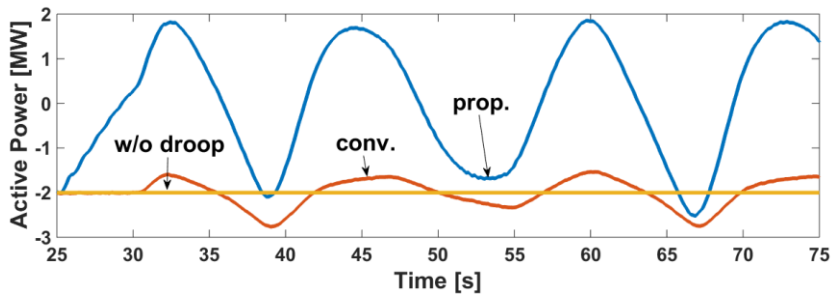

(b)

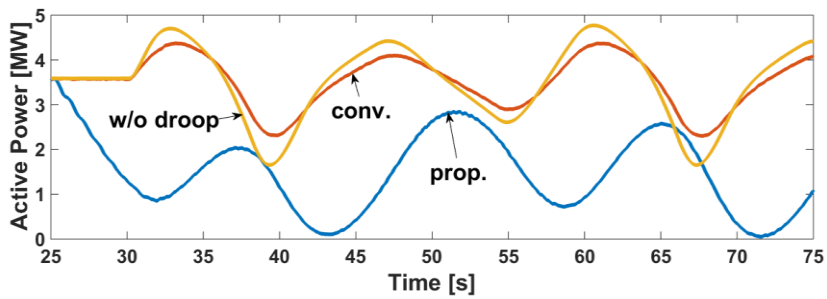

(c)

Fig. 5.5 Active power for Case 1-2. (a) PV system and WT. (b) BESS. (c) Diesel generator.

Fig. 5.5(a) shows the active powers of PV and WT. Wind speed begins to vary at 30 s and solar irradiance is 0 (at night time) and thereby the active power of PV system is 0. As shown in Fig. 5.5(b), at the beginning of the simulation, the BESS is set to charge 2 MW, since the total generation exceeds the load demand. The output power responses are similar to those of during the day, while the output power of the diesel generator tends to fall below its minimum (0 MW) at 43 and 71 s of the simulation time as shown in Fig. 5.5(c). Though the active power of diesel generator did not fall below its minimum value in this case, if it tends to happen, SOC_{ref} should be controlled to prevent it.

As shown in Fig. 5.6(a), the SOC level can be well maintained at the desired level by using the proposed control method while the others cannot. The frequency deviation becomes greater than that of during the day when applying the

conventional methods, whereas the proposed method maintains the frequency at the nominal value as shown in Fig. 5.6(b).

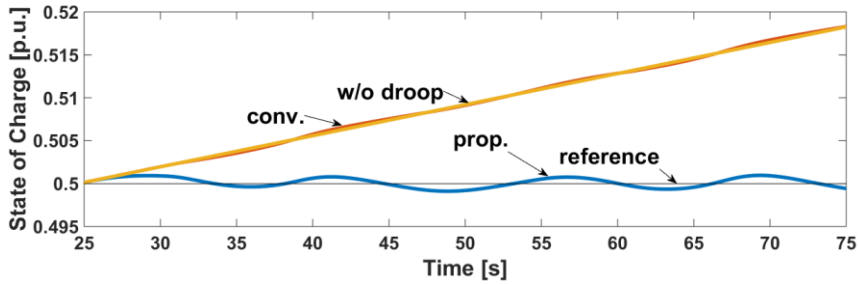

(a)

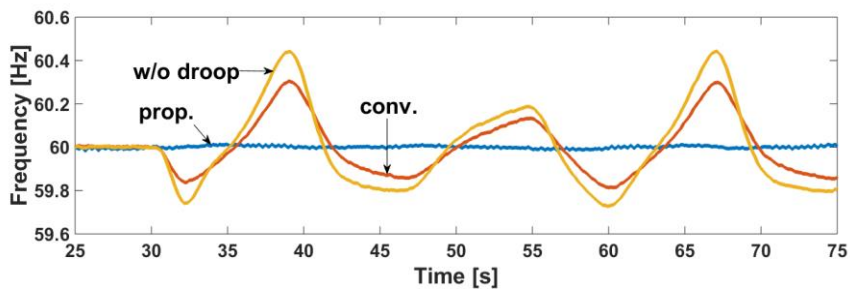

(b)

Fig. 5.6 SOC and frequency for Case 1-2. (a) SOC and its reference of the BESS. (b) Frequency.

Figs. 5.7(a) and (b) show the reactive power output of the WT and PV system, respectively. Since the output active power fluctuation of the WT is greater than that of during the day, more reactive power is compensated than during the day. By contrast, for the PV system, there is little difference between the conventional droop and the proposed control methods since the solar irradiance at night is 0 W/m^2.

Voltage fluctuation is prevented as shown in Fig. 5.8(a) despite the marked wind speed fluctuation compared to the day time. The bus voltage of the PV system differs little between the conventional and the proposed control methods since there is no solar irradiance.

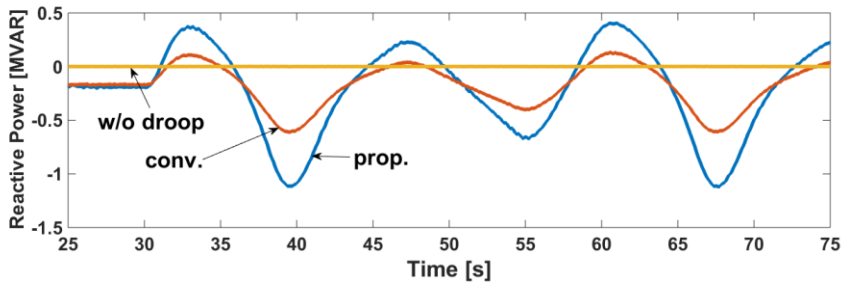

(a)

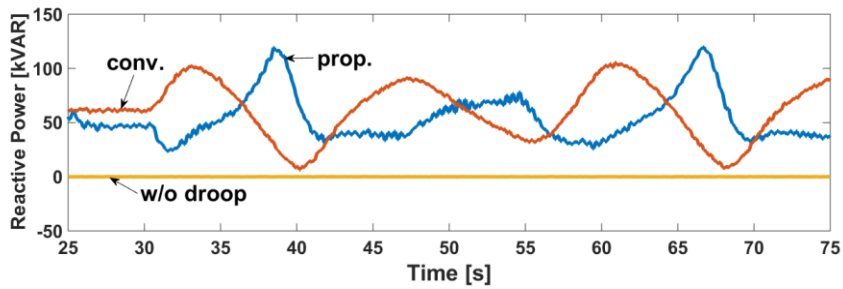

(b)

Fig. 5.7 Reactive power for Case 1-2. (a) WT. (b) PV system.

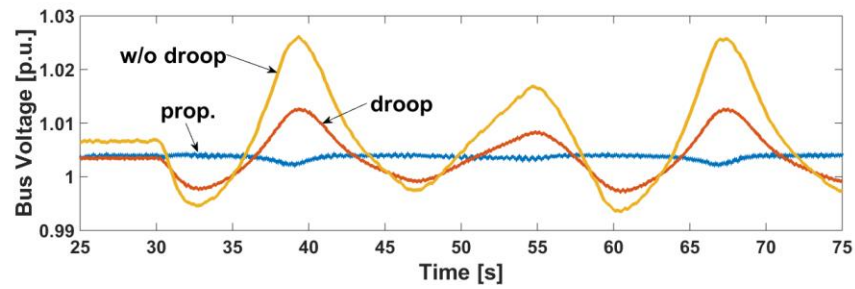

(a)

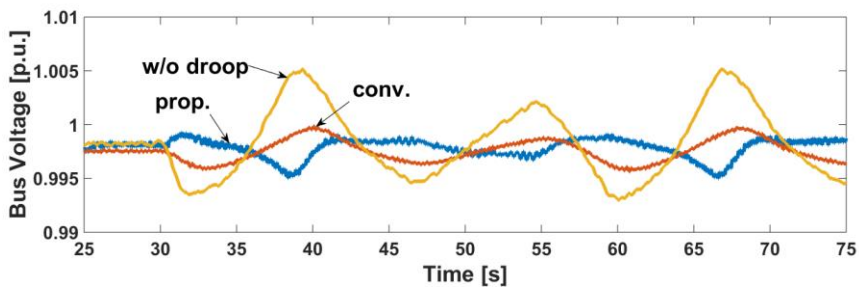

(b)

Fig. 5.8 Bus voltage for Case 1-2. (a) WT. (b) PV system.

5.2 Case 2 – Worst case

This case study deals with the case where wind speed and solar irradiance vary from 0 to the rate value in order to account for the worst scenario that could happen to the RESs and thereby to prove that the system can be stably operated even in the worst case.

Simulation settings – Case 2-1

The basic simulation settings are same with Case 1 except wind speed and solar irradiance. Wind speed varies from 3 to 12 m/s and solar irradiance varies from 0 to 1000 W/m^2. Since solar irradiance has to be considered, the load demand is same as the day time.

Simulation results and discussions – Case 2-1

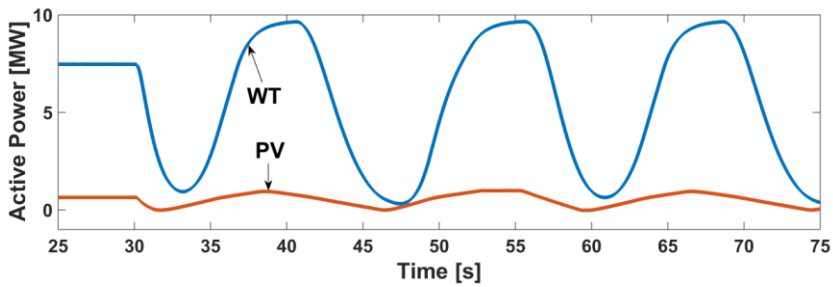

(a)

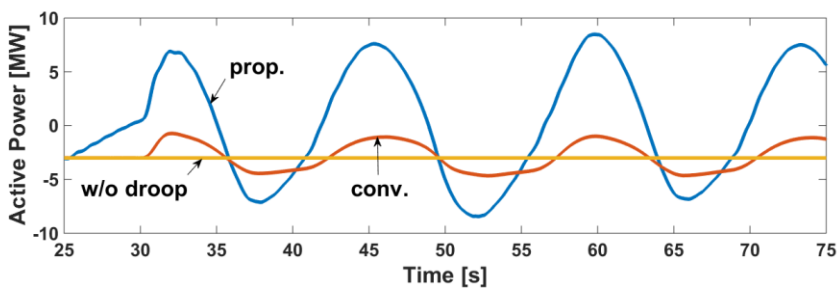

(b)

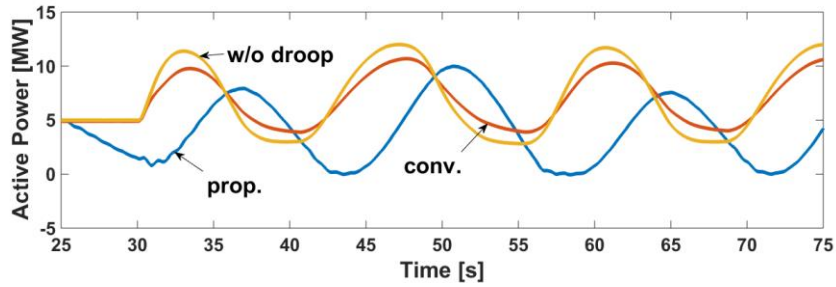

(c)

Fig. 5.9 Active power for Case 2-1. (a) PV system and WT. (b) BESS. (c) Diesel generator.

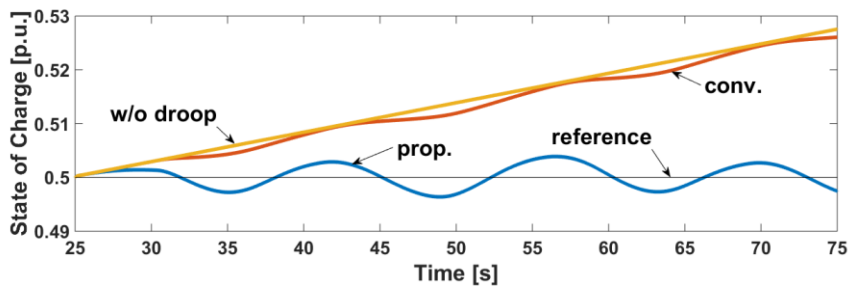

(a)

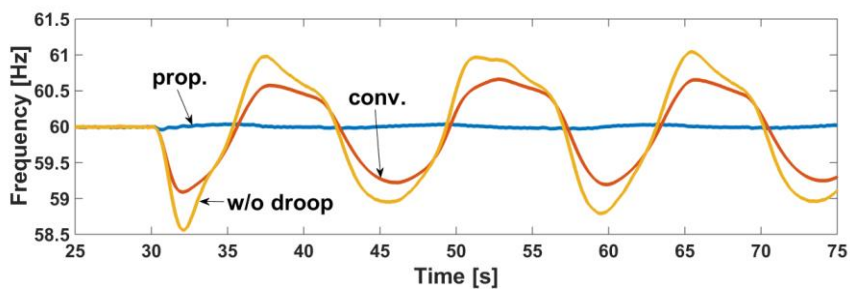

(b)

Fig. 5.10 SOC and frequency for Case 2-1. (a) SOC and its reference of the BESS. (b) Frequency.

As shown in Fig. 5.9(a), the active powers of the WT and the PV system are vary from 0 to the rating power. Figs. 5.9(b) and (c) show the active powers of the BESS and the diesel generator, respectively. Due to severer fluctuation of wind

speed and solar irradiance than those of Case 1, the active power of the BESS and the diesel generator as well as the SOC (see Fig. 5.10(a)) fluctuates more than those of Case 1. Nevertheless, the frequency is tightly maintained at the nominal value still as shown in Fig. 5.10(b).

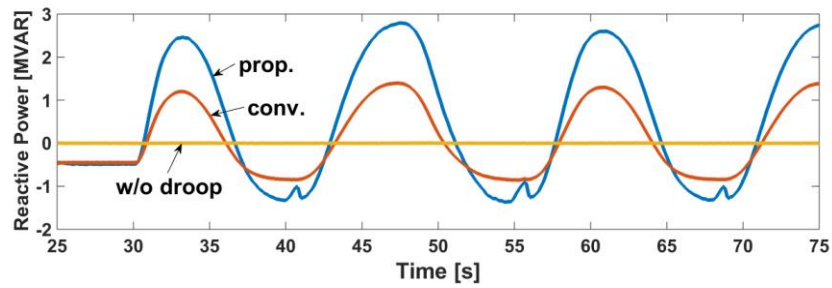

(a)

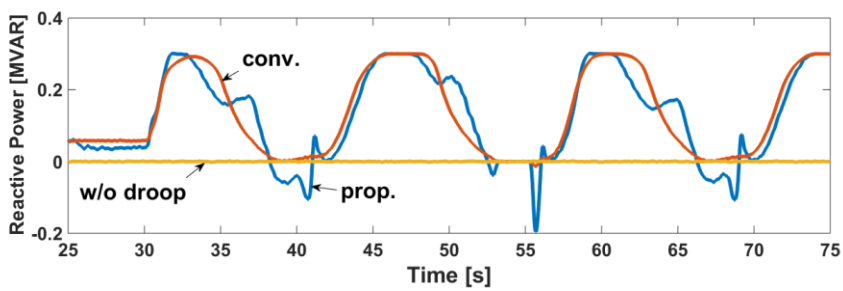

(b)

Fig. 5.11 Reactive power for Case 2-1. (a) WT. (b) PV system.

Figs. 5.11(a) and (b) show the reactive power of the WT and the PV system, respectively. In the proposed methods, there are several points where the reactive powers of the WT and PV system are limited according to (4.2). They are occurred at around 41, 56, and 68 s of the simulation time as shown in Fig. 5.11. As a result that can be shown in Fig. 5.12, at these points, there are little bounces of voltage and the voltage magnitude becomes same with that of applying the conventional method, but overall, the proposed method performs better than the others still. It can also be noticed that the voltage control performance by the proposed control method at the PV system bus is noticeably improved compared to Case 1 though

the improvement seems not absolutely effective. Moreover, this case study ensures that even if the output active power of the RES largely deviates from the forecasted value, the voltage fluctuation is effectively mitigated. This is reasonable result since that the sensitivity matrix, which determines *P*–*Q* droop coefficient, is dominantly influenced by the line impedance instead of active/reactive power of each bus. Note that *P*–*Q* droop coefficients for day time (0.413 for WT, 0.495 for PV) and night time (0.473 for WT, 0.514 for PV) have a little difference.

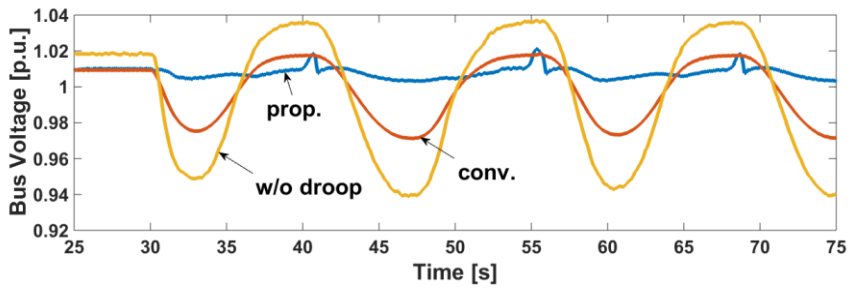

(a)

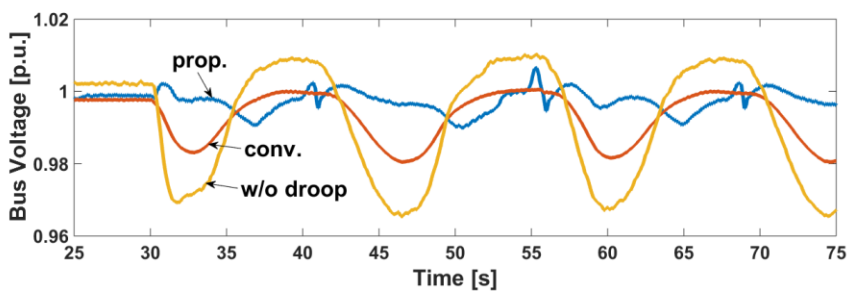

(b)

Fig. 5.12 Bus voltage for Case 2-1. (a) WT. (b) PV system.

Simulation settings – Case 2-2

In Case 2-1, one 14-MW diesel generator is operated in the standalone microgrid. However, as discussed in Chapter 3.1.4, there are two or more generators at the power plant commonly. Hence, the case that two diesel generators are installed at the same bus is examined in this case and the effectiveness of the control method proposed in Chapter 3.1.4 is proved. The simulation environment is

as same as Case 2-1 except that two 7-MW diesel generators are installed instead of one 14-MW diesel generator.

Simulation results and discussions – Case 2-2

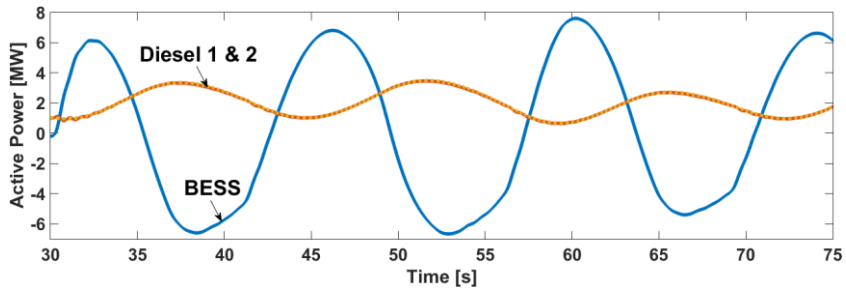

(a)

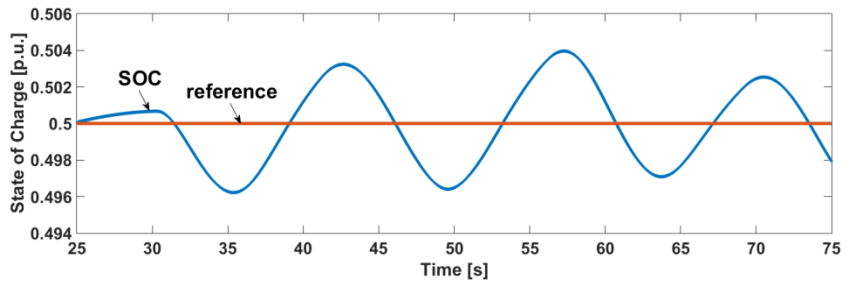

(b)

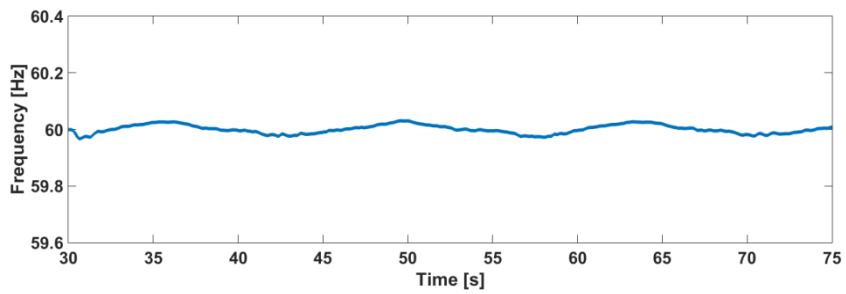

(c)

Fig. 5.13 Simulation results for Case 2-2. (a) Active power. (b) SOC. (c) Frequency.

Fig. 5.13 shows the simulation results for Case 2-2. As shown in Fig. 5.13(a), the BESS responds to the RES's output change and the diesel generators respond to the change of SOC. Two diesel generators share exactly same amount of active power with each other since the ratio of k_p and k_i (see Fig. 3.16) gains among two

generators are set to 1:1. Hence, it can be concluded that the active power sharing among synchronous generators can be implemented by the proposed control method (SOC-based active power sharing) just as same as the conventional frequency droop control method. Though there are some fluctuations in the SOC (due to slow response speed of the diesel generator and the large fluctuation of output of the RESs), the SOC and the frequency can be maintained steadily as shown in Figs. 5.13(b) and (c).

5.3 Case 3 – Reactive power control of BESS and DGs

From Fig. 5.11(a), it can be noticed that the reactive power of WT is limited the maximum active power output. As a result, the voltage fluctuation is occurred as shown in Fig. 5.12(a). This voltage fluctuation can be mitigated by the proposed control method in Chapter 4.1.2.

Simulation settings

The simulation environment is as same as that of Case 2 except that the reference voltage magnitude of the diesel generator and the BESS are substituted by that in Fig. 4.2(a). Two control methods – the BESS and the diesel generator do not support the reactive power control of the WT (w/o. support) and the BESS and the diesel generator support the reactive power control of the WT (w. support).

Simulation results and discussions

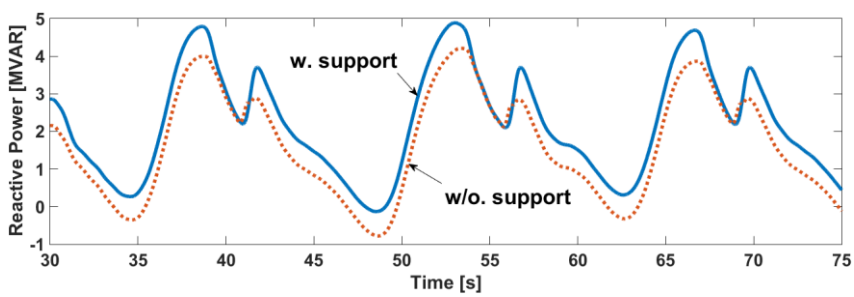

(a)

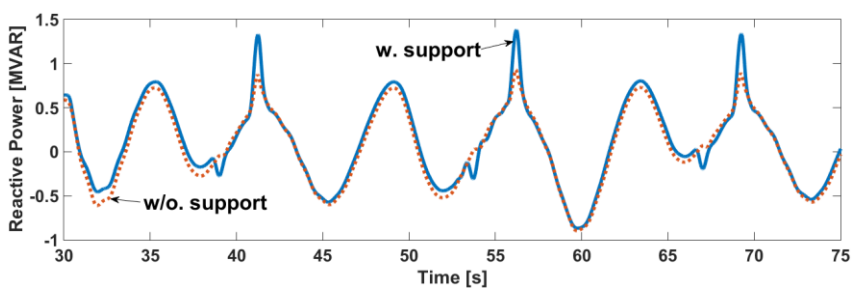

(b)

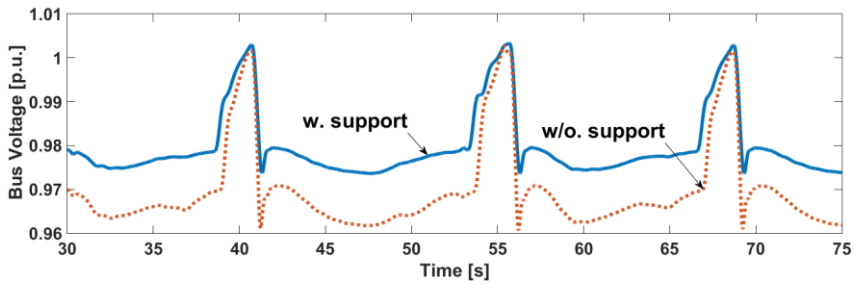

(c)

Fig. 5.14 Simulation results for Case 3. (a) Reactive power of diesel generator. (b) Reactive power of BESS. (c) Bus voltage of WT.

Fig. 5.14 shows the simulation results for Case 3. By using coordinated control method (w. support) of the BESS and the DGs (the diesel generator and the WT), more reactive power is injected to the grid than the case of the BESS and the diesel generator do not support the WT (w/o. support) as shown in Figs. 5.14(a) and (b). Particularly, the reactive power support from the BESS and the diesel generator is noticeable at the points where the reactive power of the WT is limited (at 40, 55, 68 s). As a result, the voltage fluctuation at the WT bus is mitigated by adopting w. support method as shown in Fig. 5.14(c).

5.4 Case 4 – Small active power fluctuation

Through Cases 1 and 2, it can be noticed that the proposed voltage control strategy performs well for the WT bus whereas it barely affects the PV system bus. A major reason for this is because that the active power fluctuation of the WT is much larger than the PV system. So this case considers the active power fluctuation of the PV system only while the WT outputs constant power to make sure that the proposed voltage control strategy also positively affects the PV system bus.

Simulation settings

The simulation settings for this case are exactly same as that of Case 2 except that the wind speed is at its average value (11 m/s) constantly.

Simulation results and discussions

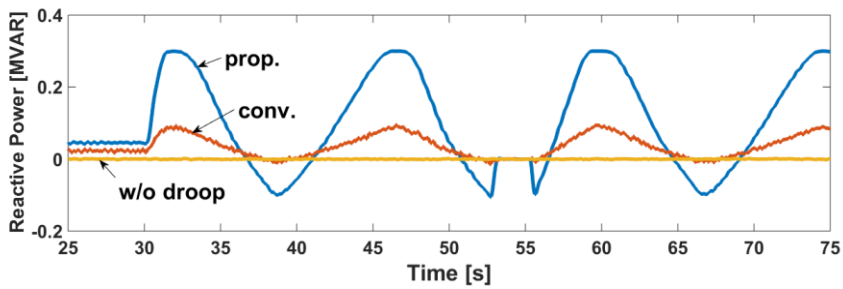

Fig. 5.15 Reactive power of PV system for Case 4.

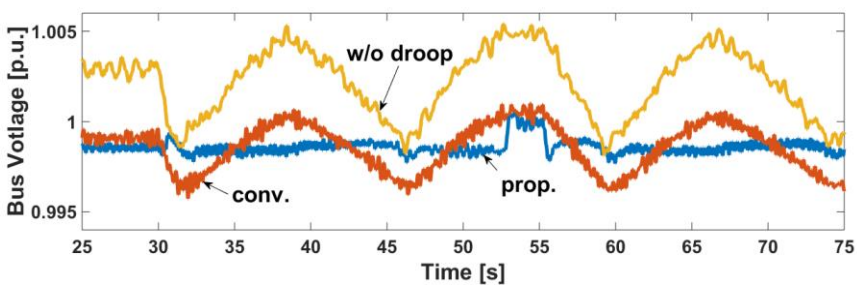

Fig. 5.16 Bus voltage of PV system for Case 4.

Since this case is only for proving the effectiveness of the proposed voltage control strategy at the PV system bus, the simulation results only show the reactive power and the voltage of the PV system as shown in Figs. 5.15 and 16. As shown in Fig. 5.15, the reactive power is compensated more than the other methods except at the moment around 53–56 s where the reactive power is limited according to (4.2). It can be noticed that the active power of the PV system is at the maximum value (1 MW) as shown in Fig. 5.9(a). By using the proposed control method and without any voltage disturbance by the WT, the voltage fluctuation is well prevented compared to the other methods though the bus voltage has similar value with that of the method adopting conventional *V*–*Q* droop at around 53–56 s.

5.5 Case 5 – Tripping of the BESS

One of advantages of using a synchronous generator as a grid-forming source is the characteristic that it can maintain a grid for a while after it trips out from a grid due to some disturbances such as faults. This is possible because a synchronous generator has a rotational mass (a rotor) with inertia. However, an inverter-interfaced BESS has no inertial mass that keeps rotating (generating AC voltage) after a trip event. This case deals with the event that the BESS is tripped out from the grid and provides a simple solution.

Simulation settings

The simulation test is applied to the standalone microgrid shown in Fig. 3.2 and the simulation settings are same as Case 1-1 except that the RESs are assumed to output constant power. After tripping of the BESS, any controllable source has to replace the role of the BESS. To this end, the controller of the diesel generator, which is the only controllable source in the studied standalone microgrid, should be modified from that of shown in Fig. 3.4 with the incorporation of mode change function. The modified controller of the diesel generator is shown in Fig. 5.17.

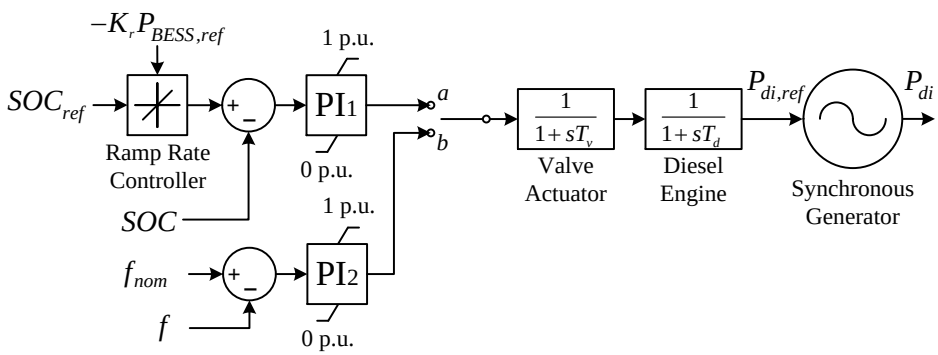

Fig. 5.17 Modified controller of the diesel generator [23].

As shown in Fig. 5.17, the ramp rate controller, load–frequency controller

(PI_2), and the switch with node *a* and *b* is included in the controller. The function of the ramp rate controller will be discussed in the next section. During normal operation, the switch shown in Fig. 5.17 is connected to node *a* and hence the diesel generator is controlled to maintain the SOC at the reference value SOC_{ref} as described in Chapter 3. Since the system frequency entirely depends on the BESS in this control strategy, the reliability problem may be raised due to tripping event of the BESS. To prevent this problem, the switch connection is changed from node *a* to *b* when the BESS tripped out from the system. During the switch is connected to node *b*, the diesel generator is controlled as same as the conventional one. Since the BESS and the diesel generator are connected to the same bus, it is assumed that the tripping of the BESS can be instantaneously sensed by the diesel generator controller. Hence, the transition of the diesel generator's control mode is able to be operated as soon as the BESS trips out.

Simulation results and discussions

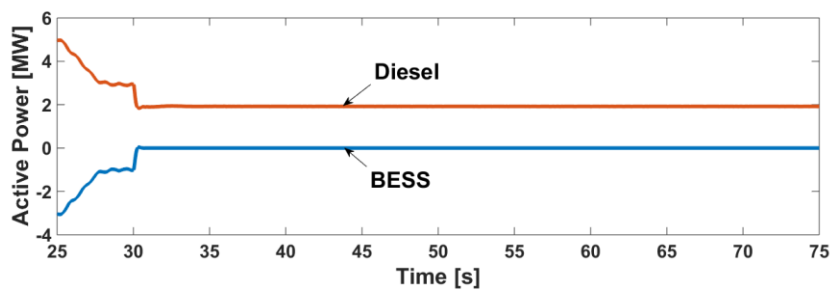

Fig. 5.18 Active power of the BESS and the diesel generator for Case 5.

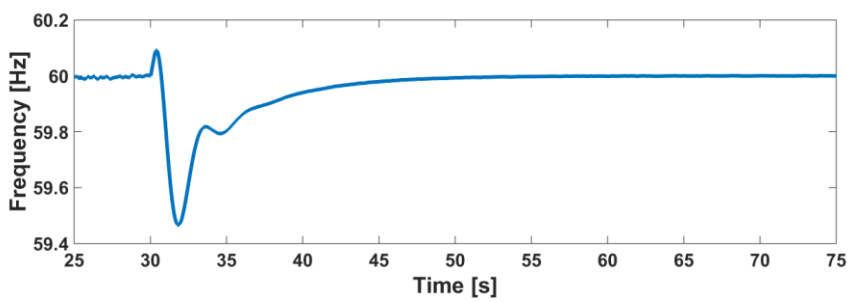

Fig. 5.19 Frequency for Case 5.

Figs. 5.18 and 5.19 show the simulation results for the case of tripping of the BESS. If the BESS is tripped out from the system at 30 s of the simulation time as shown in Fig. 5.18 due to cases such as a fault, a maintenance, and etc., the diesel generator changes its operation mode by changing its switch (see Fig. 5.17) from node *a* to *b*. As a result, the active power of the BESS becomes 0 and the active power of the diesel generator is decreased as shown in Fig. 5.18. The time delay between the tripping of the BESS and the switch transition is ignored in this study. Even if the time delay exists, it may be very short, since the diesel generator is in the vicinity of the BESS, to influence the system stability harmfully. The switch transition to node *b* makes the diesel generator to operates as same as that of using the conventional isochronous governor. Consequently, the frequency behaves as same as the conventional method as shown in Fig. 5.19. Though this control strategy make the standalone microgrid operates as same as the conventional one, it enhances the system reliability against the tripping event of the BESS.

5.6 Case 6 – Adjusting active power reference of the BESS

Typically, the main objective of the BESS is not forming the grid by controlling voltage but feeding the grid by controlling output power. With the proposed control method (see Fig. 3.1), the output active power of the BESS cannot be controlled to output desired level. For instance, the active power reference is not provided to the BESS controller (see Fig. 3.1). To overcome this problem, the ramp rate controller shown in Fig. 5.17 is incorporated into the controller of the diesel generator. With this controller, the feasibility of controlling active power of the BESS is investigated in this section.

Simulation settings

The simulation settings for this case are same with those of Case 5 except that the BESS is not tripped out from the system. The standalone microgrid shown in Fig. 3.2 is used and the RESs output constant power. Since there is only one active power controllable unit (the diesel generator) in the standalone microgrid, the active power of the grid-forming unit (the BESS) can be controlled indirectly by controlling the active power of the diesel generator. However, the diesel generator controls the SOC level as shown in Fig. 5.17. Hence, the ramp rate of the SOC is controlled instead of the active power. This is possible since the active power is proportional to the derivative of the SOC as can be noticed in (3.12). From (3.12), since K_r is the constant value, the ramp rate of the SOC can be controlled by adjusting P_{BESS} (which is $P_{BESS,ref}$ in Fig. 5.17) as a control variable. For example, when the BESS needs to be discharged with 1 MW output, the ramp rate controller operates as the following procedure:

- Set $P_{BESS,ref}$ = 1 MW.
- Decrease SOC_{ref} lower than the current value.
- This newly set SOC_{ref} can be determined by the operator.
- The output active power becomes 1 MW until the current SOC level

meets the newly set SOC_{ref} and then becomes 0 MW.

In case of charging, SOC_{ref} should be increased. With this control method, the output active power of the BESS can be controlled indirectly and simultaneously, the BESS can be controlled as the grid-forming unit.

As mentioned in the previous section, the capacity of the BESS is scaled down to 1/20 of its practical value, 30 MWh, in the simulation to illustrate the change in the SOC clearly.

Simulation results and discussions

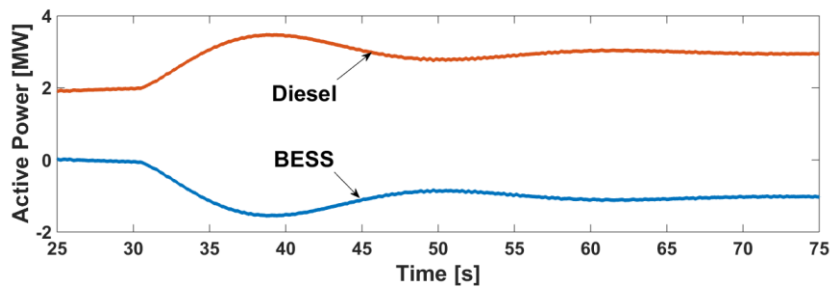

(a)

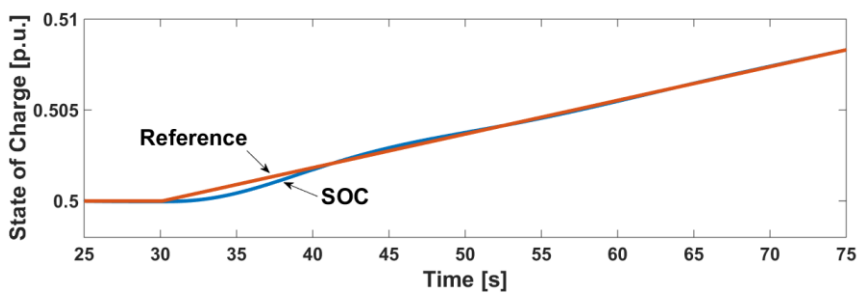

(b)

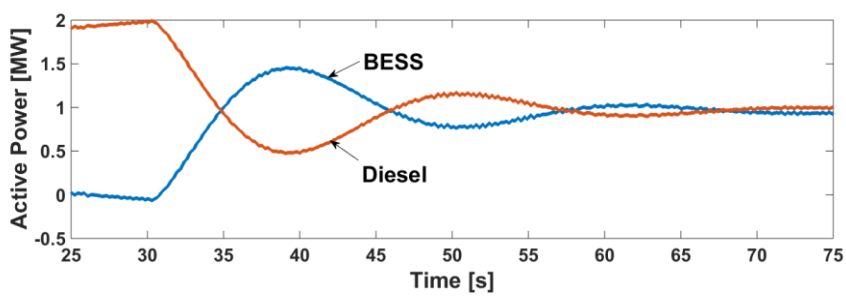

(c)

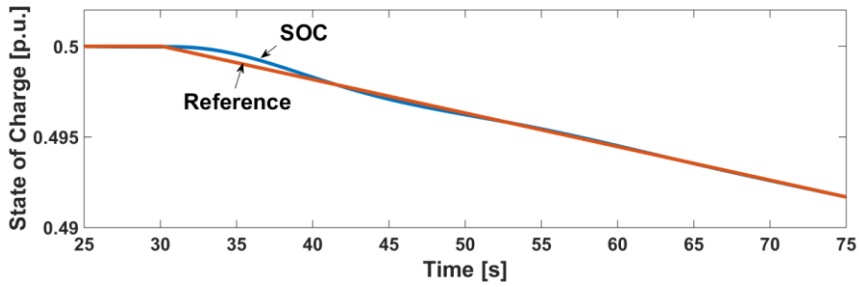

(d)

Fig. 5.20 Active power and SOC for Case 6. (a) Active powers of the BESS and the diesel generator during charging. (b) SOC and its reference of the BESS during charging. (c) Active powers of the BESS and the diesel generator during discharging. (d) SOC and its reference of the BESS during discharging.

Figs. 5.20(a) and (b) show the simulation results for charging case and Figs. 5.20(c) and (d) show the results for discharging case. In the beginning of the simulation, both cases begin with 2 MW output of the diesel generator and 0 MW of the BESS. In Fig. 5.20(a), the ramp rate of the SOC is adjusted for the BESS to charge 1 MW. As a result that can be shown in Fig. 5.20(b), the diesel generator increments its output power and the BESS outputs –1 MW of active power. Similarly, the ramp rate of the BESS is adjusted to discharge the BESS as shown in Fig. 5.20(c). Consequently, the diesel generator decrements its output and the BESS outputs 1 MW of active power. In this way, the BESS can be controlled to output any desired amount of active power indirectly by adjusting the SOC ramp rate controller which is included in the controller of the diesel generator.

5.7 Case 7 – Intermittent output active power

In Chapter 3.2.4, the case of load change in the standalone microgrid with multiple DG units (see Fig. 3.17) is tested. DG4, non-dispatchable (uncontrollable) DG unit, is considered to output constant power in Chapter 3.2.4 though its output power may be intermittently changed. This case study deals with the situation of that the output active power of DG4 changes intermittently.

Simulation settings

The simulation settings are same with that of Chapter 3.2.4 except that there is no load change and that the output active power of uncontrollable DG unit (DG4) fluctuates. The fluctuation starts at 1 s. Two control methods are compared with each other where the conventional method (conv.) adopts *P–f* droop and *f–P* droop control and the proposed control method (prop.) adopts the method developed in Chapter 3.2.4. The applied control method at each unit is listed in Table 3.4.

Simulation results and discussions

Figs. 5.21(a) and (b) show active powers of the conventional method and the proposed method, respectively. As can be seen from Fig. 5.22(a), the SOC can be maintained at the desired level in the proposed method whereas it cannot be in the conventional method.

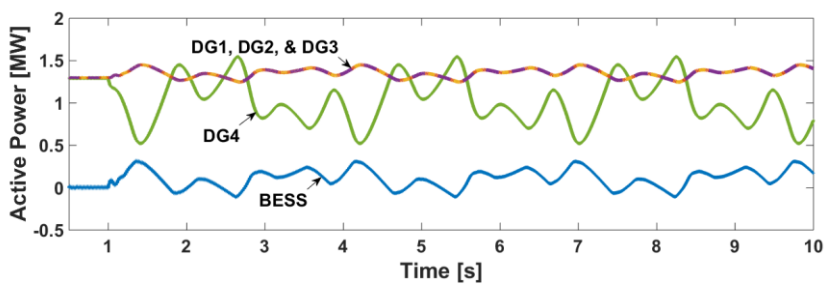

(a)

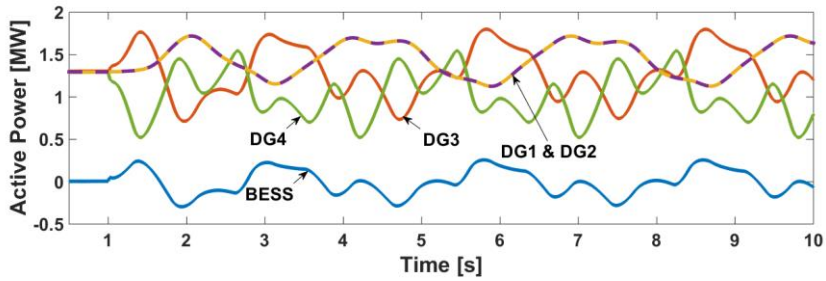

(b)

Fig. 5.21 Active power for Case 7. (a) Conventional method. (b) Proposed method.

Moreover, the frequency also can be maintained at the nominal value in the proposed method as shown in Fig. 5.22(b) while it cannot be in the conventional method. Consequently, the proposed method performs as purposed for both situations of load change and output fluctuation in the perspective of maintaining the SOC and the frequency simultaneously.

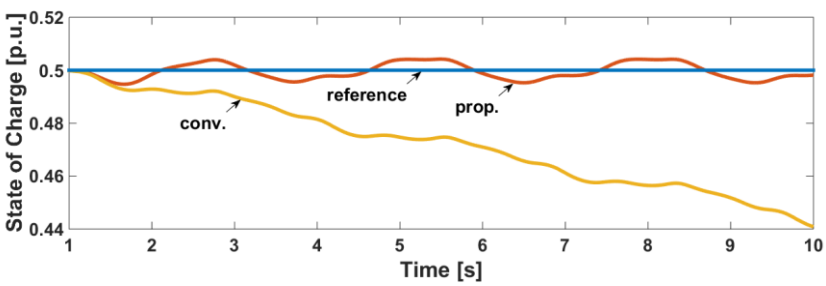

(a)

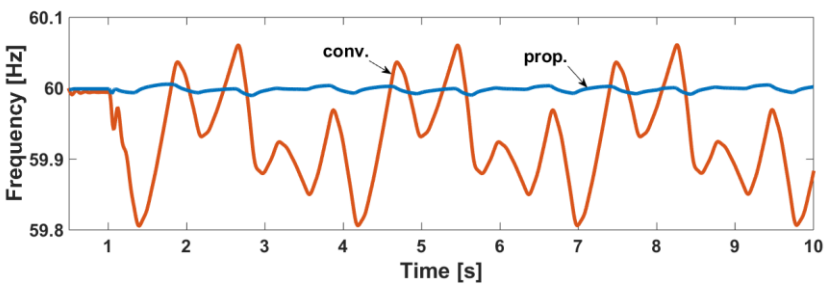

(b)

Fig. 5.22 SOC and frequency for Case 7. (a) SOC. (b) Frequency.

5.8 Case 8 – Communication system failure

This case deals with the standalone microgrid system composed of multiple controllable DG units. In this standalone microgrid system, as developed in Chapter 3.2.1 (see Fig. 3.17), the communication system is indispensable for adopting the proposed control strategy. The effectiveness of the proposed control strategy is already proved in Chapter 3.2.4 though the reliability problem that may be caused by communication system (a microgrid CC) failure is still remained. To cope with communication failure and thereby enhance system reliability, the controller of the BESS (see Fig. 3.1) is slightly modified in this section.

Simulation settings

The studied standalone microgrid and the simulation settings are same with that of Chapter 3.2.1 (see Fig. 3.17) except that the communication system fails at 1.6 s of the simulation time and that the controller of the BESS is modified as shown in Fig. 5.23 where m_P is a droop coefficient and is set to 0.01 in this study.

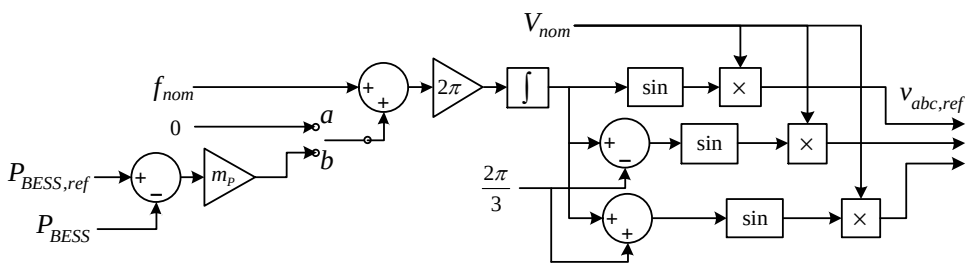

Fig. 5.23 Modified controller of the BESS

As shown in Fig. 5.23, the switch with node *a* and *b* is newly incorporated into the controller compared to the controller in Fig. 3.1. During normal operation, the switch is connected to node *a* which operates the proposed constant frequency control method whereas during abnormal operation of communication system

failure, the switch is connected to node *b* which operates the conventional *P–f* droop control. The time delay between the communication system failure and the switch mode transition from *a* to *b* is neglected in this study.

Simulation results and discussions

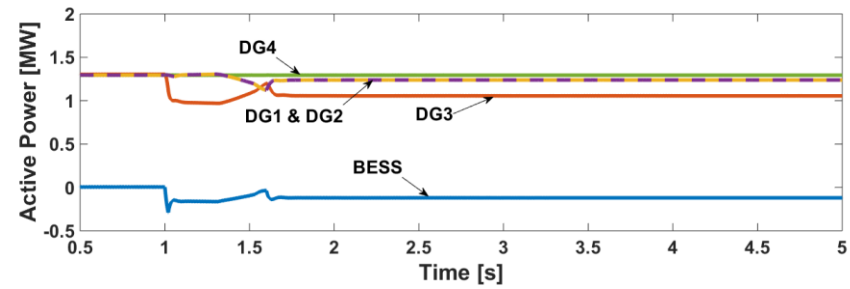

(a)

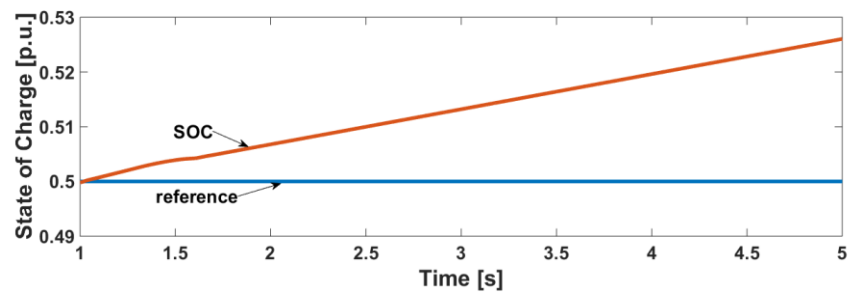

(b)

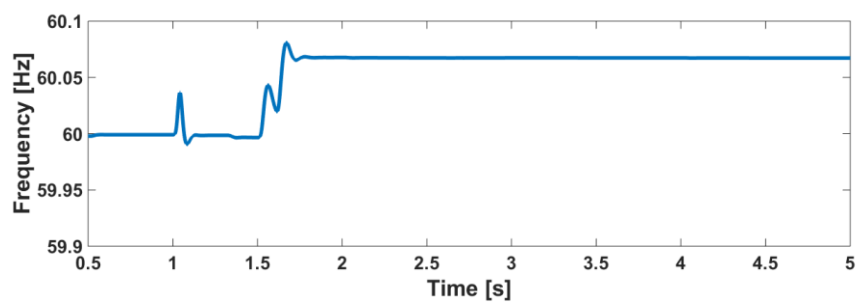

(c)

Fig. 5.24 Active power, SOC, and frequency for Case 8. (a) Active power of each unit. (b) SOC and its reference. (c) Frequency.

Fig. 5.24(a) presents the active powers of the BESS and DG units. After the

load change event at 1.0 s, the active power is shared according to the proposed method (primary and secondary SOC control) based on the SOC. As the communication system fails at 1.6 s, the switch shown in Fig. 5.23 is changed from node *a* to *b* and thereby the active power is shared as same as the conventional method (*P*–*f* droop for the BESS and *f*–*P* droop for DG1 and DG2). Note that the *f*–*P* droop control shown in Fig. 3.20 is incorporated to the controller to cope with this case. DG3 is controlled as shown in Fig. 3.19 and thereby compensates active power as much as the amount of active power deviation of the BESS from 0. DG4 is non-dispatchable (uncontrollable) unit as explained previously. The SOC cannot be maintained at the desired level as can be seen in Fig. 5.24(b). Also, the frequency cannot be maintained at the nominal value as shown in Fig. 5.24(c). Though the SOC and frequency cannot be maintained, the proposed method enhances the system reliability during the communication system failure with a change of the BESS control mode. Note that the other DG units do not need any change of control mode.

Chapter 6. Conclusions and Further Studies

6.1 Conclusions

This dissertation presents the control strategies for a standalone microgrid which has low inertia and weak grid characteristics to enhance voltage and frequency stability.

This study is motivated by the growth of energy self-supporting islands (e.g., Samso Island, Ulleung Island), microgrids, RESs, DGs, and BESSs. Especially, energy self-supporting islands inevitably need to be fostered as a form of a standalone microgrid. In this dissertation, a standalone microgrid represents an autonomous islanded microgrid that is permanently disconnected from a main grid due to economical and/or geographical factors (e.g., islands, mountains).

There are two major factors among the grid code requirements that have to be regulated properly in operation of power systems. One of them is the frequency which is typically correlated with active power in conventional power systems. A deviation of the frequency from its nominal value is occurred when active power mismatch between supply and demand happens. The other is the voltage magnitude which is typically correlated with reactive power in conventional power systems. Due to these relationships, P–f (and/or f–P) droop and Q–V (and/or V–Q) droop controls are usually applied to standalone microgrids in order to emulate conventional power systems. However, the conventional droop control methods are suitable to power systems including large synchronous generators with large inertia and mainly inductive line parameters which do not correspond to standalone microgrids. For standalone microgrids, which have low inertia and weak grid, novel control strategies need to be developed.

In the frequency control perspective, decoupling of the frequency and the inertia (rotational mass of synchronous generators) is proposed. The BESS, instead

of the diesel generator, forms the constant grid voltage and frequency without any droop control. The BESS is inverter-interfaced device which can instantaneously change output voltage angle so that the frequency is hardly changed. However, without frequency droop, active power mismatch in the system cannot be noticed by other generation units. In the proposed method, the SOC, instead of the frequency, is used to notice active power mismatch. Since the BESS is employed as the only grid-forming unit, maintaining the SOC at the desired level is of paramount importance.

The ways of maintaining the SOC is classified into two categories. One is used when the proposed method is applied to a standalone microgrid with a single controllable generation unit. In this type of standalone microgrid, uncontrollable DG units can be seen as negative loads and the net active power mismatch can be presented by change of the SOC. The only controllable DG unit plays a role of load–SOC control unit, which emulates load–frequency control unit of conventional power systems, in order to maintain the SOC to the desired level. This controllable generation unit should be installed in the vicinity of the BESS in order to measure the SOC data without communication time delay. In addition to SOC-maintaining function, the controllable generation unit can also control for the BESS to output constant active power indirectly by adjusting ramp rate of the SOC reference. Moreover, to enhance system reliability, the controllable generation unit is able to switch its control mode to the conventional frequency droop right after the BESS is tripped out from the system due to accidents such as faults.

The other method of maintaining the SOC is used when the proposed method is applied to a standalone microgrid with multiple controllable generation units. One of the controllable DG units acts as primary SOC control unit which compensates active power as much as the amount of deviation of active power of the BESS. To this end, the primary SOC control unit should be installed in the vicinity of the BESS in order to measure the SOC data without communication time delay. The other controllable DG units act as secondary SOC control unit

which attempts to make zero SOC error by using PI controller. Thus, they also called as load–SOC control unit which is named after load–frequency control of conventional power systems. The secondary SOC control units are usually located far from the BESS hence they should receive the SOC data via communication system (a microgrid CC). The communication time delay is considered and the switching of control mode of the BESS is developed in order to improve the system reliability.

In the voltage control perspective, new droop concepts are proposed in order to mitigate voltage fluctuation (or deviation) caused by active power fluctuation (or deviation). Since relationship between voltage and active/reactive power is highly correlated with grid line parameters, proposed droop concepts are developed with respect to network voltage level.

For medium voltage network standalone microgrids, employing *P–Q* droop control, which is developed in this dissertation, to a RES is proposed to mitigate voltage fluctuation caused by active power fluctuation of a RES itself. Unlike conventional voltage control methods, which correlate voltage only with reactive power, *P–Q* droop control considers correlation between voltage and active power as well as reactive power. *P–Q* droop coefficient of each RES is properly determined by a sensitive matrix of a standalone microgrid. With this control method, each RES in a standalone microgrid can properly compensate reactive power where this reactive power compensation is limited not to disturb MPPT control scheme in order to maximize energy efficiency. Moreover, voltage damping effect can be observed by adopting *P–Q* droop control to RESs.

For low voltage standalone microgrids, *P–P* droop and *V–P* droop control methods are developed for a BESS to apply them to active power controller. Low voltage network standalone microgrids have mainly resistive line parameters, so voltage is highly correlated with active power instead of reactive power. Hence, active power of a BESS is controlled for voltage regulation. *P–P* droop control is for counterbalancing of a RES's active power deviation from its forecasted value.

The BESS adopting *P–P* droop control should be installed in the vicinity of the RES so that the BESS can measure the active power deviation of the RES directly. *V–P* droop control is developed to overcome the disadvantage of *P–P* droop control that the BESS should be installed in the vicinity of the RES. *V–P* droop control measures local voltage deviation and then adjusts active power based on the voltage deviation, so it can be applied to BESSs located far from the RES. Though, *P–P* droop control is much more effective than *V–P* droop control in the voltage control perspective.

To prove the effectiveness of the proposed control strategies, they are tested on three different standalone microgrids and are compared with the conventional control strategy. The simulation was modeled and tested by MATLAB/SimPowerSystems. By using the proposed control strategies, not only the frequency can be tightly held on to its nominal value but also the SOC of the BESS can be maintained at the desired value. The ramp rate controller of SOC is also developed in order to adjust the output active power level of the BESS indirectly. Moreover, the voltage fluctuation (or deviation) is dramatically mitigated in both low and medium voltage network standalone microgrids. By incorporating a switch that transits its control mode after fault or communication failure event, the system reliability is also improved.

By using the proposed control strategies, increased hosting capacity of intermittent RESs in standalone microgrids and increment of standalone microgrids themselves are anticipated.

6.2 Further studies

The proposed control strategies indeed enhance frequency and voltage stability of a standalone microgrid as shown in various simulation studies in the previous chapters. However, some problems still remain as further studies.

One of the further studies is that the proposed control strategy should test small-signal stability considering communication time delay. The proposed control strategy for a standalone microgrid with multiple controllable DG units needs communication system which inevitably accompanies time delay. Since the time delay influences the system stability [45], [46], small-signal analysis should be implemented on the proposed control strategy.

Another further study that should be considered is to suggest an alternative for improving system reliability while tripping of the BESS. In the proposed control strategy, a standalone operates as same as the conventional method after the BESS trips out from the system due to emergency such as faults. Returning to the conventional control method has no advantages in the frequency and voltage control perspectives.

Determining the PI controller gains of secondary SOC control units may be another further study. In this dissertation, the PI controller gains were arbitrarily determined to show that the secondary SOC control units share active power as per predetermined ratio (ratio among PI gains of secondary SOC controllers). However, they need to be determined with careful consideration, e.g. generation cost and power loss.

Finally, a way of sensing emergency events such as tripping of the BESS and communication failure should be investigated and developed. In this dissertation, the processes of sensing emergency events are assumed to be done automatically and instantaneously.

Bibliographies

[1] L.-Y. Chen, Y.-T. Yin, T.-Y. Ho, and Y.-Z. Chen, "Sensitized solar cells via nanomaterials: A recent development in quantum dots-based solar cells," *IEEE Nanotechnol. Mag.*, vol. 8, no. 2, pp. 16–21, Jun. 2014.

[2] B. Lasseter, "Microgrids [distributed power generation]," in *Proc. IEEE Power Engineer. Soc. Winter Meet.*, Columbus, OH, Jan. 2001, vol. 1, pp. 146–149.

[3] R. H. Lasseter, "Microgrids," in *Proc. IEEE Power Engineer. Soc. Winter Meet.*, Jan. 2002, vol. 1, pp. 305–308.

[4] Int. Energy Agency, "Photovoltaic Power Systems Programme, trends in photovoltaic applications – Survey report of selected IEA countries between 1992 and 2012," IEA-PVPS T1-23:2013, 2013.

[5] R. Thresher, M. Robinson, and P. Veers, "To capture the wind," *IEEE Power Energy Mag.*, vol. 5, no. 6, pp. 34–46, Nov./Dec. 2007.

[6] Ministry of Trade, Industry and Energy. (2014, Feb.). 2014 Business Planning Report. Korea government. Seoul, Korea. [Online] (accessed Dec. 30, 2015).

[7] M. Saastamoinen. (2009, Mar.). Case Study 18: Samsø - renewable energy island programme. NCRC. Samsø island, Denmark. [Online] (accessed Dec. 30, 2015).

[8] S. Ottewell, "Ireland's renewable island," *IET Power Eng.*, vol. 17, no. 3, pp. 10–11, Jun./Jul. 2003.

[9] M. Vandenbergh, R. Geipel, M. Landau, and P. Strauss, "Performance evaluation of the Gaidoroumandra mini-grid with distributed PV generators," *4th European PV-hybrid and mini-grid conference*, Athens, 29-30th, May 2008.

[10] K. L. Wang, Y. G. You, and Y. Q. Zhang, "Energy management system of renewable stand-alone energy power generation system in an island," *Automation of Electric Power Systems*, vol. 34, no. 14, pp. 13–17, 2010.

[11] Ministry of Knowledge Economy. (2013, Feb.). The 6th Basic Plan for Long-term Electricity Supply and Demand (2013~2027). Korea government. Seoul, Korea. [Online] (accessed Dec. 30, 2015).

[12] A. D. Paquette, M. J. Reno, R. G. Harley, and D. M. Divan, "Sharing transient loads : Causes of unequal transient load sharing in islanded microgrid operation," *IEEE Ind. Appl. Mag.*, vol. 20, no. 2, pp. 23–34, Mar./Apr. 2014.

[13] R. Majumder, A. Ghosh, G. Ledwich, and F. Zare, “Power management and power flow control with back-to-back converters in a utility connected microgrid,” *IEEE Trans*. *Power Syst*., vol. 25, no. 2, pp. 821–834, May 2010.

[14] L.-R. Chang-Chien, W.-T. Lin, and Y.-C. Yin, “Enhancing frequency response control by DFIGs in the high wind penetrated power systems,” *IEEE Trans*. *Power Syst*., vol. 26, no. 2, pp. 710–718, May 2011.

[15] L.-R. Chang-Chien and Y.-C. Yin, “Strategies for operating wind power in a similar manner of conventional power plant,” *IEEE Trans*. *Energy Convers*., vol. 24, no. 4, pp. 926–934, Dec. 2009.

[16] K. V. Vidyanandan and N. Senroy, “Primary frequency regulation by deloaded wind turbines using variable droop,” *IEEE Trans*. *Power Syst*., vol. 28, no. 2, pp. 837–846, May 2013.

[17] S. Chowdhury, S. P. Chowdhury, and P. Crossely, *Microgrids and Active Distribution Networks*, London, U. K.: The Institute of Engineering and Technology, 2009.

[18] F. Katiraei, R. Iravani, N. Hatziargyriou, and A. Dimeas, “Microgrids management: Controls and operation aspects of microgrids,” *IEEE Power Energy Mag*., vol. 6, no. 3, pp. 54–65, May/Jun. 2008.

[19] D. E. Olivares *et al*., “Trends in microgrid control,” *IEEE Trans*. *Smart Grid*, vol. 5, no. 4, pp. 1905–1919, Jul. 2014.

[20] B. Singh, K. Kant, A. Chandra, and K. Al-Haddad, “Design and implementation of single voltage source converter based standalone microgrid,” in *Proc*. *IEEE Power and Energy Soc*. *General Meet*., 2014, pp. 1–5.

[21] I. M. Bugaje, “Renewable energy for sustainable development in Africa: a review,” *Renewable Sustainable Energy Rev*., vol. 10, no. 6, pp. 603–612, Dec. 2006.

[22] B. Zhao, X. Zhang, J. Chen, C. Wang, and L. Guo, “Operation optimization of standalone microgrids considering lifetime characteristics of battery energy storage system,” *IEEE Trans*. *Sustainable Energy*, vol. 4, no. 4, pp. 934–943, Oct. 2013.

[23] Y.-S. Kim, E.-S. Kim, and S.-I. Moon, “Frequency and voltage control strategy of standalone microgrids with high penetration of intermittent renewable

generation systems," *IEEE Trans*. *Power Syst*., vol. 31, no. 1, pp. 718–728, Jan. 2016.

[24] H. Karimi-Davijani and O. Ojo, "Dynamic operation and control of a multi-DG unit standalone microgrid," in *Proc*. *IEEE Power and Energy Soc*. *Innovative Smart Grid Technologies*., 2011, pp. 1–7.

[25] N. Duic, M. Lerer, and M. G. Carvalho, "Increasing the supply of renewable energy sources in island energy systems," *Int*. *J*. *Sustain*. *Energy*, vol. 23, no. 4, pp. 177–186, 2003.

[26] S. A. Papathanassiou and M. P. Papadopoulos, "Dynamic characteristic of autonomous wind-diesel systems," *Renewable Energy*, vol. 23, no. 2, pp. 293–311, Jun. 2001.

[27] M. Ilic-Spong, J. Christensen, and K. L. Eichorn, "Secondary voltage control using pilot point information," *IEEE Trans*. *Power Syst*., vol. 3, no. 2, pp. 660–668, May 1988.

[28] J. M. Guerrero, J. C. Vasquez, J. Matas, L. G. de Vicuna, and M. Castilla, "Hierarchical control of droop-controlled AC and DC microgrids–A general approach towards standardization," *IEEE Trans*. *Ind*. *Electron*., vol. 58, no. 1, pp. 158–172, Jan. 2011.

[29] Y. A.-R. I. Mohamed and A. A. Radwan, "Hierarchical control system for robust microgrid operation and seamless mode transfer in active distribution systems," *IEEE Trans*. *Smart Grid*, vol. 2, no. 2, pp. 352–362, Jun. 2011.

[30] A. Mehrizi-Sani and R. Iravani, "Potential-function based control of a microgrid in islanded grid-connected modes," *IEEE Trans*. *Power Syst*., vol. 25, no. 4, pp. 1883–1891, Nov. 2010.

[31] "*Advanced Architectures and Control Concepts for more Microgrids: Definitaion of Ancillary Services and Short-Term Energy Markets*," *Deliverable DD4, MORE MICROGRIDS*, Dec. 2009 [Online] (accessed Dec. 30, 2015).

[32] H. Karimi, H. Nikkhajoei, and M. R. Iravani, "Control of an electronically-coupled distributed resource unit subsequent to an islanding event," *IEEE Trans*. *Power Del*., vol. 23, no. 1, pp. 493–501, Jan. 2008.

[33] F. Katiraeri, M. R. Iravani, and P. W. Lehn, "Micro-grid autonomous operation during and subsequent to islanding process," *IEEE Trans*. *Power Del*., vol. 20,

no. 1, pp. 248–257, Jan. 2005.

[34] H. Karimi, A. Yazdani, and M. R. Iravani, "Negative-sequence current injection for fast islanding detection of a distributed resource unit," *IEEE Trans. Power Electron.*, vol. 23, no. 1, pp. 298–307, Jan. 2008.

[35] P. Kundur, *Power System Stability and Control*, New York: McGraw-Hill, 1994.

[36] E. P. Wiechmann, P. Aqueveque, R. Burgos, and J. Rodriguez, "On the efficiency of voltage source and current source inverters for high-power drives," *IEEE Trans. Ind. Electron.*, vol. 55, no. 4, pp. 1771–1782, Apr. 2008.

[37] J. A. P. Lopes, C. L. Moreira, and A. G. Madureira, "Defining control strategies for microgrids islanded operation," *IEEE Trans. Power Syst.*, vol. 21, no. 2, pp. 916–924, May 2006.

[38] F. Blaabjerg, R. Teodorescu, M. Liserre, and A. V. Timbus, "Overview of control and grid synchronization for distributed power generation systems," *IEEE Trans. Ind. Electron.*, vol. 53, no. 5, pp. 1398–1409, Oct. 2006.

[39] F. Gao and M. R. Iravani, "A control strategy for a distributed generation unit in grid-connected and autonomous modes of operation," *IEEE Trans. Power Del.*, vol. 23, no. 2, pp. 850–859, Apr. 2008.

[40] M. C. Chandorkar, D. M. Divan, and R. Adapa, "Control of parallel connected inverters in standalone ac supply systems," *IEEE Trans. Ind. Appl.*, vol. 29, no. 1, pp. 136–143, Jan./Feb. 1993.

[41] S. Conti, R. Nicolosi, and S. Rizzo, "Optimal dispatching of distributed generators in an MV autonomous micro-grid to minimize operating costs and emissions," in *Proc. IEEE Internat. Symp. on Industrial Electron.* (*ISIE*), Jul. 2010, pp. 2542–2547.

[42] N. Hatziargyriou *et al.*, "Energy management and control of island power systems with increased penetration from renewable sources," in *Proc. IEEE Power Engin. Soc. Winter Meet.*, 2002, vol. 1, pp. 335–339.

[43] C. Colson, M. Nehrir, and S. Pourmousavi, "Towards real-time microgrid power management using computational intelligence methods," in *Proc. IEEE Power and Energy Soc. General Meet.*, Jul. 2010, pp. 1–8.

[44] C. Colson, M. Nehrir, and C. Wang, "Ant colony optimization for microgrid multi-objective power management," in *Proc. IEEE Power Syst. Conf. and Exposit.* (*PSCE '09*), Mar. 2009, pp. 1–7.

[45] A. Kahrobaeian and Y. A.-R. I. Mohamed, "Network-based hybrid distributed power sharing and control for islanded microgrid systems," *IEEE Trans*. *Power Electron*., vol. 30, no. 2, pp. 603–617, Feb. 2015.

[46] S. Liu, X. Wang, and P. X. Liu, "Impact of communication delays on secondary frequency control in an islanded microgrid," *IEEE Trans*. *Ind*. *Electron*., vol. 62, no. 4, pp. 2021–2031, Apr. 2015.

[47] H. Laaksonen, "Protection principles for future microgrids," *IEEE Trans*. *Power Electron*., vol. 25, no. 12, pp. 2910–2918, Dec. 2010.

[48] T. Ustun, C. Ozansoy, and Zayegh, "Modeling of a centralized microgrid protection system and distributed energy resources according to IEC 61850-7-420," *IEEE Trans*. *Power Syst*., vol. 27, no. 3, pp. 1560–1567, Aug. 2012.

[49] A. Ruiz-Alvarez *et al*., "Operation of a utility connected microgrid using an IEC 61850-based multi-level management system," *IEEE Trans*. *Smart Grid*, vol. 3, no. 2, pp. 858–865, Jun. 2012.

[50] A. Colet-Subirachs *et al*., "Centralized and distributed active and reactive power control of a utility connected microgrid using IEC 61850," *IEEE Syst*. *J*., vol. 6, no. 1, pp. 58–67, Mar. 2012.

[51] A. L. Dimeas and N. D. Hatziargyriou, "Operation of a multiagent system for microgrid control," *IEEE Trans*. *Power Syst*., vol. 20, no. 3, pp. 1447–1455, Aug. 2005.

[52] W.-D. Zheng and J.-D. Cai, "A multi-agent system for distributed energy resources control in microgrid," in *Proc*. *IEEE 5th Internat*. *Conf*. *on Critical Infrastructure* (*CRIS*), Sep. 2010, pp. 1–5.

[53] Project reports: *Program on technology innovation: The galvin path to perfect power-a technical assessment*, EPRI, Mar. 2007.

[54] T. Ackermann, *Wind Power in Power Systems*, 1st ed. Chichester: John Wiley & Sons, 2005.

[55] B. Fox *et al*., *Wind Power Integration: Connection and system operational aspects*, 1st ed. London, U.K.: The Institution of Engineering and Technology, 2007.

[56] C. Knospe, "PID control," *IEEE Control Systems Mag*., vol. 26, no. 1, pp. 30–31, Feb. 2006.

[57] J. He and Y. W. Li, "An enhanced microgrid load demand sharing strategy,"

IEEE Trans. *Power Electron*., vol. 27, no. 9, pp. 3984–3995, Sep. 2012.

[58] M. A. Eltawil and Z. Zhao, "Grid-connected photovoltaic power systems: Technical and potential problems–A review," *Renewable Sustainable Energy Rev*., vol. 14, no. 1, pp. 112–129, Jan. 2010.

[59] Project reports: *Control and design of microgrid components*, PSERC, Jan. 2007.

[60] S.-K. Kim, J.-H. Jeon, C.-H. Cho, E.-S. Kim, and J.-B. Ahn, "Modeling and simulation of a grid-connected PV generation system for electromagnetic transient analysis," *Sol*. *Energy*, vol. 83, no. 5, pp. 664–678, May 2009.

[61] A. Stiel and M. Skyllas-Kazacos, "Feasibility study of energy storage systems in wind/diesel applications using the HOMER model," *Appl*. *Sci*., vol. 2, no. 4, pp. 726–737, Oct. 2012.

[62] L. Gao, S. Liu, and R. A. Dougal, "Dynamic lithium-ion battery model for system simulation," *IEEE Trans*. *Compon*. *Packag*. *Technol*., vol. 25, no. 3, pp. 495–505, Sep. 2002.

[63] F. Milano and M. Anghel, "Impact of time delays on power system stability," *IEEE Trans*. *Circuits Syst*. *I*, *Fundam*. *Theory Apply*., vol. 59, no. 4, pp. 889–900, Apr. 2012.

[64] J. MacDowell, "Installations connected to a power transmission system and generating equipment: Minimum design requirements, equipment, operations, commissioning and safety," NERC Corp., Atlanta, GA, USA, Nov. 2009 [Online] (accessed Dec. 30, 2015).

[65] H.-Y. Jung *et al*., "A study on the operating characteristics of SMES for the dispersed power generation system," *IEEE Trans*. *Appl*. *Supercond*., vol. 19, no. 3, pp. 2028–2031, Jun. 2009.

[66] A.-R. Kim *et al*., "Performance analysis of a toroid-type HTS SMES adopted for frequency stabilization," *IEEE Trans*. *Appl*. *Supercond*., vol. 21, no. 3, pp. 1367–1370, Jun. 2011.

[67] H. Laaksonen, P. Saari, and P. Komulainen, "Voltage and frequency control of inverter based weak LV network microgrid," in *Proc*. *2005 Internat*. *Conf*. *on Future Power Systems*, Dec. 2005, pp. 1–6.

[68] A. Engler, "Applicability of droops in low voltage grids," *DER Journal*, no. 1, Jan. 2005.

[69] J. Yaoqind, L. Dingkun, and P. Shengkui, “Improved droop control of parallel inverter system in standalone microgrid,” in *Proc. 8th Internat. Conf. on Power Electronics – ECCE ASIA*, May 30–Jun. 3, 2011, pp. 1–8.

[70] J. M. Guerrero, M. Chandorkar, T.-L Lee, and P. C. Loh, “Advanced control architectures for intelligent microgrids–Part I: Decentralized and hierarchical control,” *IEEE Trans. Ind. Electron.*, vol. 60, no. 4, pp. 1254–1262, Apr. 2013.

[71] Y.-S. Kim, E.-S. Kim, and S.-I. Moon, “State of charge (SOC)-based active power sharing method for distributed generations in an islanded microgrid,” in *Proc. 2015 Internat. Conf. on Circuits and Systems (CAS 2015)*, Aug. 9–10, 2015, pp. 1–5.

[72] Y.-S. Kim, I.-Y. Chung, and S.-I. Moon, “Tuning of the PI controller parameters of a PMSG wind turbine to improve control performance under various wind speeds,” *Energies*, vol. 8, no. 2, pp. 1406–1425, Feb. 2015.

[73] *Lithium-ion Battery Life Technical Sheet*, Saft Inc., Bagnolet, France, 2014.

Appendix A. The Parameters Used in the Study

A.1 The parameters of the synchronous generator

The salient rotor type synchronous generator model in the library of MATLAB/SimPowerSystems is used for the diesel generator in the standalone microgrid shown in Fig. 3.2. Most of the parameters are default values of the library of MATLAB/SimPowerSystems. They are shown in Table A.1. The details of the synchronous generator model used in this study can be found in the library of MATLAB/SimPowerSystems.

Table A.1 Parameters of synchronous generator.

Parameter		Value	Unit
Reactance	X_d	1.305	pu
	X'_d	0.296	pu
	X''_d	0.252	pu
	X_q	0.474	pu
	X''_q	0.243	pu
	X_l	0.18	pu
Stator resistance	R_s	0.003	pu
Time constants	T'_{do}	4.49	s
	T''_{do}	0.0681	s
	T''_q	0.0513	s
Inertia	H	3.7	s
Pole pairs	p	20	-

A.2 The parameters of the excitation system

The excitation system of IEEE type AC5A in the library of MATLAB/SimPowerSystems is used for the synchronous generator used in this dissertation (see Fig. 3.2). All of the parameters are default values of the library of MATLAB/SimPowerSystems. They are shown in Table A.2. The details of the excitation system model used in this study can be found in the library of MATLAB/SimPowerSystems.

Table A.2 Parameters of excitation system.

Parameter		Value	Unit
Low pass filter time constant	T_r	20e–3	s
Voltage regulator gain and time constant	K_a	100	-
	T_a	0.02	s
Voltage regulator output limits	VR_{min}	–7.3	pu
	VR_{max}	7.3	pu
Damping filter gain and time constants	K_f	0.03	-
	T_{f1}	1	s
	T_{f2}	0	s
	T_{f3}	0	s
Exciter gain and time constant	K_e	1.0	-
	T_e	0.02	s
Filed voltage value	E_{fd1}	5.6	pu
	E_{fd2}	0.75×5.6	pu
Exciter saturation function values	S_eE_{fd1}	0.86	pu
	S_eE_{fd2}	0.5	pu
Initial values of terminal voltage and field voltage	V_{to}	1	pu
	E_{fdo}	1	pu

A.3 The parameters of the PI controllers

The parameters of PI controllers used in this dissertation (Figs. 3.4, 3.5, 3.20, 4.1, 5.17) are shown in Table A.3.

Table A.3 Parameters of PI controllers.

Controller	K_p	K_i
PI_1	80	30
PI_2	20	4
PI_3	0.4	40
PI_4	50	100
PI_5	0.4	40
PI_6	50	100
PI_7	30	30

The parameters of PI_2 are for isochronous governor and are referred from [26] to emulate practical characteristics of a diesel generator. The parameters of PI_3–PI_6 are for the inverter control so they are determined heuristically through simulation trial-and-error method in order to have fast response characteristics. The parameters of PI_1 and PI_7 are for load–SOC control units. Some of them (PI_3–PI_6) are determined by method used in [72] and the others are by trail-and-error with the simulation test. Some of them have different values since they are applied to different standalone microgrids (PI_1 for synchronous generator-based standalone microgrid and PI_7 for inverter-based standalone microgrid).

Appendix B. Influence of Forecasting Error on *P–Q* Droop Control

As mentioned in Chapter 4.1.2, the *P–Q* droop coefficient is determined based on the forecasted load demand and RESs' generation data and the network impedance (see (4.3)–(4.7)). Hence, badly forecasted data affects the droop coefficient and hence the voltage control performance. In this chapter, an influence of forecasting error on the voltage control performance is investigated.

Simulation test

The simulation environment used in Chapter 4.1.2 is used again in this chapter to investigate the influence of forecasting error on the *P–Q* droop control performance. In this case, however, the *P–Q* droop coefficients calculated with the night time data (including load demand and the RESs' forecasted output power) is used whereas the day time load and the RESs' output power of the worst case (the RESs' output power vary from 0 to the rated value) are used in the practical simulation test in order to reflect the worst forecasting error. The simulation test system's practical data and the forecasted data are shown in Table B.1.

Table B.1 Comparison between practical and forecasted data.

RES	Average RESs' output [MW]		Bus Number	Load [MW]	
	Practical	Forecasted		Practical	Forecasted
WT	7.47	3.45	2	3	1.5
			3	2	1
			5	1	0.5
			6	1	0.5
			8	2	1
PV	0.66	0	9	0.2	0.1
			10	0.2	0.1
			11	0.1	0.05
			12	0.5	0.25

With the practical data, the droop coefficients ($1/m_{PQ}$) for the WT and the PV

should be 0.413 and 0.495, respectively, however the droop coefficients of 0.473 and 0.514 (calculated by using the wrongly forecasted data) are applied to the WT and the PV, respectively. Case 2 (worst case) in Chapter 5.2 is used to compare with the case of using wrongly forecasted data.

Fig. B.1 shows the simulation results comparing three control methods tested in Case 2 of Chapter 5.2 and the proposed method considering the worst forecasting error (denoted as "prop. w. error" in Fig. B.1). The WT by using the proposed control method with the huge forecasting error ("prop. w. error") absorbs more reactive power as shown in Fig. B.1(a) since the forecasted value P_{pre} (see Fig. 4.1) is significantly different from the actual active power. The reactive power bounces at 39, 43, 67 s since it reaches its limitation according to (4.2). The PV outputs zero reactive power as shown in Fig. B.1(b) since it forecasts that solar irradiance would be zero. By using the proposed control method with the forecasting error, the fluctuation of the WT bus voltage is still well alleviated though it bounces at 39, 43, 67 s as shown in Fig. B.1(c) since the reactive power reaches its limitation according to (4.2). However, the voltage deviation (not fluctuation) from the nominal value cannot be well prevented. The PV bus voltage seems to be aggravated by wrongly forecasted data as can be seen in Fig. B.1(d). If the forecasting error is huge, the proposed control method applying to the PV may be better than that of control method without droop (denoted as "w/o droop" in Fig. B.1) but it may be worse than that of the conventional method (denoted as "conv." in Fig. B.1). It seems, at the very least, that the worst forecasting error does not lead the degradation of the system stability.

It can be concluded that the exact forecasting is somewhat significant for determining the *P*–*Q* droop coefficient. Fortunately, an extremely huge forecasting error investigated in this study is not likely to happen and the droop coefficient can be modified based on re-forecasted data. Again, the secondary control issues (such as forecasting and scheduling) are not discussed in this dissertation.

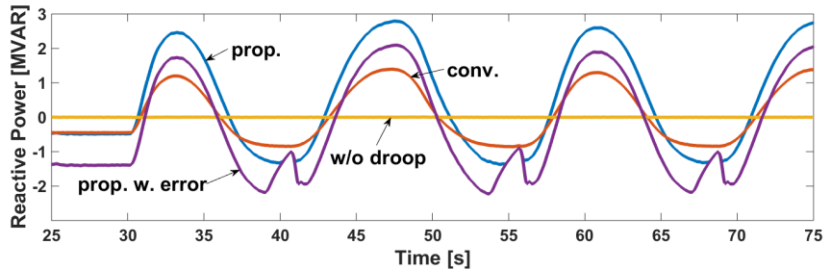

(a)

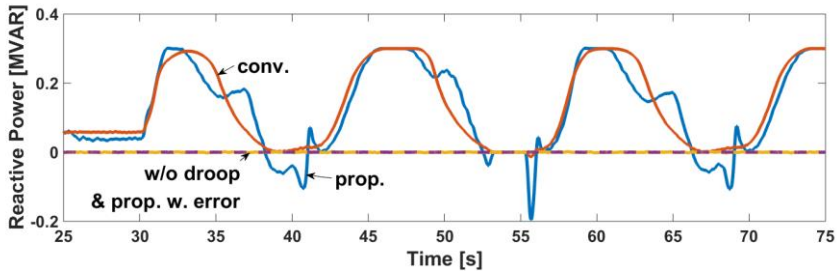

(b)

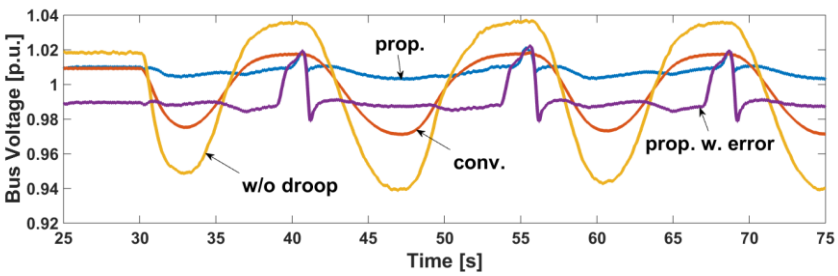

(c)

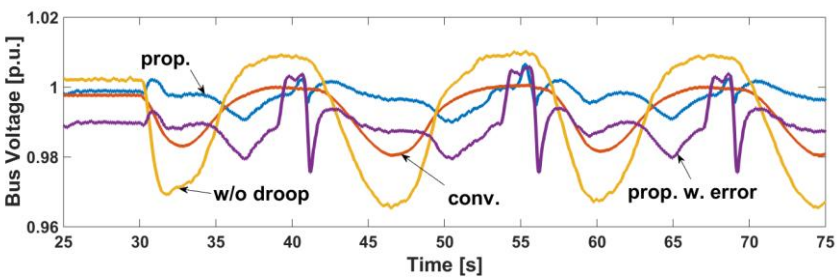

(d)

Fig. B.1 Simulation results considering forecasting error. (a) Reactive power of WT. (b) Reactive power of PV. (c) WT bus voltage. (d) PV bus voltage.

Appendix C. Relationship between Expected Life and SOC of Battery

In Chapter 3.1.3, the control strategy of diesel generator considering fuel efficiency is developed. However, considering fuel efficiency of the diesel generator causes the SOC not to be maintained at the certain level. It is mentioned in Chapter 3.1.3 that the change of SOC might affect the life of the battery and hence could be economically inefficient. Fig. C.1 [73] shows the relationship between expected life and SOC of a lithium-ion battery.

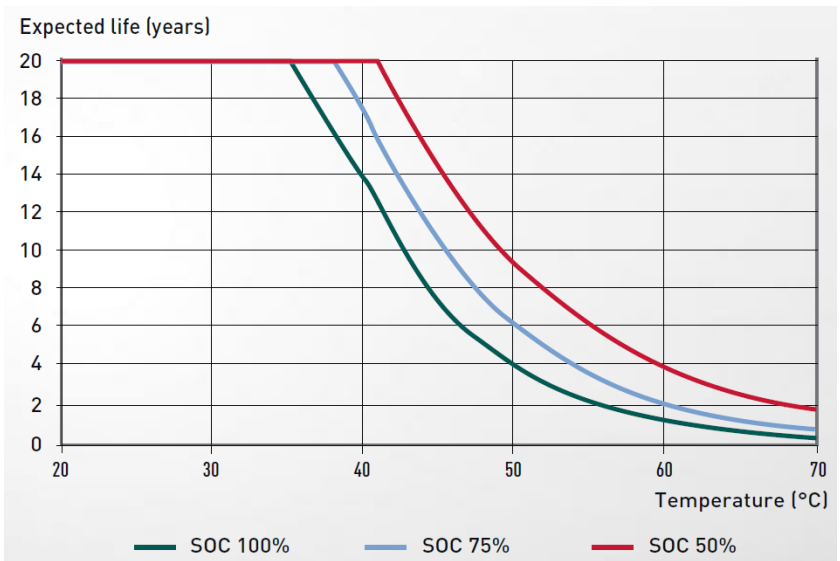

Fig. C.1 Relationships between expected life, temperature, and SOC of a battery [73].

As shown in Fig. C.1, it can be concluded that the expected life of the battery could be expanded if the SOC of the battery is maintained near 50 %. The life expansion of the battery increases economic efficiency in the perspective of a standalone microgrid operation. The SOC affects not only the expected life but also the number of charge/discharge cycles. The relationship between the number of

cycles and the SOC (expressed as DOD in this Fig.) is shown in Fig. C.2.

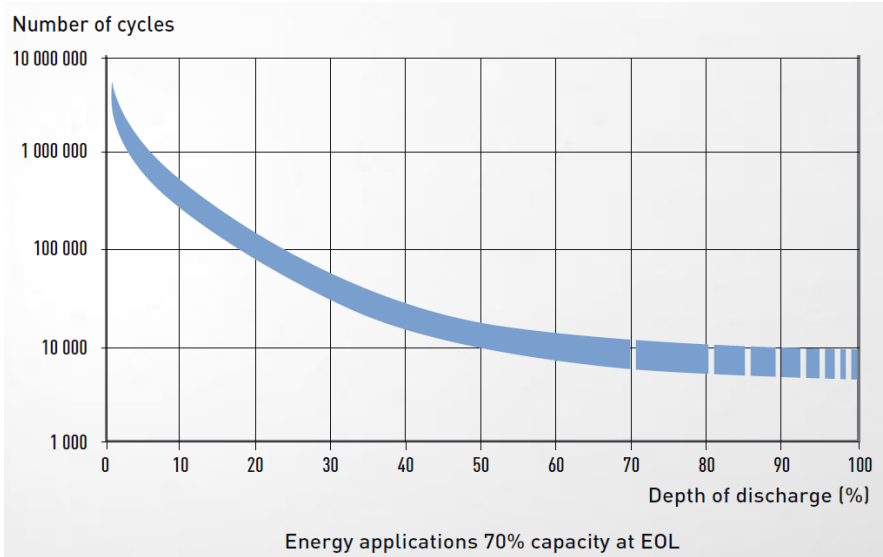

Fig. C.2 Relationship between number of cycles and SOC of a battery [73].

As shown in Fig. C.2, the number of charge/discharge cycle can be increased during the high level of SOC operation.

From Figs. C.1 and C.2, it can be concluded that not only the fuel efficiency of the diesel generator but also the SOC is the important factor that affects the economic efficiency of a standalone microgrid operation. Hence, the fuel efficiency, the SOC, and all the other factors (e.g., power loss and start-up cost of the generator) must be considered in order to assess the economic efficiency of the proposed control strategies for a standalone microgrid.

초 록

전기적으로 고립되어 주 계통에 영구적으로 연계되지 못하는 경우의 마이크로그리드를 독립형 (Standalone) 마이크로그리드로 정의한다. 계통연계형 마이크로그리드에서는 주 계통이 주파수 및 전압을 안정적으로 유지시켜주지만 독립형은 그렇지 않다. 일반적으로, 독립형 마이크로그리드의 유·무효전력 분배 방법은 기존 계통을 모방하여 주파수 및 전압 droop 제어 기법을 적용해왔다. 하지만 독립형 마이크로그리드는 계통 관성이 작고 강인도가 낮기 때문에 부하나 신·재생에너지 발전기 출력의 변화에 대해 주파수 및 전압의 안정도가 취약하다.

본 논문에서는 독립형 마이크로그리드에서 부하나 신·재생에너지 발전기의 출력 변동 등과 같은 외란 발생 시 주파수와 전압을 안정적으로 유지할 수 있는 분산전원들의 제어 방법을 제안한다. 기존의 주파수 droop 제어 기법은 부하 변동 시 주파수가 공칭 값에서 벗어나는 정도를 기준으로 유효전력 수급 균형을 맞추기 때문에 주파수 변화가 불가피하다. 이를 해결하기 위해 본 논문에서는 배터리 에너지저장장치 (Battery Energy Storage System, BESS)의 충전상태 (State of Charge, SOC)를 기준으로 유효전력을 분배하는 방법을 제안한다. 배터리 에너지저장장치는 droop 제어 없이 일정한 주파수와 전압을 형성하도록 제어가 되고 나머지 분산전원들은 원하는 유·무효전력을 내도록 제어된다. 따라서 독립형 마이크로그리드의 유효전력 부하가 변하면 배터리 에너지저장장치의 출력과 충전상태가 변한다. 나머지 분산전원들은 배터리 에너지저장장치의 충전상태의 변화를 기준으로 유효전력을 분배하게 된다. 배터리와 물리적으로 가까운 분산전원들은

배터리의 출력변화를 직접 측정하여 일차 충전상태 제어 (Primary SOC Control)를 하고 물리적으로 멀리 있는 분산전원들은 통신 설비를 통해 충전상태 정보를 얻어 이차 충전상태 제어 (Secondary SOC Control)를 한다. 시스템의 신뢰도를 높이기 위해 통신 설비가 고장이 났을 경우에는 배터리와 분산전원들이 기존의 주파수 droop 제어로 작동되도록 제어기를 설계했다.

전압 안정도의 향상을 위해서는 새로운 droop 방법을 제안했다. 기존에는 독립형 마이크로그리드의 모선 전압을 어느 정도 유지하는 동시에 무효전력을 분배하기 위해 전압-무효전력 droop 제어를 사용하였다. 이 방법은 모선 전압의 공칭 값에서 벗어난 정도를 기준으로 무효전력을 조절한다. 따라서 전압이 변해야지만 무효전력이 보상되기 때문에 전압의 변동을 근본적으로 방지할 수는 없다. 특히 신·재생에너지 발전기와 같이 유효전력 출력이 간헐적으로 변동한다면 그에 비례하게 모선 전압도 변동한다. 계통의 강인도가 낮을수록 전압 변동은 더욱 심해진다. 이 문제를 해결하기 위해 본 논문에서는 신·재생에너지 발전기의 유효전력 출력 변동에 비례하게 무효전력 출력을 변화시킴으로써 모선 전압 변동을 방지하는 유효전력-무효전력 droop 제어를 제안했다. Droop 계수는 민감도 행렬을 기반으로 구했다. 또한, 무효전력 보상으로 전압을 제어하는 데에 한계가 있는 저압계통 독립형 마이크로그리드에 대해서는 BESS의 유효전력을 보상하여 전압을 제어하는 유효전력-유효전력 droop 제어방법도 제안하였다.

제안한 방법은 MATLAB/SimPowerSystems로 설계 및 모의실험 되었다. 제안한 방법은 기존의 주파수 및 전압 droop 제어 방법들과 비교해보았으며 실험결과를 통해 효과를 검증할 수 있었다.

제안한 방법은 신·재생에너지 발전기의 수용률이 높은 전기적으로 고립된 계통에 적용할 수 있을 것으로 기대된다. 특히 신·재생에너지

발전기들이 일으키는 주파수 및 전압 문제를 아주 안정적으로 해결할 수 있다. 결과적으로 전세계의 신·재생에너지 발전기 수용률을 높이고 전기적으로 고립된 도서지역의 에너지 자립화에 크게 기여할 것으로 기대된다.

주요어 : 정주파수, SOC 기반 유효전력 제어, Droop 제어, 독립형 마이크로그리드, 배터리 에너지저장장치, 신·재생에너지 발전기
학 번 : 2010-20776